Energy Research and Development Division

FINAL PROJECT REPORT

Distributed Generation Impacts, Cyber Security Issue Identification, and Home Area Network Design

California Energy Commission

Edmund G. Brown Jr., Governor

December 2017 | CEC-500-2017-040

PREPARED BY:

Primary Author(s):
Atousa Yazdani
Mahyar Zarghami
Mohammad Vaziri
Russ Tatro
Suresh Vadhva
Emir Macari

California Smart Grid Center
California State University, Sacramento
6000 J Street
Sacramento, CA 95819-6019
916-278-6011
www.ecs.csus.edu/csgc/

Agreement Number: 500-09-039

Prepared for:

California Energy Commission

Quenby Lum
Agreement Manager

Fernando Piña
Office Manager
Energy Systems Research Office

Laurie ten Hope
Deputy Director
ENERGY RESEARCH AND DEVELOPMENT DIVISION

Drew Bohan
Executive Director

ACKNOWLEDGEMENTS

The California State University-Sacramento (CSUS) thanks the electric utility companies, equipment vendors, and staff of the California State University, Sacramento. It was through the combined efforts of this diverse group that the projects were made possible. The authors highlight the following persons in particular:

Mike Gravely and Pedro Gomez of the California Energy Commission for approaching the University and providing the funding for this research.

Industry Advisors: Don Jacobs, Sacramento Municipal Utility District, Alex McEachern, Power Standards Laboratory, Mark Morosky, Trimark Associations, Pat Mantey, University of California, Santa Cruz, Merwin Brown, California Institute for Energy and Environment

CSU, Sacramento Staff: Denise Anderson, Coordination Support, Cynda Dart, Coordination Support, Jim Ster, Technical Support

CSU, Sacramento Student Researchers

Afzal, Masoud	Gant, Murphy	Meadows, Alex	Supnet, Chris
Ahmed, Omar	Gee, Neil	Miller, Troy	Tamblyn Jeffery
Al Ruwaili, Mohammed	Giles, Craig	Modini, Santosh Babu	Tavatli, Farshad
Alsasua, Gianni	Greene, Alexandra	Mponte, Didier	Tesfasilassie, Musie
Alzanoon, Abdulkarim	Honnavali Prabhkara, Rakesh	Nei, Ling	Thouta, Nikitha
Bandak, Carlos	Icenhower, Joshua	Nguyen, Linh	Throne, Jonathan
Brimer, Steven	Imtiaz, Aisha	Nugent, Jessica	Tosspon, Chris
Bustaman, Sufian	Isle, Daniel	Nunes, Kasey	Trublood, Zachariah
Cahail, Darrell	Jadhav, Poonam	Nyugen, Thoa	Tudor, Cody
Carmi, Eric	Kaviani, Babak	Oneal, Trevor	Wade, Austin
Chadha, Ayush	Keita, Mamadou	Patel, Mohit	Wernecke, Aaron
Chandrasekara, Lakmal	Konrad, Tanya	Prior, Robert	Wingo, Rebecca
Cloninger, Anna	Krepelka, Franklin	Rahimi, Ali	Wong, Carissa
Cooney, Kevin	Liang, Tao	Razigh, Shahab	Wortman, Robert
Cummins, Erik	Lima, Brian	Relangi, Sirisha	Xiong, Tou
Davidson, Andrew	Loria, William	Rossi, Shanna	Yamasaki, Matthew
Diab, Aaron	Ludlow, Trevor	Sharma, Rishi	Zein, Arief
Dixon, Jeremy	Mackinlay, Helena	Shete, Shreedevi	Zhang, Dongyi
Feranil, Mark	Makasarashvili, Aleksey	Spencer, Andrew	
Frost, Deborah	Makhzani, Amirsaman	Sprung, Eric	
Fu, Wenjie	Manzyuk, Diana	Subburaj, Vishnu Priya	

PREFACE

The California Energy Commission Energy Research and Development Division supports public interest energy research and development that will help improve the quality of life in California by bringing environmentally safe, affordable, and reliable energy services and products to the marketplace.

The Energy Research and Development Division conducts public interest research, development, and demonstration (RD&D) projects to benefit California.

The Energy Research and Development Division strives to conduct the most promising public interest energy research by partnering with RD&D entities, including individuals, businesses, utilities, and public or private research institutions.

Energy Research and Development Division funding efforts are focused on the following RD&D program areas:

- Buildings End-Use Energy Efficiency
- Energy Innovations Small Grants
- Energy-Related Environmental Research
- Energy Technology Systems Integration
- Environmentally Preferred Advanced Generation
- Industrial/Agricultural/Water End-Use Energy Efficiency
- Renewable Energy Technologies
- Transportation

Distributed Generation Impacts, Cyber Security Issue Identification, and Home Area Network Design is the final report for the California State University, Sacramento Research Projects: Distributed Generation Impacts, Cyber Security Issue Identification, and Home Area Network Design project (contract number 500-09-039) conducted by the California State University, Sacramento. The information from this project contributes to Energy Research and Development Division's Energy Technology Systems Integration program area.

When the source of a table, figure or photo is not otherwise credited, it is the work of the author of the report. All quoted sections of this report have been taken from the papers listed in the References that have been published and presented at various Institute of Electrical and Electronics Engineers (IEEE) conferences.

For more information about the Energy Research and Development Division, please visit the Energy Commission's website at www.energy.ca.gov/research/ or contact the Energy Commission at 916-327-1551.

ABSTRACT

This report describes research activities to investigate active distribution networks with high volumes of renewable energy. Improvements must be made to distribution networks to facilitate safe and reliable interconnection of distributed generation at higher penetration levels. Major concerns such as voltage, protection, and power quality related to distributed generation interconnections, and the issues with existing design standards and criteria, are identified and presented. Several different Distribution Network changes have been proposed to help resolve these issues.

This report discusses integrating renewable energy in distribution systems and presents the new challenges. It also provides solutions such as changes in operating the system, using accurate measurements, and diligent algorithms. Finally, the research illustrates the benefits of using industry-approved energy storage.

Keywords: *Distribution Network, Active Distribution System, smart grid, advanced metering infrastructure, AMI, photovoltaic, PV, solar, battery, energy storage, energy monitoring, energy awareness, energy management, renewable energy, power monitoring*

Please use the following citation for this report:

Yazdani, Atousa; Mahyar Zarghami; Mohammad Vaziri; Russ Tatro; Suresh Vadhva; Emir Macari. (California State University, Sacramento). 2017. ***Distributed Generation Impacts, Cyber Security Issue Identification, and Home Area Network Design.*** California Energy Commission. Publication number: CEC-500-2017-040.

TABLE OF CONTENTS

LIST OF FIGURES

LIST OF TABLES

EXECUTIVE SUMMARY

Introduction

Concerns about burning fossil fuels have encouraged a variety of renewable generation technologies to be considered that could provide a sizeable amount of power to the nation's electricity generation portfolio. Some advantages of renewable distributed generation include emission-free power generation, relief of electricity line congestion by providing local generation to high load areas, load frequency control, and ancillary services. There are, however, numerous challenges associated with integrating this power to the existing system that must be addressed since generating electricity from renewable resources is not consistent. It is also essential to resolve the grid impacts from renewable distributed generation, cyber security issues and using smart home energy technologies.

Project Purpose

Growth of renewable energy will affect the operation, controls, and protection equipment of the electrical grid. Additionally, the current distribution network was not designed to integrate renewable generation at significant volumes. The California State University-Sacramento team researched distributed generation impacts on California's electric distribution system operation and delivery. They also documented cyber security issues and explored how home area networks could allow smart energy systems to use renewable energy and increase energy efficiency.

A series of studies was carried out to improve operating distribution networks with high amounts of renewable distributed generation. Major concerns from integrating renewable distributed generation are identified as voltage fluctuation and improperly operating utility distribution system protection equipment. The concerns involve deviations from conservation voltage reduction levels set by current operational standards. Furthermore, several mitigation measures that would alleviate the impacts of distributed generation are considered and proposed.

A major concern is also related to significant amounts of electricity generated during daytime hours, resulting in reversal of power flow in distribution feeder lines which are designed for one-way power flows. Such reversal power flows are often associated with abnormally high and/or low voltages along the feeder. Current rules and standards do not allow any distributed generation to participate in local voltage regulation. For example, photovoltaic (PV) inverters are only allowed to feed live power to ensure maximum power production. However, this type of operation may result in undesirable voltage conditions. A coordinated active/reactive power control by distributed generation, including PV inverters, can help resolve the issues associated with voltage profile, while reducing the total demand of the system.

Project Results

The research team explored distributed generation and the impacts of integrating renewable energy in distribution systems. Case studies used utility and standardized feeders to display and/or verify these perceived concerns. Possible solutions for mitigating some of these concerns were researched, analyzed and simulated. Operational, protection, and control impacts were

analyzed. Conceptual studies and formulas for advanced technologies such as state estimation were also considered and documented. Despite the issues and concerns, research has shown that strategic investments in enabling technologies can greatly increase the distribution network's ability to utilize an increasing level of DG. National Standard IEEE 1547 is a stepping stone to furthering the possibilities of DG integration, along with the IEEE 2030 standards.

Researchers identified and explained the consumer's cyber security and privacy risks, recommending best practices when using various smart home devices. Additionally, they identified industry resources that will guide the next generation of engineers and security professionals. The final recommendations are for the utilities to consider the possibility of upgrading their smart meters to ZigBee SEP 2.0 compliant hardware and firmware. ZigBee SEP 2.0 offers the possibility of stronger encryption and more robust communication channels.

In the Customer Premise Network (CPN) and Home Area Network (HAN) research, industry partners have begun to roll out HAN devices that are Zigbee enabled and are available for purchase by consumers. Researchers have conducted many studies and test experiments on creating smart sensors and robust data management of CPN/HAN tool systems integrated with current grid technology. These studies show promising results of consumers saving up to 29 percent in energy consumption with automated control systems fed by real-time energy usage and pricing data.

Project Benefits

Integrating distributed generation from renewable resources promotes cleaner and less hazardous energy. Connecting more distributed renewable generation helps meet the Renewable Portfolio Standard goals set by the California legislature.

The project's researchers verified the adverse impacts of integrating renewable energy into the electric grid and proposed possible mitigation measures to alleviate these effects. The suggested recommendations can benefit the utilities' day-to-day operations and could enhance the quality of energy being delivered to end customers. Results from the analysis, simulation and testing have been documented and shared with the industry through technical publications and presentations in national and international conferences.

CHAPTER 1:
Steady State and Flicker Impacts of DG Penetration on Distribution Systems

State and federal regulatory commissions have set California's target penetration levels for renewable sources of energy. California is leading the United States by requiring that 33 percent of all retail electricity sales be from renewable resources by the year 2020. This massive integration of renewable energy to California's electrical grid, especially to the distribution feeders, has system owners and stakeholders concerned. Therefore, a series of analyses should be performed to expand the knowledge as to how these newly introduced generations will impact the security and reliability of load delivery.

Adding DG to the electrical grid can affect the direction of the flow along the feeder lines. In North America the distribution system is unidirectional, and generally uses radial feeders. The power flows in a radial nature from the substation to the various loads along the feeder. This radial design is to maintain the voltage within an acceptable range for the minimum and maximum load demands and enhance the voltage regulation capability on the feeders. Often these renewable resources are located in remote areas and limited in size. These small remote generation sites are often connected to the distribution feeders without any detailed studies or analysis. The implementation of DG alters the performance of the entire distribution feeder. In this condition the distribution feeder is no longer a radial topology with a unidirectional power flow pattern and the bi-directional flow inside the distribution feeders will be amplified as the size of the distributed generator is increased. Some of the known impacts of DG integrated in radial distribution feeders are voltage quality deterioration, alteration on the protection equipment settings, desensitized relays, increased fault currents, and increased maintenance of "hunting" equipment. One of the main issues associated with this type of generation is the islanding affect and addition of new protection schemes to the feeder. A considerable amount of research has been done identifying these concerns and issues, and this will be a call for change in standards and feeder design strategies. (Vaziri, Zarghami and Yazdani 2014), (Afzal, Zarghami and Yazdani 2013)

There are advantages to integrate DG into distribution feeders; one is the reduction of demand on the main feeder and its tie lines, resulting in the delay or postponement of equipment upgrades at the point of common coupling due to load growth. Evenly dispersed generation also has the ability to support local voltage, making the voltage profile more consistent along the feeder. Considering a feeder that is suffering from low voltage conditions in case of high demands, in this scenario the evenly distributed DG can boost the voltage along the feeder and bring a more consistent voltage profile. The analysis has shown that in distribution feeders with strong voltage regulation, the addition of small amounts of generation (usually below 25 percent of an individual customer's power consumption) will not bring a significant impact on the feeder. This type of generation is non-exporting in nature and maintains the system's unidirectional power flow, and, therefore, it reduces the load on the feeder. The DG is generally equipped with anti-islanding protection schemes and does not need to be monitored for such

problems. The DG can slightly destabilize the protection equipment by changing the demand values and short circuit ratings originally used in the protection study. The bidirectional power flow disrupts the simple protection equipment, requiring more protection equipment and a complete review of the protection system and coordination of devices. The losses in the system are also reduced, benefiting the distribution system operator's costs. At the Point of Common Coupling (PCC) on a weak network the DG can cause the voltage to rise on the lateral, while nearby laterals can be operating at significantly lower voltages. The voltage discrepancies can cause challenges for voltage control on the feeder, possibly requiring additional voltage regulating equipment or the re-location of existing equipment. Some larger DGs are capable of islanding a portion of the feeder. It is required to monitor them and prevent unintentional islanding, and, most importantly, prevent the island from re-connecting with the grid while out of phase. (Vaziri, Zarghami and Yazdani 2014), (Afzal, Zarghami and Yazdani 2013)

Losses in the network begin to increase costs for the distribution system operator and become worse as more DG is added. When there is the presence of a large number of small exporting DG units, or a few large DG units that are capable of reverse power flow on the laterals and main feeders, the distribution feeder requires a complete re-design. The voltage regulating equipment will be incorrectly programmed, the protection equipment is completely inadequate in terms of components and the coordination for the power flow, and there is serious risk to the DG equipment and the distribution system operator. Many islanding scenarios of the feeder sections are possible with high probabilities. Such conditions require preventative measures to safeguard the DG and Distribution System equipment.

In this chapter the impacts of the DG on a feeder is analyzed and each subsection is the outcome of studying the effects that are briefly mentioned here. (Vaziri, Zarghami and Yazdani 2014), (Afzal, Zarghami and Yazdani 2013)

Steady State Distribution System Voltage

Standards Governing Voltage and Regulation

The process of keeping feeder voltage within a desired bandwidth is called voltage regulation. The standard provided by the American National Standards Institute (ANSI), also known as ANSI-C84.1, specifies the upper and lower limits of the utility voltages for the distribution feeders

- Under normal operating conditions, the regulation requirement is +/- 5 percent on a 120-volt base.
- Under unusual conditions, the allowable range is -8.3 percent to +5.8 percent.

The desired voltage level can be achieved by using two different methods. The first is by directly controlling the voltages, or in other words, by lowering or raising the number of turns on the secondary side of a regulating device. Step voltage regulators and OLTC transformers are examples of the devices used for direct voltage control. The second is that voltages can also be regulated indirectly by controlling the flow of reactive power in the feeder. Devices used to indirectly control voltages utilizing reactive power are shunt capacitors and SVCs.

In a normal distribution network the highest voltage is within the feeder, usually at the output of the Load-Tap Changing transformers (LTC). The lowest voltage is usually at the customer's site located furthest from the LTC of the feeder. Both the low and high voltages must be kept within tightly regulated standards of 114 V to 126 V respectively (.95 pu – 1.05 pu on a 120V base) as stated by the American National Standards Institute (ANSI) Service Voltage Standard C84.1.

To maintain the voltage level at a customer's site, automatic voltage control is provided by bus regulation, individual feeder regulators at the substation, and supplementary pole top line regulators along the feeder. A Voltage-Regulating Relay (VRR) controls the tap changes based on the voltage settings, the bandwidth, and the time delay. LTCs are limited to raising or lowering the voltage levels at the point of the tap-changing transformer. Capacitors installed in a radial network affect the voltages between the transformer and the capacitor. One of the most economical and, therefore, prevalent ways to achieve voltage control is the use of LTC at the substation as well as shunt capacitors on the feeders and at the stations. (Vaziri, Zarghami and Yazdani 2014), (Afzal, Zarghami and Yazdani 2013)

Appendix F discusses a common methodology to calculate Voltage Drop Percentage.

Voltage Regulator

A voltage regulator is an autotransformer with a mechanism responsible for tap changing as well as a voltage sensing and control unit. By changing its tap, voltage regulators can increase or decrease their output voltage, hence controlling voltages on the sections downstream from its locations on the feeder. A typical voltage regulator can increase (boost) or decrease (buck) the voltages up to 10 percent, providing a total of 20 percent of regulation range. This boost or buck process is carried out in 32 steps with a 0.62 percent voltage change per step. Voltage control components have three basic settings:

- Base voltage and Line Drop Compensator (LDC) settings. The base voltage set point is the desired output voltage of the regulator at zero current flow.
- Bandwidth, which is the tolerance/difference at which the voltage regulator starts regulating voltages.
- Time delay, or the time difference, at which the regulator first detects the difference between set points and measured voltages and corrective action starts.

Voltage sensing control receives input from current and voltage transformers to constantly measure the system voltage. These measured system voltages are compared to the "set point." If the difference between measured and set voltage is more than one half of the bandwidth and it maintains itself for a period equal to the time delay setting, the control sends a command to raise or lower the tap changing mechanism for proper action. If the measured voltage is less than the set voltage, a boosting procedure will be activated. If the measured voltage is higher than the set point, a bucking process will be initiated.

The LDC setting is used by line-voltage regulators to additionally compensate for the voltage drop on the line when the current increases (Figure1). LDC in a voltage regulator can be

controlled by changing the X and R settings on the unit. In the simulations, the LDC functionality of the voltage regulator was disabled by setting the resistance and reactance elements to zero. The voltage regulator was set to regulate the output determined by the base voltage setting alone. This is known as "Regulator Terminal" mode in the simulation. Other available operating modes include, "Fixed Tap" and "Load Center". Each of these settings for the voltage regulator reacts differently with DG. (Vaziri, Zarghami and Yazdani 2014), (Afzal, Zarghami and Yazdani 2013)

Figure 1: Example of LDC Regulation Issues

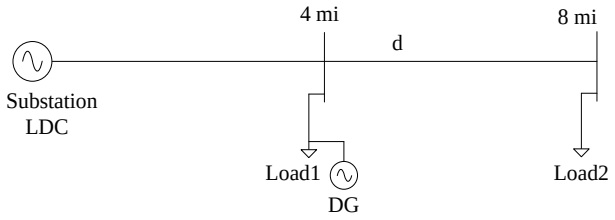

Voltage Regulating Devices Concerns

Capacitor-Related Concerns

Pole-mounted, switched capacitors are utilized to correct power factor and improve voltage profile between the capacitor and power source. Due to daily load curves, mixtures of switched and fixed capacitors are often used on distribution feeders. Most capacitor banks are placed near the location of reactive demand or roughly 2/3 of the distance down the mains on evenly loaded feeders. The addition of DG alters the effectiveness of the capacitors in several ways. If the DG is near unity PF, or if it is a synchronous generator (which is normally set at a fixed power factor schedule), the voltage at the PCC will usually rise, requiring the reduction of fixed capacitive support, and even the possibility of switching reactors to bring the voltage down. However, if the DG is an induction unit, the reactive support of the capacitors may no longer be adequate. Also, the dynamic nature of DGs must be taken into account. The output of solar concentrating panels is greatly reduced with cloud shadows and wind turbines that are equally affected by wind variability. This non-uniform output further stresses the voltage control schemes. (Vaziri, Zarghami and Yazdani 2014), (Afzal, Zarghami and Yazdani 2013)

Tap Changer Settings Concerns

On-Load Tap Changing (OLTC) transformers driven by Automatic Voltage Control (AVC) relays are usually used in feeders. With increasing levels of DG generation in a distribution feeder, voltage regulation problems can arise, altering the performance of the AVC relay. Both the power factor of the DG and the power factor of the load seen by the OLTC can cause the voltage measured by the AVC relay to be shifted. This results in inaccurate voltage control. At the very minimum, any introduction of DG into a system requires a re-evaluation of the control equipment settings to verify that standards are upheld in individual worse case scenarios and loading conditions. (Vaziri, Zarghami and Yazdani 2014), (Afzal, Zarghami and Yazdani 2013)

A simplified example of inaccurate voltage control is shown in Figure 2. Using equations for Voltage Drop (VD) (Appendix F) the VD is calculated both for the LDC and the actual VD at distance "d". Before the DG delivers power into the system, the LDC is accurate. As shown in Figure 2 once the DG begins to inject power at Load1, the accuracy of the LDC deteriorates.

Figure 2: Accuracy of LDC Compared to Actual Voltage Drop and a Function of Generator Output

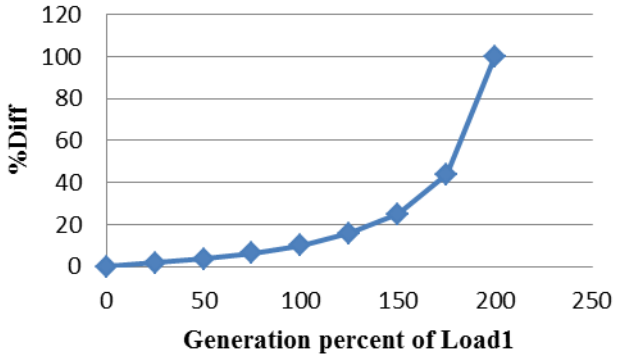

Transient Voltage Flicker

Transient Voltage Flicker Sample System Test and Mitigation Measures

As penetration levels of renewable resources, such as wind and solar power, increase in the low-voltage grid, the problem of voltage fluctuations arises. These fluctuations cause voltage flickers depending on the voltage's rate of change. This phenomenon cannot only cause annoying flickering of lights, but also the loss of efficiency in industrial plants and interference with the protection system.

To overcome the fluctuations in power due to renewable resources, such as wind or solar plants, battery energy storage systems (BESS) have been proposed to mitigate the problem. BESS, when implemented at the point of common coupling through converters, can provide support for power quality through exchange of active and reactive power. (Vaziri, Zarghami and Yazdani 2014), (Afzal, Zarghami and Yazdani 2013)

Simulation Parameters and System Description

The distribution feeder selected for this project is an actual 12kV distribution circuit with several single phases and three phase laterals feeding multiple loads. The simulation is modeled using a utility grade computer program known as "CYMEDIST®". The load allocations are all set to 99 percent with the following power factors: Domestic=0.95, Commercial=0.87, Industrial= 0.85 and Agricultural= 0.85. Major items of interest for this voltage study are a synchronous generator as a variable DG connected at 30,000 feet from substation, a voltage regulator, SVC units connected at distances of 27,500 feet and 28,800 feet respectively, as well as a switched capacitor rated at 100 kVAr/phase installed at a distance of 18,500 feet from the substation. Other locations of interest are the end of feeder at 36,000 feet, and an automatic reclosing breaker switch located at 21,837 feet from the substation. Figure 3**Error! Reference source not found.** shows the structure of the studied distribution feeder. The synchronous generator ran in

voltage-controlled mode, and the 'voltage drop-unbalanced' load flow calculation method was used, which allowed the team to independently plot the voltage profile of the system for each of the three phases.

Figure 3: Case Study Feeder

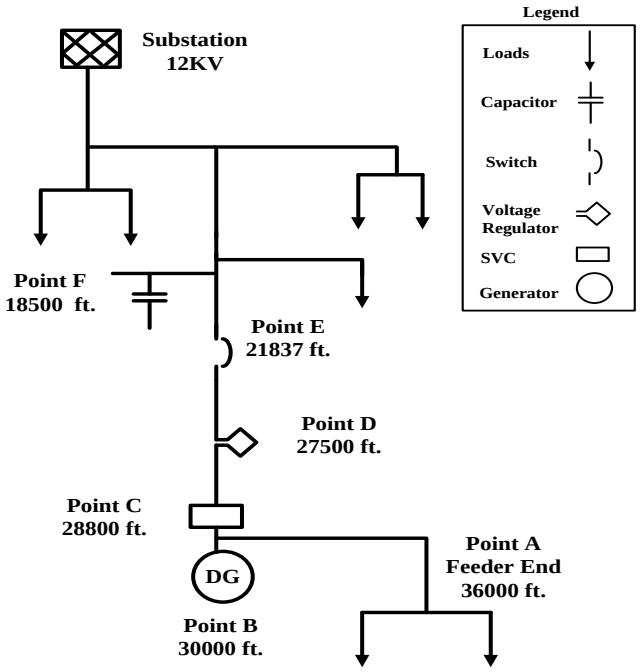

An actual peak load of 11.5 MW has been considered as full load and 30 percent of this load will be referred to as light load for the simulations. A synchronous generator capable of producing a maximum of 10 MW of real power was used as the variable DG source. 1 MW of generator output was considered as minimum generation, while 10 MW output is referred to as maximum generation. The generator output was changed from its minimum to maximum in the intervals of 0.5 MW and results were recorded as the level of DG output was varied. (Vaziri, Zarghami and Yazdani 2014), (Afzal, Zarghami and Yazdani 2013)

The effects of increasing penetration of DG in the circuit were studied. The feeder under consideration was evaluated under full load and light load conditions and the results are presented in the following sub-sections.

Full Load with No DG

With no DG connected to the system the power flow was determined to be in one direction, which implies that the voltages will drop as you measure them further away from the substation, due to the increase in distance from the substation and the fact that the load increases with distance.

Figure 4 shows the recreated voltage profile of the circuit under consideration at full load and light load conditions without any DG connected to it. This profile will serve as a base for

comparison studies between different scenarios. Locations for the generators, capacitors, voltage regulators, and SVCs along with other points of interest are marked on the base case. From the simulation results shown in Table 1, the voltages on all the phases are sagging for this loading condition as the distance is getting farther from the distribution substation. Towards the end of the feeder the voltages tend to go lower, and they can drop below the lower limit of ANSI standard. The switched capacitor installed at "point F" is injecting reactive power into the circuit, hence keeping the voltages within acceptable range. Without any DG connection, there were not any voltage problems that were noted at any of the locations along the feeder for this peak loading condition.

Figure 4: Voltage Profile of Feeder at Full and Light Load with No DG

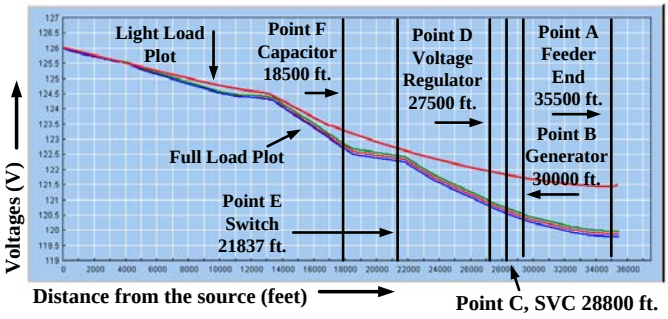

Table 1: Voltages at Different Generator Output under Full Load

DG output (MW)	Voltages (V)					
	Point A	Point B	Point C	Point D	Point E	Point F
1	122.2	122.56	122.68	122.7	123.7	123.7
2	118.7	119.12	119.12	119.12	119.7	119.7
3	120.57	121.07	120.85	120.9	120.77	120.76
4	122.47	122.6	122.47	122.3	121.85	122
5	123.8	124.3	124.13	123.87	122.8	122.7
6	125.3	125.7	125.37	125	123.7	123.2
7	126.6	127.12	126.8	126.3	124.46	123.8
8	127.9	128.5	127.9	127.6	125.1	124.1
9	129.2	129.5	129	128.56	125.7	124.6
10	130.4	130.8	130.3	129.7	126.4	124.9

At about 7 MW of DG output, the voltages at points A, B, and C rise to the extent that they begin to violate the upper limit of the allowable voltage band. The Point of Common Coupling (PCC) between the DG units and the feeder, designated by "B" in Figure 5, is being affected the most. Customers being serviced in proximity of such locations will also experience high voltage at this generation level. Minimum voltage increase was noted on Points E and F since these locations are farthest from the DG. At maximum generation of 10 MW, flow of power is

completely reversed, and the voltages in the vicinity of the generator are well outside the acceptable voltage bandwidth limits.

Figure 5: Voltage Profile at 10 MW of DG output, Full and Light Load

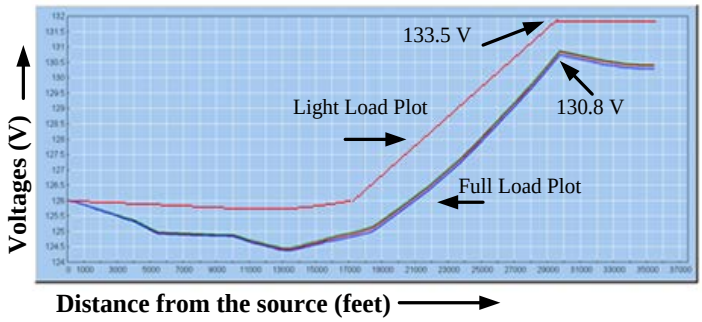

Light Load with No DG

As expected, simulations showed that under the conditions of light load, the voltages drop along the feeder as the distance from the substation increases, similar to the base case scenario. However, the voltage drop in this case was not as much as what was observed during full load condition. Minimum voltages around point A are in the neighborhood of 123 V as compared to 117 V at the same location during full load condition. This is expected behavior because the light load draws less current and, hence, causes less voltage drop along the line.

Light Load with Max Generation

Again a DG was connected to the system and its output was varied from 1MW to 10 MW in the intervals of 0.5 MW similar to the full load scenario. Resulting voltage levels on all the observation points A through F at various DG output levels are shown in

Table 2. Again, it was noted from simulations that the voltages at all the points A through F of the feeder increase as the DG penetration level increases. It is obvious that increasing DG penetration has more adverse effects on the feeder voltage levels during light loading conditions when compared to full loading conditions. Voltages quickly increase beyond the acceptable limit on all the checkpoints. Point B, the location of the generator's interconnection and its surrounding areas are being affected the most. The voltage levels near the PCC are unacceptable even at the DG output of 6 MW.

Table 2: Voltages at Different Generator Output under Full Load

DG output (MW)	Voltages (V)					
	Point A	Point B	Point C	Point D	Point E	Point F
1	121.09	121.1	121.1	121.15	121.05	121.1
2	122.8	122.9	122.85	122.8	122.7	122.1
3	124.4	124.6	124.4	124.2	123.08	122.6
4	125.99	126.12	125.8	125.02	123.99	123.27
5	127.3	127.4	127.1	126.8	124.7	123.7
6	128.6	128.7	128.4	127.8	125.5	124.15
7	129.9	130.01	129.63	129.07	126.19	124.7
8	131.16	131.29	130.7	130.1	126.8	125.2
9	132.3	132.4	131.7	131.1	127.4	125.4
10	133.3	133.5	132.7	132.01	127.9	125.78

Figure 6 is the graphical representation of the voltages at points B and C at different levels of generator output. From the graph it is clear that the voltages are rising above the 126 volts maximum bandwidth limit. (Vaziri, Zarghami and Yazdani 2014), (Afzal, Zarghami and Yazdani 2013)

Figure 6: Voltage Graph under Full and Light Load at Variable DG Output

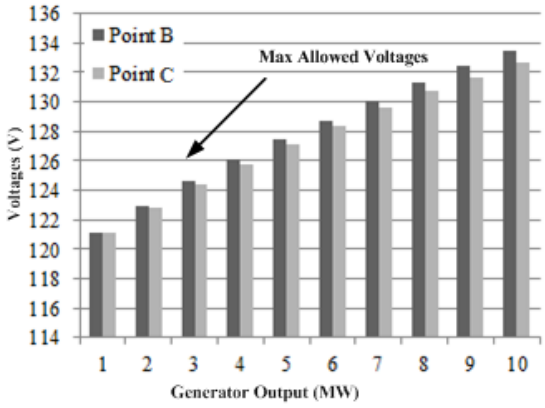

Possible Solutions

Addition of Voltage Regulators

Addition of a voltage regulator at point D could be a solution to low or high voltages with or without the presence of DG. In this section of the report, effects of the voltage regulator will be studied under full load and light load conditions with and without DG. A reproduced voltage profile in Figure 7 shows the comparison of the voltages under full and light load conditions with a voltage regulator in the absence of DG. In these simulations the voltage regulator was used without LDC by setting the R and X values to zero.

Full/ Light Load with No DG

From Figure 7 it is obvious that the voltage regulator is boosting the declining voltages at the point of its installation under full load condition, bringing them closer to the set point. In both cases the regulated voltage level on all three phases are within the acceptable limit.

Figure 7: Voltage Profile with Voltage Regulator at Full and Light Load (no DG)

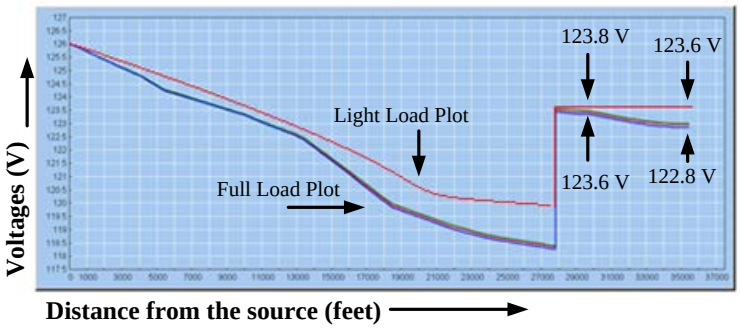

Full Load with DG and Regulator

With the voltage regulator connected to the feeder, and DG connected at point B, the output was increased as before and the voltages at all the points of interest were recorded. The simulations' results are shown in

Table 3. The voltage profile for this case is presented in Figure 8. The resulting voltages for the full load scenario with DG and the voltage regulator can be compared to the case that did not have the regulator.

Figure 8: Voltage Profile with Voltage Regulator at Full and Light Load (with DG)

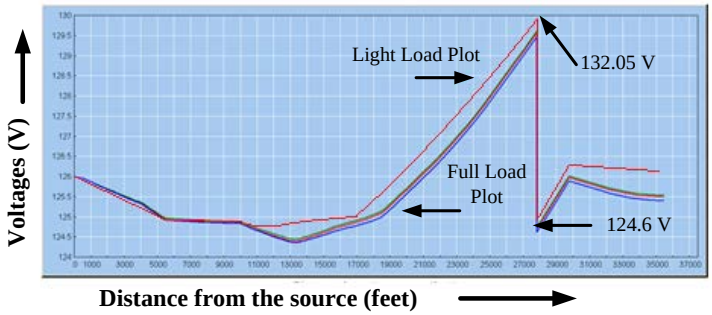

It is clear that voltage regulator is bucking the voltages down to reference voltage level, partly solving the high voltage problems caused by the DG. It can be concluded that with the installation of a voltage regulator, the DG output can reach much higher penetration levels than the case for the same feeder without the voltage regulator.

Table 3: Voltages at Different Generator Output under Full Load (with DG)

DG Output (MW)	Voltages (V)					
	Point A	Point B	Point C	Point D	Point E	Point F
1	122.98	123.4	123.4	123.6	123.8	123.8
2	123.2	123.6	123.5	123.7	119.6	120.2
3	123.4	123.6	123.8	123.7	120.73	121.09
4	123.88	124.3	124.2	124	121.9	122.1
5	123.9	124.32	124.1	123.9	122.8	122.7
6	124.4	125	124.5	124.2	123.6	123.2
7	125	125.5	125.1	124.6	124.3	123.7
8	124.7	125.2	124.7	124.1	125.1	124.2
9	125.2	125.6	125.1	124.4	125.8	124.6
10	125.5	126	125.3	124.6	126.01	124.9

Light Load with DG and Voltage Regulator

The simulation process was repeated for the same circuit under light loading condition as in the previous section and the results are shown in Table 4. Light loading conditions with and without the voltage regulator can be reviewed by comparing the data in the tables presented. From the point-by-point comparison of these tables and figures, it can be concluded that the installation of voltage regulators partially solves the high voltage problem caused by DG by bucking the voltages down to within acceptable limits. For example, in the vicinity of point D the voltages are around 132.02 V without the regulator. However, with the regulator installed at that point, the regulated voltages are in the neighborhood of 124.9 V.

Table 4: Voltage at Different Generator Output with Light Load and Regulator

DG Output (MW)	Voltages (V)					
	Point A	Point B	Point C	Point D	Point E	Point F
1	124.1	124.1	124.1	121.08	121.06	121.1
2	124.4	124.49	124.4	124.3	122.1	121.9
3	124.4	124.6	124.5	124.2	123.13	122.68
4	125.2	125.3	125.1	124.7	124	123.28
5	124.5	124.6	125.6	125.2	124.7	123.7
6	125.6	125.7	125.26	125.5	124.2	124.33
7	126.07	126.2	125.75	125.18	126.23	124.7
8	126.4	127	126.05	125.4	127	125.39
9	125.95	126.09	125.49	124.75	127.7	126
10	126.3	126.6	125.8	124.9	128.1	125.78

Interaction of DG with Voltage Regulators

Simulation results seem to clearly indicate that installation of a voltage regulator near the PCC solves the high voltage problem caused by DG in certain cases and low voltage problems in the absence of DG. However, this solution comes with its own set of problems. One of the most

important problems is voltage flicker, which can be defined as a rapid voltage magnitude variation between two consecutive levels. This sudden change may be caused by switching between the DG output levels or an abrupt complete disconnection of DG at a relatively high output level. If DG is disconnected abruptly, the voltages suddenly drop at the PCC to the values that existed before the DG was connected. The low voltage is exacerbated because the voltage regulator at this instant is usually in the bucking position to lower the high voltages caused by the DG prior to disconnection. Since the process that voltage regulators use to regulate voltage can't change instantly, this bucking process continues causing a steady state low voltage condition until the regulator has fully responded to the change in conditions. This can take up to several minutes depending on the number of steps needed to move from the current buck position to the boost position requited by the setting. The resulting voltage flicker difference between the two voltage levels may be beyond acceptable limits. This flicker can be calculated as follows:

$$V_{Flicker} = V_{Max} - V_{Min} + V_{Reg} \quad 1$$

Where:

$V_{Flicker}$ = Voltage Flicker

V_{Max} = Voltage at PCC with the DG and regulator connected

V_{Min} = The voltage at PCC without regulator and DG connected

V_{Reg}= Voltage buck caused by the regulator

For example, from the previous figures consider point B at 10 MW of generation level for the full load scenario, resulting in the voltage flicker being $V_{Flicker}$ = 126.1 – 120.2 +5 = 10.9.

Table 5 shows the voltage flicker calculated at different levels of generation for full load and light load scenarios. Minimum voltages (V Min) for full load are in the neighborhood of 120.2 V and for light load they are around 122.3 V.

Table 5: Voltage at Different Generator Outputs with Light Load and Regulator

DG Output (MW)	V(Max)		V(Reg)		V(Flicker)	
	Full Load	Light Load	Full Load	Light Load	Full Load	Light Load
5	124.3	124.6	1	1.5	5	3.8
6	125	125.7	1	3.3	5.8	6.2
7	125.5	126.2	1.7	4	7	7.9
8	125.2	126.9	3.2	6	8.2	10.7
9	125.6	126.09	4	6.5	9.4	10.3
10	126.1	126	5	7.3	10.9	11

IEEE Standard 519-1992 specifies acceptable values of voltage flicker versus the frequency of its occurrence. According to this standard as the frequency of flicker increases, the max value of flicker magnitude decreases. For example, during a one-hour period if flicker occurs twice, 5 percent flicker is acceptable. On the other hand, if this occurrence is 20 times within a one-hour period, the maximum allowable flicker level decreases to only 1.8 percent. Similarly, on a per minute basis if voltage fluctuation is 2 occurrences per minute, the flicker can be 0.5 percent of the base value. However, if there are 60 fluctuations per minute, then the flicker must be below 0.12 percent of the base value.

Solution by Installing SVC

SVC units are capable of a high speed response to any voltage changes in the system, and the addition of these units at one or multiple locations on the feeder can help maintain a smooth voltage profile under differing network conditions. These SVC units are also effective for overcoming the voltage flicker problem. Simulation results presented below for various scenarios verified SVC as a viable solution for both steady state and transient voltage problems.

From the simulations for both light load and full load scenarios, it was observed that the SVC helps maintain a smooth voltage on all phases and points of observation in the circuit. SVC is smoothly boosting the voltages in the areas where voltages were declining before, as well as smoothly bucking where the voltages were previously rising.

At Full Load

A composite (light load and full load) voltage profile for the circuit with the SVC and DG at its maximum output level of 10 MW is shown in Figure 9 and Table 6. Comparing the results from Table 1 and Table 6, the researchers concluded that installation of SVC has efficiently solved the high voltage problem caused by high penetration of DG. With no DG when the voltages tend to go low toward the end of feeder, SVC boosts the voltages to bring them within the desired limit by injecting reactive power into the feeder. In the presence of an increasing penetration level of DG, the voltages tend to go high, and as a result the SVC brings the voltages down to acceptable limits by absorbing reactive power from the circuit.

Figure 9: Full Load and Light Load Profile at 10 MW of Generation, with SVC

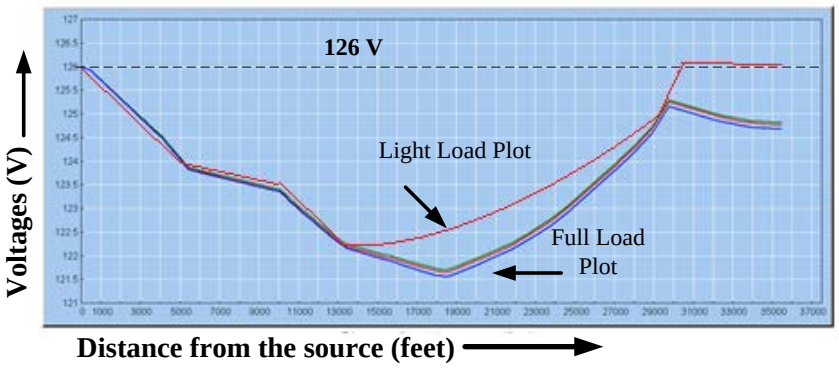

Table 6: Voltages under Full Load Condition at Different Generator Output with SVC

DG Output (MW)	Voltages (V)					
	Point A	Point B	Point C	Point D	Point E	Point F
1	124.2	124.6	124.7	124.6	123.8	123.7
2	124.4	124.5	124.6	124.6	123.6	123.4
3	123.4	123.6	123.8	123.7	120.73	121.09
4	124.3	124.6	124.5	124.3	123.4	123.1
5	124.4	124.8	124.7	124.5	123.3	123.05
6	124.4	124.9	124.7	124.4	123.1	122.7
7	124.5	125.04	124.6	124.4	122.9	122.5
8	124.7	125.2	124.7	124.1	125.1	124.2
9	124.7	125.25	124.7	124.3	122.54	122.02
10	124.8	125.3	124.7	124.3	122.28	121.7

At Light Load

Figure 10 shows the voltage profile of the circuit under light load condition, with SVC connected and DG at 10 MW of output. Table 7 shows the voltage for 1 to 10 MW of DG output. SVC is equally effective in full load and light load conditions. It can be concluded that SVC is a viable solution for the high voltage problem caused by DG. For example, at 10 MW of DG output, without SVC the voltages at all the points are much higher than the voltages recorded with the SVC in place. Use of SVC is also a superior solution when compared to voltage regulators. Without SVC units in place the maximum DG output must be below 6MW to avoid high voltage conditions. With the SVC in place on the other hand, the DG output penetration level can be as high as 10 MW without any high voltage problems. On the other hand, high voltage problems at most of the points of interest were solved using voltage regulators, except for the fact that the feeder still sees high voltage problems on the section right before the voltage regulator, as depicted from Table 7. SVC controls voltages smoothly as compared to voltage regulator, so the overvoltages seen on the line sections between point E and point D do not exist on the feeder when using SVC.

Figure 10: Voltages at Point B with Voltage Regulator and SVC

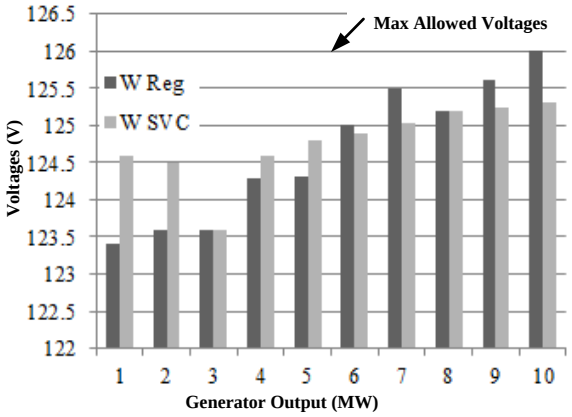

Table 7: Voltages under Full Load Condition at Different Generator Output with SVC

DG Output (MW)	Voltages (V)					
	Point A	Point B	Point C	Point D	Point E	Point F
1	124.9	125.04	125	124.9	124.3	123.9
2	125.07	125.1	125.03	124.9	124.2	123.8
3	125.01	125.07	124.9	124.7	123.9	123.57
4	125.1	125.18	124.9	124.8	123.8	123.37
5	125.2	125.27	124.9	123.6	123.1	122.7
6	125.39	125.45	125.07	124.8	123.5	122.9
7	125.4	125.47	125.02	124.8	123.3	122.64
8	125.46	125.55	125	124.7	123	122.33
9	125.63	125.7	125.09	124.8	122.8	122.07
10	126.08	126.1	126.13	125.5	123	122.14

Other advantages of using SVC units over voltage regulators is that SVC responds almost instantly to any changes in the circuit voltages as compared to a regulator that takes much longer. SVC recovers voltages back to the desired levels within a few cycles as compared to the several minutes taken by the voltage regulator. The fast response time of SVC also reduces the possible problem of voltage flicker. Table 7 shows the comparison of the voltages at point B in the presence of a voltage regulator versus SVC at increasing level of DG penetration.

Interconnection of DG on distribution feeders is causing high voltage problems under both steady state and transient conditions, which are known as voltage flickers. Proper measures need to be taken into consideration to overcome these issues. As the DG output penetration level increases, the voltages on various points in the circuit start to rise. Under light load condition this rise is worse than the full load condition. This rise in voltage could be so high that it can violate the maximum high voltage limit of 126 V. To solve this problem a voltage regulator was connected close to the DG. The LDC functionality of the regulator was disabled, and its reverse operation mode was also turned off. It was concluded from the simulations that, though the voltage regulator can solve the high voltage problem on most of the locations, it does not provide a comprehensive solution. Line sections just before the voltage regulator still face high voltage problems. Even in the presence of voltage regulators the DG penetration cannot go beyond a certain level. In addition, it amplifies the problem of voltage flickers due to its nature of functionality. Additionally, increased penetration of DG may also interfere with the objectives of CVR and its control schemes. The idea behind CVR is to reduce the feeder voltage in order to reduce losses and conserve energy. Feeder voltages are lowered primarily by using voltage regulators. Since increasing DG penetration increases voltages, it tends to nullify the purpose of CVR. Consequently, the CVR control scheme may need to be revised.

SVC was introduced as an alternative solution. From simulations its role was studied under light and full load conditions. It was concluded that SVC controls the voltages throughout the circuit very smoothly. Without the presence of DG it can boost the voltages and in the presence of DG it can lower the voltage levels down to the desirable limits in a smooth and continuous manner. With the SVC connected, the DG output penetration level can be much higher

compared to the output level for the voltage regulator before any voltage problems become noticeable. Another characteristic of SVC that makes it a better solution than voltage regulators is its high-speed response to any change in the system voltage. This implies that it can raise or lower the voltages as needed within a few power system cycles, hence reducing the magnitude of possible voltage flicker. The downside of SVC is its high cost as compared to voltage regulator, so there are some tradeoffs when it comes to selecting any one of these solutions. Voltage regulators offer results which are not so satisfactory but they are cheap. SVC provides a much better solution at higher costs. There are other solutions such as to "re-conductor" the feeder to larger wire sizes or higher voltages, installations of synchronous condensers, or voltage controls at the DG units.

Protection Concerns

Relay Desensitization

Increased penetration levels of DG at certain locations can cause flow reversals with undesirable effects on the system voltage profile. It can also cause protection related concerns, such as relay desensitization, overstressed equipment, automatic reclosures, unintentional islanding, nuisance tripping, neutral shifting, and series resonance. As a result, the protection relays at the substation and other sources may take longer, or in some cases be unable to detect and clear the faults due to decreased levels of fault current contributions from each source. This reduces sensitivity and reliability of relay protection.

The total fault current is the vector summation of the individual fault current contributions from each of the sources. This is primarily the short circuit ratings of the feeder and all rotating loads. With the introduction of DG, the total fault current rises while at the same time the contributions from each source decreases. Depending on the type and size of the cumulative DG, the larger the size of the DG, the larger the contribution it could have to the fault current. As the total fault current increases, the interrupting rating of the protective equipment must be re-evaluated for its adequacy. Protection equipment is installed and set according to the current load profile and short circuit ratings. These settings are altered with the introduction of DG, and require the addition of more protection equipment, with updated protection schemes. Currently, to limit the need for large changes to the distribution feeder, National Standard IEEE 1547 requires all DG to disconnect in the presence of a fault or disturbance on the feeder. As DG increases, the need to keep more generation online during nearby faults becomes more advantageous for system stability and reliability.

For example, in

Figure 11 the power flow from the substation to a main feeder is equipped with other lateral feeders protected by breakers at each of the relays R1 through R3. If a fault occurred at location "F", the protection scheme would be designed to trip R2 before R1, with R1 providing backup protection in case of miss-operation by R2. (Nie, et al. 2016), (Fu, et al. 2015)

Figure 11: Example of DN before DG is Added

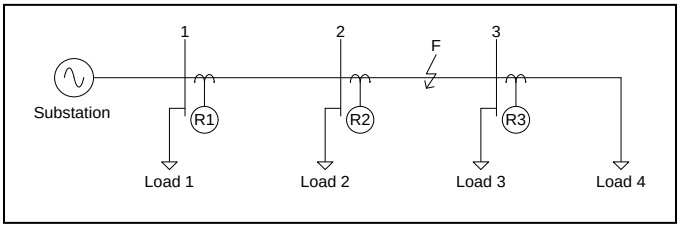

However, if DG capable of exporting power is added as seen in Figure 12, then a fault at location "F1" must also be detected by each of the new DG sources, namely G2 and G3. As the DG penetration levels increase, the contributions from each source will decrease, thus making fault detection less sensitive with longer clearing times from each of the sources. This is highly undesirable. (Nie, et al. 2016), (Fu, et al. 2015)

Figure 12: Example of DN with No Upgrades and DG

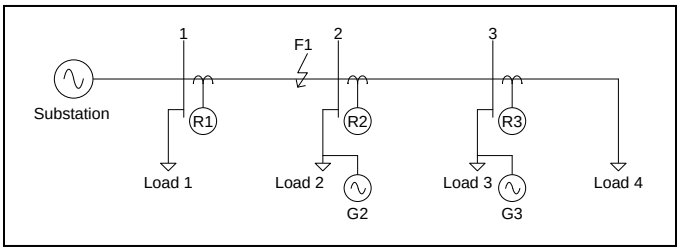

The variability due to changing system conditions present further issues. As G2 and G3 change dynamically due to lack of wind, or clouds on concentrating solar panels. The maximum and minimum fault values also change. As the fault values drift, the protection scheme may not operate properly. Sympathetic tripping of G2 or G3 can also occur when fault "F2" occurs, and the DG's contribution to the total instantaneous fault current exceeds the DG's relay setting before the relay R2 or R3 senses and opens.

The DG is also capable of rendering a relay completely insensitive. If fault F2 occurs the G4 generator adds to the total fault current, while the R3 relay sees lower fault values of fault current due to the reduced contributions from other sources depending on the type of DG and the distances between relay, generator, and load. This desensitization of the relay R3 causes a slower response, or even a lack of tripping, until the unit G4 trips. (Nie, et al. 2016), (Fu, et al. 2015)

The primary goals of distribution protection are to detect and isolate a fault and minimize the number of customers affected by a fault. Protection tools are located to minimize the duration of a fault and possibly locate it. The most common fault experienced on a Distribution System is a line to ground fault, which may be sustained or momentary. A sustained fault indicates conditions requiring repair of the line, such as a conductor that has fallen to the ground due to

an accident. Momentary or transient faults refer to a condition where the line may be re-energized without a need for any repairs. In case of a momentary fault where a fuse is blown on a fused lateral, the customers who are fed by that lateral will lose electricity; therefore, the fault needs to be cleared before fuses are blown. In this case high-speed tripping breakers are utilized to prevent the fuses from being blown by clearing them beforehand. Then, an automatic reclosing scheme can re-energize the system by closing the breaker again to resume services to the customers. If the fault is a sustained or permanent type, then the fuse closest to the fault should blow to limit the number of customers affected and isolate the troubled location of the line for repairs. To have the fuse closest to the permanent fault blow, the fuse and all other interrupting devices connected in series with it up to the feeder breaker must be time coordinated with one another. Usually, the main feeder and feeder tie line are protected by breakers or reclosers, rather than fuses. Proper coordination of protective devices eliminates service interruptions, minimizes the extent of customers affected, and helps determine the location of faults. As one can see in Figure 13 and Figure 14, it should also minimize the expensive equipment that is utilized to achieve the goals of protection with a bidirectional power flow condition. (Nie, et al. 2016), (Fu, et al. 2015)

Figure 13: Example of DN with Possibility of Relay Desensitization

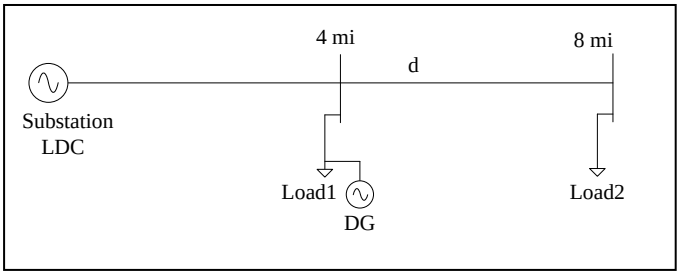

Figure 14: Example of a DN with Switches, Fuses, and Protection Overlap

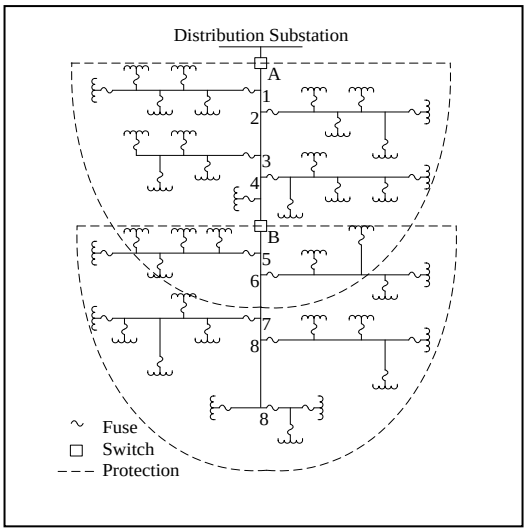

Higher I^2t Stress on Equipment

Considering the required time, labor and material to accomplish distribution line, DG is normally constructed near the load centers. Interconnection of DG can alleviate the loading on transmission and distribution systems and enhance productiveness in power industry. However, the installation of DGs also introduces changes to the structure of power systems. With increased penetration of DGs, the I^2t effects due to varying fault contributions from the substation and existing DG varies sharply. Increased levels of total I^2t validly raise the protection concerns about increased levels of stress on the equipment. Meanwhile, the fault current contributions through the substation and all existing DG sources decrease such that the relays from some of the sources may not detect the fault current. When the I^2t stress levels on any equipment exceeds beyond its capability, ruptures or disintegrating failures can be expected to occur during faulted conditions. Solution for overstressed equipment would be to replace the equipment when detected or upon equipment failure. It is recommended that the I^2t stress levels be evaluated periodically with increased levels of DG penetration levels and equipment replacement be considered when needed. This phenomenon is known as relay desensitization.

Islanding Concerns

Islanding is possible when the DG is independently capable of supporting any portion of the Distribution network. Human safety issues are a concern, as equipment may be energized when the servicemen believe it is de-energized. Improper grounding, voltage, frequency, and adequate protective equipment are the main drawbacks for a sustained island. Also, reconnecting the sustained island to the rest of the system can be problematic if it is done out of phase. This condition can induce fault like currents into the system. Passive islanding detection and disconnection is a requirement when dealing with an active distribution network. That will be accomplished by monitoring voltage, frequency, and other system parameter variations and rate of changes at the DG's PCC. However, if the DG and the islanded network load are balanced, then the island can become located in a Non-Detection Zone (NDZ). Active anti-islanding monitoring is accomplished by the introduction of fluctuations in frequency, phase shifting, reactive power injection, current injection, positive feedback, and other methods. These small fluctuations result in negligible changes when the system is operating under normal conditions, yet it creates significant detectable changes when the DG is part of an island. A combination of active and reactive islanding detections will provide more robust systems of detection and protection for the various islanding conditions. (Nie, et al. 2016), (Fu, et al. 2015)

Concepts for Mitigating DG Impacts to Allow Maximum Penetration

Strategic investments in enabling technologies can greatly increase the distribution networks ability to utilize an increase in DG integration. There are research studies and ideas on how to increase the capacity of the renewable generation on a distribution feeder while maintaining the quality of service. There are simplistic and revolutionary methods as to achieve the mentioned objective. The following subsection presents some of their benefits and/or shortcomings of the proposed methods to increase the DG and maintain the quality of power delivery. (Afzal,

Zarghami and Yazdani 2013), (Zarghami, Kaviani, et al. 2014), (Zarghami, Vaziri, et al., Applications of Battery Storage to Improve Performance of Distribution Systems 2013)

Upgrading Conductors

Upgrading the distribution conductors is considered to be one of the original solutions to improving the feeder power transfer capability. As an example, each DG can be put on its own, properly sized radial feeder, serving the local High Voltage (HV) / Medium Voltage (MV) substation. While this solution works, it is inherently expensive and limits the realization of DG in remote locations where renewable resources, such as wind and solar, are more likely to be found. If the DG is placed on a weak network and is incapable of realizing its full potential during low local consumption, the conductors between the DG and the HV/MV substation necessitate upgrading to increase the capacity of the feeder to accept more DG. This cannot be an optimal solution, as the cost of re-conductoring may surpass the benefits of DG integration and capacity increase. (Afzal, Zarghami and Yazdani 2013), (Zarghami, Kaviani, et al. 2014), (Zarghami, Vaziri, et al., Applications of Battery Storage to Improve Performance of Distribution Systems 2013)

Optimal Placement Planning

Individual DG related problems can be mitigated by proper placement of DG on feeders in a technical manner. However, there is concern that poorly placed or incorrectly sized DG in a DN could limit the placement of additional DG. Optimal Power Flow (OPF) is a widely available tool that most DNOs use in case studies. The OPF software can be utilized to determine the maximum capacity of the DG on DN systems. The program can also determine the optimal placement of DG in the DN. To utilize this readily available tool, DG's are modeled as negative loads. By using this method, the capacity evaluation can be modeled as a load addition problem, with the voltage and thermal limits of the lines taken into account. The system is at its capacity when the cost associated with negative load is minimized. This method can help point out where on the DN a particular DG unit would be most beneficial or, on the other hand, the locations where additional DG would degrade the remaining network capacity. For example, a 1MW increase in a poor location can lower the DN capacity for DG support at another bus by more than 2MW. Furthermore, using the OPF allows the identification of limiting factors, allowing the DN owner to accurately determine where strategic investments would allow additional DG to be added to the network. This is, however, a single point analysis and would have to be repeated each time a DG unit is connected to the system. (Afzal, Zarghami and Yazdani 2013), (Zarghami, Kaviani, et al. 2014), (Zarghami, Vaziri, et al., Applications of Battery Storage to Improve Performance of Distribution Systems 2013)

Voltage Control

Voltage control is one of the most widely studied topics and one of the most mature systems in the DN. The equipment includes tap changing transformers, reactors, capacitors, Static Var Compensators (SVC), Static Synchronous Compensators (STATCOMS), and other devices. Many algorithms and fuzzy logic systems have been proposed and analytically shown that the existing voltage control equipment, with the proper modeling, may be capable of handling the increased dynamics of intermittent or increased DG. However, all of these proposals will have

to be tested and implemented in the field to prove practical viability. With the addition of FACTS devices further control may be possible. As research in this area is so broad and widely studied, only a brief summary of two cost effective DG mitigation techniques is required.

Specific case studies have shown that local voltage rise can be mitigated with the addition of a reactor at the DG's PCC and capacitors at the HV/MV substation. Although this is an inexpensive solution for increasing capacity, this topology greatly increased the active power losses for the DN. The study also determined that when the upstream HV/MV station's voltage was lowered, it facilitated the most efficient network transfer capacity. Though this is one of the most cost-effective methods, it was noted that many DN operators would be unwilling to accommodate such a request.

DG capable of variable reactive injection support, coupled with utilization of Supervisory Control and Data Acquisition (SCADA) communication on the distribution network, would facilitate the coordination between the voltage controlling equipment and, ultimately, a better system voltage profile. With information that is more complete, a single algorithm can manage all available voltage controlling equipment in the DN. This centrally coordinated voltage algorithm allows for more accurate usage of each individual component and keeps individual voltage controlling equipment from "hunting" the regulating equipment. "Hunting" refers to a problem encountered when each regulating component utilizes only local voltage and current readings to control its output independent of other voltage controlling equipment. The local independent controls often initiate unnecessary steps depending on the corrective actions taken by other voltage regulators. With variable reactive support from the DG, the existing voltage controlling equipment requires even fewer actions. The cost to establish a centralized control system and associated communication scheme for this purpose will be significant. (Afzal, Zarghami and Yazdani 2013), (Zarghami, Kaviani, et al. 2014), (Zarghami, Vaziri, et al., Applications of Battery Storage to Improve Performance of Distribution Systems 2013)

Redesigning the Network to a Mesh System

As more DG is introduced, the power becomes bidirectional, much like the mesh networks of the HV power grid. The effects of bidirectional power flow create their own problems. The paralleling of the transmission network and the DN increase the short circuit duties on the system. The increased levels of fault currents alone will require equipment with higher interrupting ratings, which can easily go beyond the limits for distribution equipment and, thus, making this option impractical.

Another meshed option may be balanced looped secondary sub-feeders, connecting consumers and producers. Despite the increased fault values, one of the advantages of such a system is for isolation of the faults. If a fault is on the main feeder, the normally open breakers and closed breakers can be rearranged to keep as much of the system energized as possible. If the fault is inside one of the loops, the fault is localized and other loops are not affected. If the loop is equipped with fault locating relays, the fault can be further isolated, splitting the loop into two radial sub-feeders. The study showed that for a secured feeder with a maximum of 47 percent penetration of DG, the feeder could be increased to 67 percent penetration depending on the number of secondary loops. The authors verified that the looped topology is capable of service

continuity and also argued that the cost savings due to the reduced power losses make it comparable to that of the secured feeder. This point will have to be verified by future research and field implementation. (Afzal, Zarghami and Yazdani 2013), (Zarghami, Kaviani, et al. 2014), (Zarghami, Vaziri, et al., Applications of Battery Storage to Improve Performance of Distribution Systems 2013)

Conservation Voltage Reduction

Conservation Voltage Reduction (CVR) is a practice used for saving energy by decreasing the voltage of the electric distribution network to its lowest allowable level within the ANSI c84.1 range (114V to 120V). The practice is implemented through using tap changers, voltage regulators, and reactive power compensators such as shunt capacitors. In some cases, reducing the voltage by 1% has resulted in a 1% reduction in demand. Increased penetration of PV in a distribution circuit can improve the effectiveness of CVR as it weakens the constant power component of the aggregated load, thus increasing the CVR factor density and reducing the total demand of the system. (Rahimi, et al. 2014)

Islanding Mitigation

Islanding falls into two categories: intentional and unintentional. Unintentional islanding can have disastrous effects as the island may be out of phase during the reconnection, system operators may be unaware that the equipment is energized, and systems of protection and voltage regulation will be inherently compromised. Standard IEEE 1547 has a maximum delay of 2 seconds for a DG to detect and disconnect from an unintentional island. However, passive and active monitoring may not be enough for timely detection and isolation of an unintentional island. Hybrid approaches that utilize passive and active monitoring are able to improve the speed of detection, decrease the threat of NDZ's, and reduce change in the power quality of the DG. Some promising research has been completed in comparing the behavior of islanded and non-islanded Automatic Load Frequency Controllers (ALFC). The actions of the ALFC coupled with learned behavior of self-organizing map neural networks have been shown to detect the difference between islanded and non-islanded operation within 200ms with 97.98 percent accuracy. The detection would signal the relay to disconnect at the PCC far faster than the required 2 seconds. With intentional islanding, regulating and protecting the equipment is the primary concern. The benefits gained in terms of service reliability and deferments of revenue losses from larger area blackouts are promising. However, the infrastructure changes are also significant. Most synchronous generators are capable of islanded operation due to the nature of their excitation systems and the ALFC. However, induction generators absorb reactive power from the system, thus requiring voltage support from equipment such as capacitors. Inverters are currently designed and set as constant current devices, not as voltage control devices. If the inverter based DGs within the detected island are capable of sensing the islanded condition and switch to a voltage control scheme, it is possible to intentionally control the island with load shedding schemes in place to keep high priority loads in service inside the island. This controlled island must also be able to re-synchronize with the grid as part of the scheme, with the inverter-based DGs reverting back to the constant current mode of operation. (Nie, et al. 2016), (Fu, et al. 2015)

Fault Current Limiting Devices

Higher levels of DG penetration increase the short circuit current (I_{SC}) in the DN. There are ways to mitigate this increase through the use of Superconducting Fault Current Limiting Devices (SFCL). The two primary types are resistive and inductive superconductors. In a resistive type, the resistance is nearly negligible, until a large fault creates enough heat to quench the superconductor. Then, the SFCL becomes resistive and limits the fault. An inductive type is like a transformer with a closed superconductor ring for a secondary winding. During normal operation, the resistance of the secondary winding is negligible; however, in the presence of a fault the superconductor is quenched and the impedance of the primary winding rises sharply. With all protection equipment, there is a very short delay (fractions of a cycle) between a fault and when the circuit breaker is initiated to trip. With the SFCL in use, the current is limited (I_{lim}) for a duration equal to or slightly greater than the automatic switching device by design. In tests that were performed with and without SFCL, results showed that without the SFCL the I_{SC} was 1650Amps peak and did not diminish with time. With the SFCL in place the tests were repeated, and the I_{lim} was 960Amps at the beginning of the fault and 310Amps when the fault was cleared. The fault current diminished due to the temperature dependent resistive properties of the SFCL. Such devices can, theoretically, allow more DG to be added into the DN while limiting the negative impacts. Further research and field tests are required for verification of results in practical systems.

Adaptive Protective Relaying

According to the existing rules and criteria, each of the contributing energy sources—such as the substation or any interconnected DG—is responsible for detecting the faults on the DN system and interrupting its own contribution. This removes the benefit of DG offering system support during a nearby fault that may be isolated by other devices. The DN protection system could be designed to adapt to the changing environment, using a host of new equipment and communications. The configuration consists of relays with communication links to downstream and adjacent current protective equipment. Each relay would be equipped with both adaptive primary and secondary functions.

If a fault occurs in a primary zone of protection, DG and load currents upstream from the relay are sensed and communicated to the relay. The relay is capable of identifying the fault using various analytical techniques, and isolates the faulted zone with the proper breakers. If a fault occurs in the backup zone, the DG and load currents downstream from the relay are changed to branch currents, whereby the changes in the fault current associated with the loads and DG can be eliminated. This system has shown to be highly effective and able to improve the protection performance under changing load and generation. Additional research and studies are needed to verify the practicality of this concept. (Nie, et al. 2016), (Fu, et al. 2015)

Static VAr Compensator (SVC)

An SVC is a power electronic device that can provide fast acting, reactive power on electrical networks to control voltages. Typically it is made up of a coupling transformer, thyristor valves, reactors, and capacitors. By using high-speed thyristor switches and thyristor-controlled devices, an SVC provides reactive shunt compensation, which could quickly be controlled for

dynamic voltage control. Capacitors or inductors can be added to or removed from the circuit on a per-cycle basis, making control of system voltage a very fast process.

Overall, SVC units act as a shunt susceptance device that is controllable by predetermined control settings, which inject reactive power into the system based on its terminal voltages. The SVC will inject reactive power into the system if the voltages at the node it is connected to begin to fall below its predefined limits, hence increasing the bus voltage back to its net desired voltage level. On the other hand, the SVC will inject less reactive power if the node voltage it is connected to increases, resulting in the desired output voltage. Because of their large size and high cost, SVCs are predominantly used for voltage control in transmission systems and very large industrial loads at this point in time. Since their compact size allows them to be installed anywhere on the feeder they could be another viable option to solve high/low steady state or transient voltage issues. (Vaziri, Zarghami and Yazdani 2014), (Afzal, Zarghami and Yazdani 2013)

Applications of Battery Storage in Power System Improvement

Energy storage can be an instrumental part of an integrated distributed generation system. Depending on the size and type of the applied energy storage, there will be different types for such devices. These device applications can be considered in load leveling, peak-load shaving, and the dispatch during service interruptions. Energy storage devices can be utilized in short-term and long-term applications.

Short-term energy storage or power storage systems are designed and optimized for the delivery of high amounts of power in short periods of time, such as seconds or less. These devices find their application in improvement of transient stability, such as when the power system is subjected to a disturbance. Due to the intermittent nature of renewables, operation of power storage systems in parallel with most renewable generations can improve overall system behavior and the quality of power delivery.

A Superconducting Magnetic Energy Storage system (SMES) consists of a high conductance coil that stores energy in the magnetic field created by the flow of direct current. SMES are capable of discharging large amounts of power in a small period of time. Due to the fast response of the SMES, it is capable of injecting or absorbing power to compensate for power fluctuations in the distributed system. This becomes useful in hybrid systems where generators cannot respond quickly to the fluctuations in the load. An example of this can be seen in fuel cell systems where generated output is not able to match the transient shocks due to sudden changes of real and reactive loads in the system.

Another type of fast storage system is flywheel technology, which has found a role in the regulation of the system's frequency due to its high efficiency and immediate response time. As frequency increases in the system, the flywheel absorbs energy and acts as a load to lower the frequency. When the frequency decreases, the charged energy can then be discharged into the system, acting as a short-term generation source in order to raise the frequency to nominal levels.

Super Capacitor Energy Storage systems (SESS) are another type of storage capable of quickly releasing significant amounts of power on demand. SESS is rarely used alone in systems since its energy density is low compared to other storage devices. SESS can be combined with other storage systems to provide high power density. For example, although BESS have relatively high energy densities, they cannot be charged and discharged very quickly. To counterbalance the weakness of BESS and SESS, these systems are placed in parallel position to provide both high energy density and high power density.

Energy management storage systems are implemented and optimized for the dispatch of power over longer periods of time. These periods range from 15 minutes to multiple hours. Long-term storage systems find their application in the areas of peak load shaving, energy trading, integration of renewables, and/or islanded operation.

For large-scale systems, Compressed Air Energy Storage (CAES) and Pumped Hydro Storage (PHS) have become means of storage during off peak hours and dispatch during peak hours. (Zarghami, Vaziri, et al., Applications of Battery Storage to Improve Performance of Distribution Systems 2013)

In the case of CAES, energy is stored by compression of air in a storage tank during the hours when demand is low. During peak hours when generation cannot meet the load demand, air is decompressed and fed to turbines, supporting the total generation. Efficiency of these systems is less than 70 percent.

PHS is essentially a hydroelectric generation unit that uses two water reservoirs, one above the other, to store energy. The water from the lower reservoir is pumped into the upper reservoir during the hours of low demand. During peak hours, the upper reservoir discharges its water through the penstock of the damn to the lower reservoir to generate power. The disadvantages of these systems are their large size and topographic and environmental limitations.

The Battery (or chemical) Energy Storage System (BESS) is one of the most popular and frequently used means of storage due to its modularity and diverse applications (Figure 15).

Figure 15: Basic Configuration of BESS in a Power System

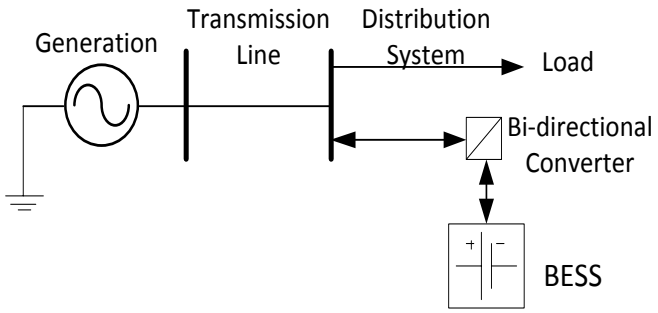

Overview of Batteries

Various battery technologies have been created for their use in large-scale application. These applications include installation of BESS onsite for industrial users or they are tied into the grid as a form of DG. As of today, two main battery types are being investigated in power systems: "conventional" cell and "flow" batteries. Both types share the same concept of integration. The batteries are connected to a power system through a DC to 3-phase AC voltage converter, and then they are stepped through a transformer before being connected to the grid.

Flow batteries have found a place in the implementation of large-scale applications in recent years. These types of batteries will have a major role in distributed generation networks due to the advantages they offer. In flow batteries, energy is stored in the system by separating the electrolytes in reservoir tanks. Flow batteries have a long life span and efficiencies ranging from 75 percent to 85 percent. There are several different types of redox flow batteries: zinc bromine (ZnBr), polysulfide bromide, cerium zinc, and all vanadium.

Vanadium Redox Flow Battery

In general, Vanadium redox flow batteries (VRB) may have a chance of being widely adopted due to their competitive cost, their simplicity, and lack of toxic materials compared to other flow batteries. An important feature of the VRB is the fact that the power (kW) and energy (kWh) ratings of the battery are independent of each other. Due to their modularity, the storage system may be optimized for delivery of energy and/or power.

Zinc Bromine Battery

Zinc bromine flow batteries have a relatively high energy density compared to lead-acid batteries, no shelf life limitations, and a negligible self-discharge. These batteries have an efficiency of 75 percent due to the losses associated with the electrochemical deviation under current flowing conditions and internal resistance. However, in comparison with other flow batteries, ZnBr flow batteries are not as technologically mature and are toxic.

Main Objective for Battery Energy Storage Systems (BESS)

Modularity of BESS enables them to be implemented for different applications and purposes. Moreover, since BESS are implemented as DG systems they can be placed in areas of most interest and profitability. Some of the applications for power system improvement are presented in the following sections.

Power Quality Improvement

For power quality improvement, BESS is designed for a fast, immediate, and high power response that lasts for seconds or less. This application finds its place in the areas of flicker compensation and voltage sag correction. The next sections provide some of these applications, such as harmonic and voltage fluctuation compensation.

Energy Management Applications

In the areas of energy management applications, BESS are optimized for high-energy capacity and discharged in the range of an hour to multiple hours. BESS are usually used for

applications such as load leveling, peak shaving, energy trading, integration of renewables, and/or islanded operation.

Ancillary Services

FERC defines ancillary services as "those services necessary to support the transmission of electric power from seller to purchaser given the obligations of control areas and transmitting utilities within those control areas to maintain reliable operations of the interconnected transmission system." These services include scheduling, system control and dispatching, voltage support, regulation and frequency response, energy imbalance, operating reserve, and black start capability. The use of energy storage systems have gained the interest of independent system operators (ISO) and regional transmission operators (RTO) due to their fast response time ranging from a few seconds to a few minutes.

Transmission Congestion management

According to New England Independent System Operator (ISO), congestion on transmission lines arises when one or more constraints on the transmission system limit the economic or cost effective supply of the load. This may include constraints, such as the ampacity and thermal capacity on a transmission line, which prevents the power from being delivered to the load. The method used to relieve and solve the problem of congestion includes Locational Marginal Pricing (LMP).

Battery storage technology can be implemented on the buses as a method to reduce the overall congestion on the transmission lines by supplying the load to those particular buses. The DG BESS systems must be placed on the buses that are responsible for much of the congestion. The BESS must be sized and optimized to reduce the load demand during peak hours when transmission lines surpass their specific ratings. This practice becomes extremely beneficial to the utilities and industries during peak hours, where the locational marginal pricing increases.

Load-Frequency Control (LFC)

The use of battery energy storage systems has become a subject of great interest to ISOs, utilities, and transmission system operators (TSOs). As stated previously, the fluctuation in power produced by renewable generation sources (or a power system in general) as well as the changes in loads can cause the frequency of the system to deviate from its permissible levels. The implementation of BESS can be used to control the frequency deviations by keeping it within an acceptable range.

Peak Load Shaving

The practice of peak load shaving, sometimes referred to as load levelling, consists of several different schemes to eliminate the peaks and valleys in the load profile. This is done by reducing the demand requested from the transmission system by using local energy storage systems. BESS are effective and feasible methods to perform the task of peak load shaving. During peak hours the price of electricity per kilowatt increases due to the increase in locational marginal pricing. The increase in price during peak hours for power usually accounts for 50 percent of the industrial consumer's electricity bill. Peak load shaving has been used for many years with on-site diesel generators and gas turbines to reduce the load, thus reducing the cost

of power. Peak load shaving has become an attractive and feasible way for large industrial plants and factories to scale back costs of electricity by optimizing energy storage usage.

From Utility's perspective, the practice of peak load shaving encompasses the use of different energy storage systems to eliminate the peaks and valleys in the load profile of a system to the desired values.

The use of BESS for peak load shaving has shown many advantages in the past few years. Utilities employing the use of BESS hybrid systems can mitigate the problem of congestion, lower the cost of locational marginal pricing, shave loads, and decrease the thermal unit commitment. An example of a BESS integrated in a distribution system is shown in Figure 16. (Zarghami, Vaziri, et al., Applications of Battery Storage to Improve Performance of Distribution Systems 2013), (Rahimi, et al. 2013)

Figure 16: Distribution System with BESS at Different Nodes

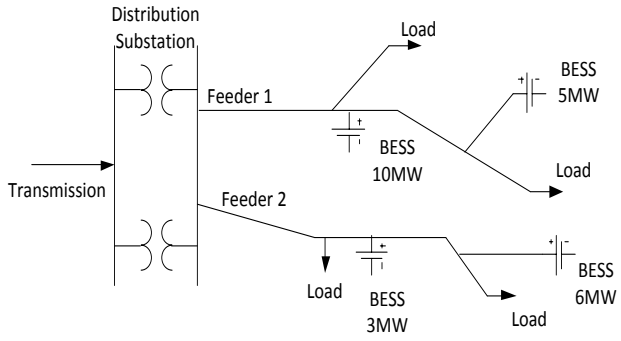

In a hybrid PV/BESS system, peak load shaving is achieved by appropriate sizing of devices and optimal operation of BESS. Optimal operation of the system is done with coordination of charging and discharging periods. The BESS is charged during off peak hours when the price of power is low, which usually falls between 12:00am to 6:00am. During the first peak hour, around noon, the BESS is discharged uniformly across the peak. The discharging of the battery along with the PV generation shaves the load by the difference between the energy production from non-renewable sources and the hybrid system. After the peak hours, when the energy prices drop, the PV units and the grid charge the batteries to supply energy back into the system during the evening peak hours when PV power generation is unavailable. The process is repeated at midnight to provide the next day's peak load. (Zarghami, Vaziri, et al., Applications of Battery Storage to Improve Performance of Distribution Systems 2013)

A Simple and Effective Approach for Peak Load Shaving Using Battery Storage Systems

Peak load shaving has become of great interest to utilities as the demand for power has grown with the increase in population, commerce, and industry. The increase in demand and variations in consumption have created a notable difference in the peaks and valleys of the load profile.

Historically, this has caused challenges regarding the operation of a reliable and stable grid. As the differences in the peaks and valleys of the load profile grow, optimal and effective charging and discharging of storage devices has gained significance in the operation of distribution systems.

The peak load shaving consists of several different schemes to eliminate the peaks and valleys in the load profile of a distribution system. This procedure can be accomplished by utilizing the means of energy storage systems to reduce the system demand during specified time intervals. The use of energy storage systems enables the utility to store power at a low rate per megawatt hour and inject power back into the grid when prices are higher, hence saving on the difference in costs. Many economically feasible schemes have been proposed for peak load shaving using energy storage devices, such as Compressed Air Energy Storage (CAES), Pumped Hydro Storage (PHS), flywheels, and BESS. Although PHS and CAES provide the greatest energy storage density, their economic benefits decline due to the capital cost and site requirements. Furthermore, energy storage systems such as flywheels suffer from the fact that they are still too small and expensive for long, large-scale energy management applications. Over the past few years, BESS has become a popular energy storage system due to its fast-ramping time, cost of operation, and capital investment.

Different methods have been proposed for finding optimal amounts of charging and discharging and their corresponding time intervals in order to eliminate the peaks and valleys from the load profile. These methods rely heavily on optimization techniques, such as non-linear programming, dynamic programming, and swarm particle optimization. Furthermore, some of these methods focus on the methodologies for the sizing of the BESS to provide optimal dimension and power, which will maximize the economic benefit by reducing the electricity bill. Peak load shaving is performed through the means of optimal operating strategies based on dynamic programming for minimizing energy payments and reducing battery deterioration for a given customer load profile. In this scheme, discharge time and maximum battery power are determined by a desired area in order to shave the peak above a given reference point. The battery capacity is then determined by the product of the discharge time and the required battery power to shave the peak load.

Once sizing is completed, optimal operating strategy is determined using dynamic programming. This strategy consists of taking the correct sequence of actions to prevent rapid degradation of the BESS while minimizing the cost of energy, battery replacement, and minimizing the number of cycles per day. The use of dynamic programming eliminates the computation of all possible sequences by selecting relevant subsequences at each step. In some research studies the proposed method uses a BESS in conjunction with photovoltaic (PV) generation units to level the load. During the charging period, the PV is dedicated solely to charge the battery. In conjunction with PV generation, the batteries can operate in three daily duty cycles: (a) Two charge cycles; two discharge cycles, (b) Two charge cycles; one discharge cycle, and (c) One charge cycle; one discharge cycle. At any given point in the optimization process, if the state of charge for the battery reaches 100 percent, all power from the PV arrays

are diverted in order to supply the grid. During the discharge period, the power from the batteries and PV arrays are discharged into the grid for leveling the load.

Another proposed method provides an algorithm for reducing the transmission and distribution losses through the means of peak load shaving. This method works based on shifting a fraction of the load from peak hours to off-peak hours in order to decrease the net resistive losses. Along with the reduction of transmission and distribution losses, the algorithm takes advantage of two other factors: the lower cost of energy and the decrease in total resistance of the system during off-peak hours. The method works by finding an adequate storage size that can be used before the losses increase again. Once the desired storage size is found, the total reduction in losses can be calculated analytically using known values such as the ratio of storage size to peak load, discharging duration, charging time, and the ratio of off-peak to peak hours. This method has benefits due to its simplicity and does not rely on processor intensive optimization algorithms.

Examples and Results

Appendix D elaborates on the methodology that has been used for the peak load shaving with BESS. The algorithm presented in the above mentioned appendix has been tested on a modified version of IEEE 34 bus distribution test feeder shown in

Figure 17. The feeder has a nominal line-to-line voltage of 24.9 kV. In the system, all loads have been treated as balanced with constant power at each time interval. The time interval and utilization period have been considered as τ=*1 hr* and *up=24 hr*, respectively. The utilization factor for all tests is considered as $uf = 93\%$. An optimum value for this factor can be determined based on the shape of the load profile.

Since the load profile of a system fluctuates daily, a one-week period has been selected for the total optimization time. For the simulations, the shape of the load profile has been adopted from past research studies. The aggregated load profile and its average for the mentioned one-week period have been shown in Figure 18. The average load profile is continuously re-evaluated during each time interval.

As shown in Figure 18, the total maximum and minimum loads seen from bus 1 during the mentioned one-week period are 0.8128 MW and 0.4027 MW, respectively. The goal of the peak-shaving algorithm is to make the aggregated load profile get as close as possible to its average during this period. Three similar battery storage systems with characteristics shown in Table 8 have been used in the simulations. Arbitrarily chosen locations of the batteries are shown in Figure 19. Simulations have been performed using MATLAB in order to verify the validity of the proposed algorithm. It is assumed that all batteries are in their minimum states of charge at the beginning of the simulation.

Figure 17: IEEE 34 Bus Test System

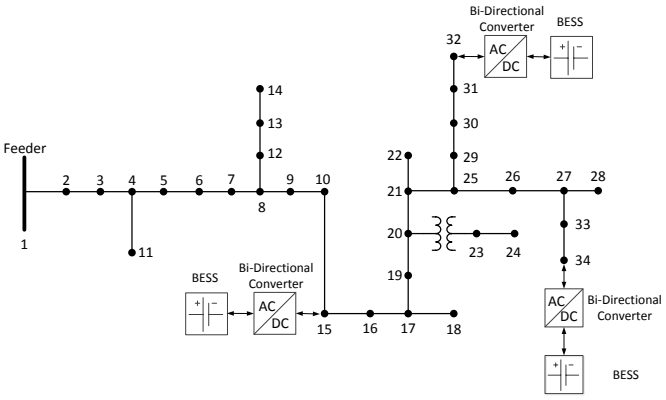

Figure 18: Aggregated Load Profiles in Different Schemes

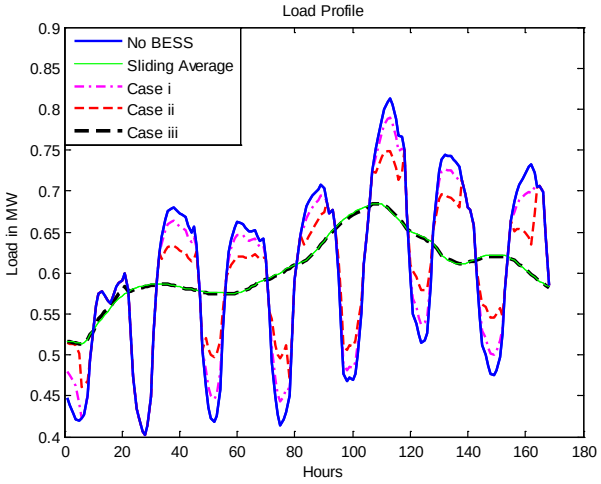

In Figure 18 the results of the aggregated load profiles considering the effects of battery storage systems in cases i, ii and iii are shown. As seen, with more penetration of storage systems, the aggregated load profile gets closer to its average. As the penetration level of the BESS in the system increases to infinity (using ideal sources with no limitation on charge/discharge of the storage facilities), the shape of the aggregated load profile will approach its average value.

Table 8: Characteristics of BESS

	Case i	Case ii	Case iii
Initial State of Charge	30 kWh	100 kWh	0
Minimum State of Charge	30 kWh	100 kWh	0
Maximum State of Charge	100 kWh	300 kWh	∞
Maximum Charge/Discharge Rate	30 kW	100 kW	∞
Efficiency	78%	78%	100%

It can be seen in Figure 19 that at the beginning of the first day, the batteries are charged up to their maximum capacity. One interesting observation is that since the peak shaving algorithm looks into the future estimation of the load profile, the batteries are not discharged in the coming peak hour (around hour 20), since this peak is relatively small with respect to the next day.

Figure 19: State of Charge of Each BESS

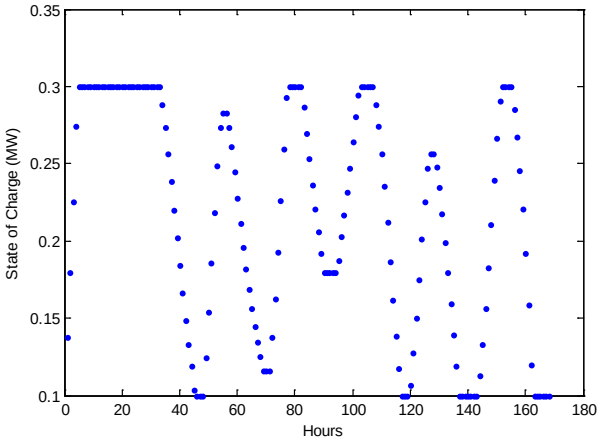

Figure 20 shows maximum system demand in kW during seven days of the week for the three studied cases. As observed, with more BESS penetration, daily maximum demand of the system can decrease considerably.

Figure 20: Maximum Demand In Each Day of the Week

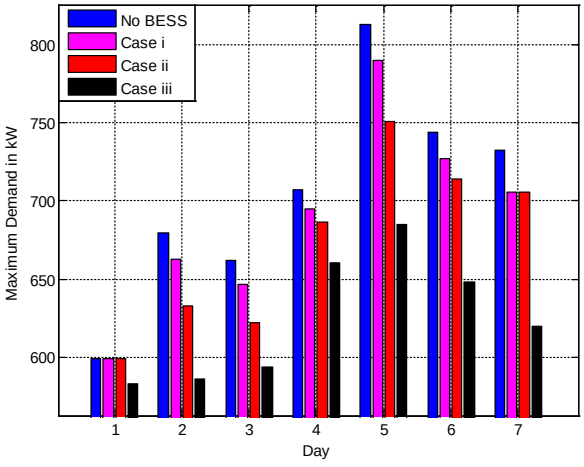

Table 9 illustrates the effects of the peak-shaving algorithm on different system characteristics. The two experimented cases i and ii have been compared with the original case in terms of total losses (MW), total loss reduction (%), average weekly load (MW), average weekly load reduction (%), total weekly demand (MWh), total weekly demand reduction (%), and system average voltage regulation. The latter has been defined as:

$$VR(\%) = \frac{\sum_{i=1}^{nBus}\sum_{j=1}^{nSamples}\left|V_{i,j}(pu) - 1\right|}{nBus.nSamples} \times 100$$

Table 9: Comparison of System With and Without BESS/PV

	No BESS	Case i	Case ii
β (%)	0	25.9	73.82
Total loss (MW)	3.7	3.67	3.64
Total loss reduction (%)	0	0.63	1.52
Average weekly load (MW)	.6012	0.6010	0.6008
Average weekly load reduction (%)	0	0.02	0.059
Total weekly demand (MWh)	101.0	100.97	100.94
Total weekly demand reduction (%)	0	0.03	0.056
Purchased power reduction (%)	0	0.3503	1.0
VR (%)	3.13	3.13	3.13

Case iii has not been included in Table 9 since it does not provide a realistic application. As seen, despite the fact that battery systems are not ideal and are only 78 percent efficient, total losses of the system will be reduced with more penetration of the BESS devices. This is because more loads are powered locally through the batteries. Moreover, the energy that the utility needs to provide to its customers will decrease as the penetration level of storage increases. This will effectively reduce the total costs for the utility since it needs to purchase less power during higher price periods. Using Locational Marginal Pricing (LMP) data of the same region, reduction of the purchased power has been shown as 0.35 percent and 1.0 percent for cases i and ii, respectively. Interestingly, the much higher penetration of BESS devices in case ii has not resulted in a significant difference between the two cases in terms of the purchased electricity.

Another important aspect in the operation of a network is its voltage profile. Comparing case i to case ii it can be seen that the overall voltage regulation of the system does not change significantly. This means that on average the storage systems do not impact the voltage profile, if solely used for active power injection. Figure 21 depicts the weekly voltage profile of Bus 28 in different cases. This bus is at the end of the distribution feeder and is subjected to low voltage problems. It can be seen that in the peak load hours, the voltage profile of the bus is slightly

better compared to the original case (No BESS), since more power is provided to the loads locally and, thus, reduces the demanded power from the slack bus 1 and will result in reducing the voltage drop throughout the feeder.

This shows that storage devices can potentially improve the voltage profile, since their injection to the grid normally takes place in the peak hours. Since batteries are connected to the grid via voltage source power electronic converters, it would be technically possible to compensate the reactive power, hence improving the voltage profile.

Figure 21: Weekly Voltage Profile of Bus 28

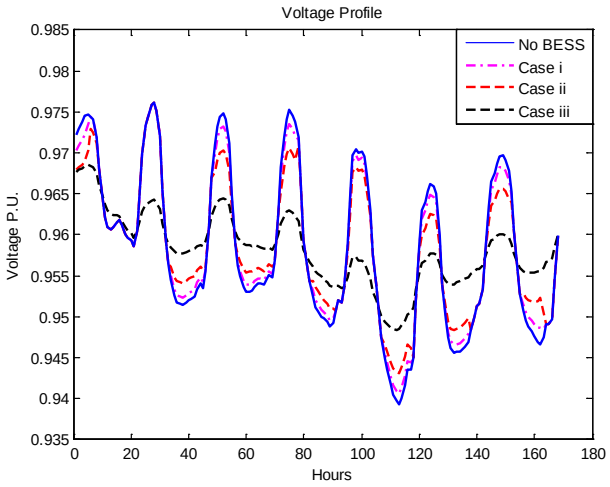

This section of the report presents a simple, fast, and effective algorithm for finding optimal charge/discharge intervals and their associated rates without the need of processor intensive techniques often required by most optimization techniques. The core of the method is based on reshaping the aggregated load profile seen from the main distribution substation such that it gets close to the average load profile during a utilization period. The utilization period is defined as the full cycle of charge and discharge of the batteries. This means that the state of charge of the batteries would remain the same at the beginning and end of the utilization period.

Implementation of this method can be easily done once the forecasted aggregated load profile of the system is known. Then, the controller in the main station will command each BESS in its territory to charge or discharge at the beginning of each time interval. In practical situations, the utilization period and the time interval can be chosen as 24 hours and 1 hour, respectively. Depending on availability of forecasted load in shorter intervals, the time interval can be a shorter value, i.e. 15 minutes. A significant advantage of the proposed method is that it does not depend on the topology of the system or its parameters, such as impedances of the lines. Further, the commands are evaluated through simple and fast mathematical procedures. As such, the commands can be reevaluated at each time interval through a sliding window with a perspective of a longer duration, i.e. the utilization period.

In the coming sections, the proposed algorithm will be explained in detail and the results will be shown by examples on a test system in order to show its effect on loss reduction, demand reduction, and voltage profile.

This work has provided a simple and effective scheme for the peak-load shaving problem from a utility's perspective. Through simulations, it has been shown that the proposed method can effectively reduce the losses and demand of the system. Moreover, it is shown that BESS devices can potentially improve the voltage profile during the peak hours, even if they only inject active power to the grid. More research is needed to investigate the potential benefits of these devices in Volt-VAR control. From the utility's perspective, since more power can be purchased during low price periods and delivered when the price is higher, BESS devices can potentially maximize the profits. However, detailed cost-benefit analysis needs to be carried out in order to verify the mentioned argument. Without a doubt, and regardless of the economic issues, battery storage systems can improve the operation of the distribution network considerably.

Compensating Harmonics

The typical load in a distribution system is nonlinear due to the number of loads connected to the circuit such as personal computers and other devices that have a nonlinear voltage-current characteristic. Injection of harmonics in a distribution system from nonlinear devices causes extra power loss in distribution transformers, feeders, and some conventional loads such as motors. More importantly, harmonics can cause abnormal operations of protection, control equipment, and loss of productivity and profits for an industrial or commercial user.

The Distribution Static Synchronous Compensator (DSTATCOM) in conjunction with DG can be used to compensate harmonic currents in order to improve the overall power quality and prevent further injection of harmonics into the grid. This is done by injecting harmonic components generated by the load back into the grid with a 180-degree phase shift. The resulting current is a pure sinusoidal waveform. This is only possible when DG is continuously injecting power into the grid. This may not be possible with wind or solar generation due to their intermittency. To solve this problem, BESS can be installed at the point of common coupling and supply power when generation is low and incapable of meeting the demand of the load. In the case of peak hours or islanding, the BESS supplies energy through the inverter, with the appropriate current and phase shift, compensating for the lack of generation and/or harmonics. When demand is low, generally from midnight till early in the morning, BESS are recharged either by DG, the upper network, or a combination of both through an optimum share.

Network Balancing with Battery Storage

When the load is balanced, the current through the neutral wire of a typical three-phase four-wire power system can be neglected. This is not the case for unbalanced loads where current flows through the neutral conductor.

BESS systems in conjunction with power converters can provide a four quadrant control of real and reactive power acting either as leading or lagging current sources at the point of common coupling. When loads are unbalanced, power converters are capable of providing independent

current injection/absorption independently at each phase in order to make the total equivalent load balanced. (Zarghami, Vaziri, et al., Applications of Battery Storage to Improve Performance of Distribution Systems 2013)

Optimal Dispatch and Control of BESS

Optimal size and dispatch of BESS can be determined using different optimization techniques. One type of optimization could focus on optimal scheduling of the BESS units to reduce the electricity bill of the system's owner. Additionally, optimizations can be performed for LFC (Load Frequency Control) to find the efficient output of BESS to increase profit made from electrical operations related to an agreement with the grid operator. Many of these methods of optimization use the Loss of Power Supply Probability (LPSP) as a parameter to measure a systems integrity and reliability. Furthermore, these techniques are constrained by the state of charge, minimum state of charge, maximum state of charge, and state of health of the BESS. These optimization techniques include: linear programming (LP), dynamic programming (DP), Model Predictive Control (MPC), and probabilistic and deterministic techniques.

LP is a mathematical process to determine the best outcomes for the linear model. The disadvantage of this technique is its limitation for reactive optimization (modification) to change the predictive strategy to accommodate unpredicted disturbances.

DP is a process of solving complex algorithms by simplifying them into a sequence of shorter algorithms. Unlike LP, this technique can be used for reactive optimization (modification) to correct the predictive strategy due to the unpredicted disturbances.

Probabilistic techniques of optimization become particularly useful when actual hour-by-hour, long-term data is not available. Instead, these techniques use the general data available to the system to predict the future values.

Model Predicative Control (MPC) is an optimization technique used to represent the behaviour of a dynamic system. The major advantage of this technique is due to its ability to operate under tight performance specifications when multiple constraints must be met.

State-Space Modeling of the BESS

A BESS is connected to the grid through an active AC/DC rectifier and a bidirectional DC/DC converter (Figure 22). The two converters are connected through a DC-link capacitor, which has been modelled by C_{dc}in parallel with R_{dc}.

Figure 22: Schematic Diagram of BESS

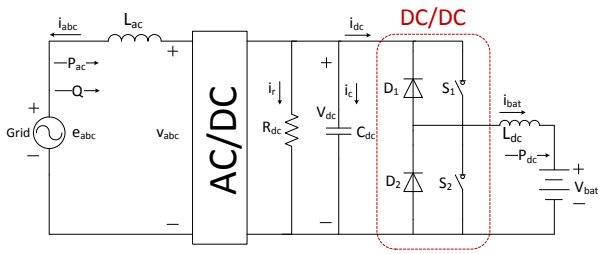

The bidirectional DC/DC converter can either charge or discharge the batteries as explained in the following.

Testing and Simulation Results

Testing and simulation of the results have been conducted in two different categories explained in the following. For simulations, the parameters shown in Table 10 have been considered.

Table 10: Simulation Circuit Parameters

$L_{ac}(mH)$	$C_{dc}(\mu F)$	$R_{dc}(\Omega)$	$L_{dc}(mH)$	$v_{dc}(V)$	$V_{LL-rms}(V)$	$f(Hz)$
0.1098	1000	∞	0.755	800	391.92	60

Comparison with Detailed Circuit Model:

To ensure the accuracy of the provided models, simulation results were conducted and compared with a detailed switching circuit model in SimPowerSystems toolbox of MATLAB/SIMULINK with similar parameters. Figure 23, Figure 24, and Figure 25 compare the results between two methods for commanded changes in active power, reactive power, and DC link voltage, respectively.

In Figure 23, before 2 sec, the BESS is charged at 40 kW. At time 2 sec, a sudden discharge of 40 kW is commanded. The state-space model has successfully captured the average behaviour of the detailed circuit model during this period.

Figure 23: Comparison of Detailed Circuit Model and State-Space Model in Simulation of Active Power

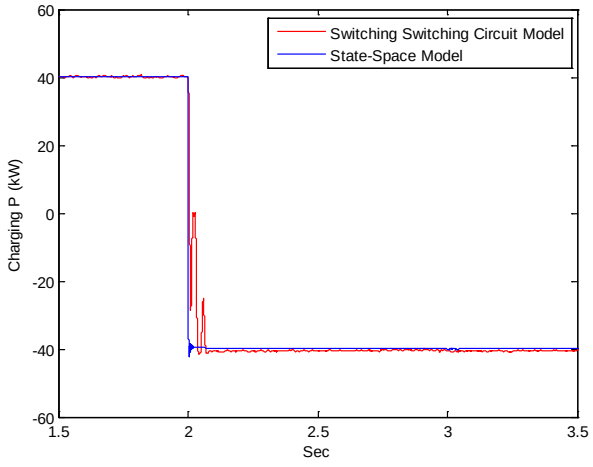

In Figure 24, before 3 sec, the reactive power injected from grid to active rectifier is at 20 kVAr. At time 3 sec, reverse direction of reactive power is commanded. As seen, the state-space model has successfully captured the average behaviour of the detailed circuit model during this period, too.

Figure 24: Comparison of the Detailed Circuit Model and the State-Space Model in Simulation of Reactive Power

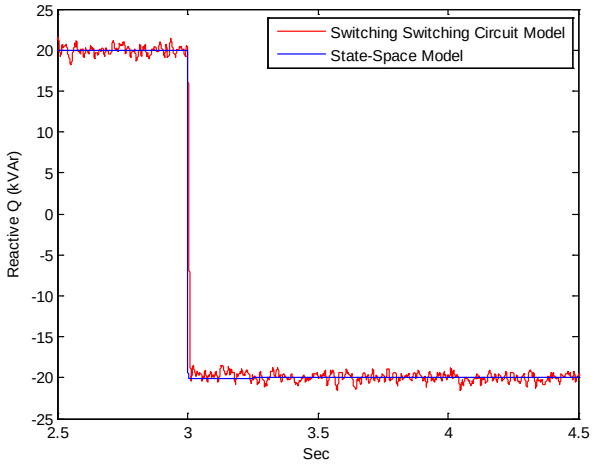

In addition to the accuracy gained through the developed state-space model, it was observed that the simulation time was reduced by more than 10 times with respect to the detailed circuit model, which shows a considerable computational gain.

As the final test, result of a command change of DC link voltage from 800 V to 820 V is demonstrated in Figure 25 It can be seen that the average behaviour of the detailed circuit has been accurately captured by the state-space model.

Figure 25: Comparison of the Detailed Circuit Model and the State-Space Model in Simulation of DC Link Voltage

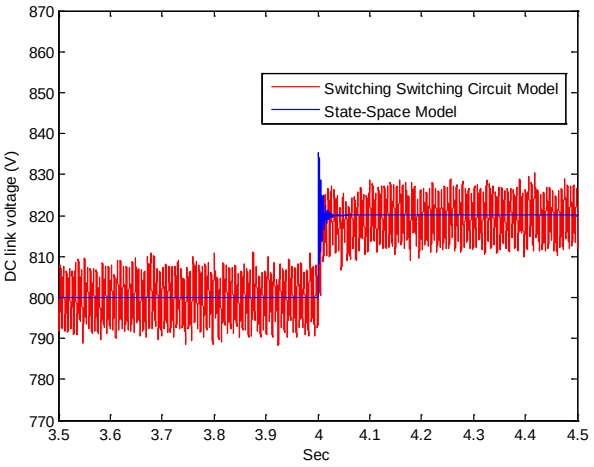

Application in Peak-Load Shaving:

The derived state-space model has been used in a peak-load shaving application based on the method explained in reference researches. Peak-load shaving has been accomplished based on comparing the load value at each hour with the estimated average load within the next 24 hours. The amount of charge/discharge will then be evaluated based on the available capacity of the battery to make the aggregated load profile as close as possible to its estimated average. This process will then continue through a sliding window based on the newly estimated values of the average load at the end of each hour.

In this example, an average household power consumption of 2 kW has been considered. This value is translated to 24 kWh of energy per day. Simulation has been conducted based on assuming the load profile of Table 11 for the first day of the week, with extension to other days based on the same load shape and the multipliers defined in Table 12. In the simulations, a capacity of 4.8 kWh for the BESS (equal to 10 percent of the daily consumption), and an initial state of charge of 50 percent for the battery has been considered. Moreover, it has been assumed that the state of charge of the batteries should remain between a minimum of 20 percent and a maximum of 80 percent at all times.

Based on the above assumptions,

Figure 26 shows the original as well as the shaved load profiles during a week of simulation using SIMULINK.

Table 11: Load Profile for Peak-Load Shaving Simulation on Monday

Time	*Load (kW)*	*Time*	*Load (kW)*	*Time*	*Load (kW)*	*Time*	*Load (kW)*
0-1	1.6	6-7	1.8	12-13	2.2	18-19	1.9
1-2	1.5	7-8	2.0	13-14	2.1	19-20	2.1
2-3	1.5	8-9	2.0	14-15	2.1	20-21	2.2
3-4	1.7	9-10	2.0	15-16	2.2	21-22	2.5
4-5	1.7	10-11	2.2	16-17	2.0	22-23	2.8
5-6	1.8	11-12	2.2	17-18	1.9	23-24	2.4

Table 12: Multipliers of the Load Profile for Seven Days of the Week

Sun.	*Mon.*	*Tues.*	*Wed.*	*Thurs.*	*Fri.*	*Sat.*
1.00	1.05	1.07	1.10	1.15	1.17	1.15

Figure 26: Peak-Load Shaving Using BESS During a Week

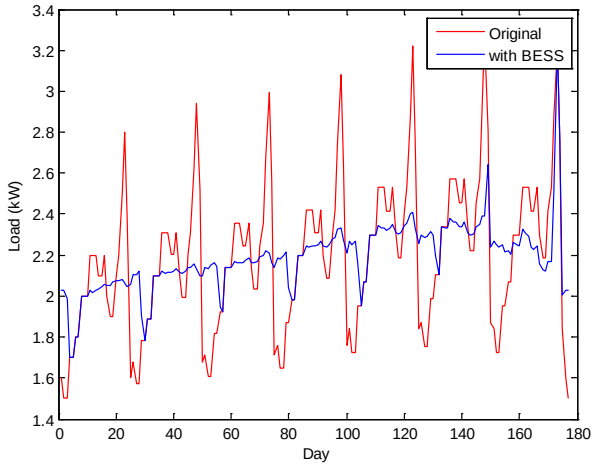

As seen, peaks and valleys of the load profile has been effectively shaved using the developed state-space model and one of the reference's peak-shaving algorithms. It is expected that using the developed state-space models, transitions of the load profile can be modelled more accurately. As a result, the developed models can be used in other important studies, such as transient stability.

Maximum Net Profit

Owners of BESS, whether it is a utility or commercial/industrial user, seek to maximize their net profit from the device. As stated, due to the intermittent behaviour of renewable DG power generation, hybrid systems need to be designed to ensure that the system will meet the demand of the load at all times. Although reliability of the system is of upmost importance, the system should also be economically optimized to guarantee the lowest cost of operation possible.

Utilities aim to increase their overall profit by reducing the amount of power purchased from the upper transmission network. In order to do this they will need to optimize their BESS units for load levelling. In this case, BESS units have to be optimally placed to reduce the congestion on power lines and prevent the utility from paying for the increase in LMP. Also the thermal unit commitment can be reduced; therefore, reducing prices of more expensive means of generation.

An industrial owner, on the other hand, installs BESS units to maximize its net profit and benefits by peak load shaving. It is stated that the specific time range of high power demand can potentially account for 50 percent of a plant's electricity bill. The applied methodology claims that with implementation of BESS units the demand can be reduced to 8 percent, hence reducing the overall bill. Another application in industry includes uninterruptable power supplies for continuous operation of data centres where data integrity is vital.

Due to the deregulation of power markets, investors looking into more profit may provide ancillary services for ISOs and/or RTOs such as frequency compensation. This is due to the recent ruling by the Federal Energy Regulatory Commission (FERC) in the United States, which states that entities providing fast-response support must be compensated for their performance.

Many different methods have been proposed to size and optimize BESS units for maximum profit and effectiveness. These methods include the security-constrained unit commitment proposed to optimize the operation of PV/BESS in a large power system with various types of thermal units, model predictive control, utilize probabilistic, and deterministic techniques, as well as others.

Owner of BESS

Owners of BESS units could be a utility, industry, business, or a community. Since all owners are looking to maximize their profits, the problem of scheduling and dispatch arises. As an example, during peak hours, an industrial user is most likely to discharge its BESS to lower its electricity bill, while the utility, depending on the particular situation, might prefer to sell more power to its industrial customer in order to gain more profits. This conflict of interest might result in unwanted situations that can endanger the security of the whole power system. This situation is similar to a game being played by multiple partners, in this case the utility and the industry. It is obvious that in any game there should be some rules governing the situations and, more importantly, all the players must respect these rules. More research needs to be done in this area to verify different scenarios that can happen in a system when multiple energy storage owners exist. Understanding these scenarios can be useful for legislators and lawmakers when dealing with the next generation of power systems, often indicated as smart grids.

Export of Power into the Grid by the End-User

California's Sacramento Municipal Utility District (SMUD) has set up programs for homeowners to export their excess power back into grid to reduce their bill. However, once their bill hits zero, the homeowner does not receive any incentives for their export of power to grid. Export of PV is permissible for end-users, although nothing is mentioned about selling stored energy such as BESS. In other countries, such as Germany, the export of power is prohibited from end-user installations to prevent the abuse of benefits from the purchase of electricity, due to the incentive attributed to the feed-in tariff associated with PV power.

FERC's Ruling for Ancillary Services

Due to current compensation methods and inefficient economic dispatch of frequency regulation resources, FERC has passed rules concerning frequency regulation compensation in the wholesale power markets. The final ruling "requires RTOs and ISOs to compensate frequency regulation resources based on the actual services provided, including a capacity payment that includes the marginal unit's opportunity costs and a payment for performance that reflects the quality of frequency regulation service provided by a resource when the resource is accurately following the dispatch signal".

Complex Power Optimization of Photovoltaic Systems

Power demand around the world is growing due to factors such as population and industrial growth. In recent years, the use of renewable energy resources has increased because of environmental constraints and economic feasibility. Among these sources, photovoltaic systems are employed to a great extent because of their easy installation and low maintenance. The state of California has mandated 33 percent penetration of renewables by the year 2020, among which PV systems will have a considerable share. There are some concerns associated with PV systems at high penetration levels, especially during high generation periods, e.g. around noon and early afternoon, when load demand is relatively low. Under these conditions, problems including backflow of power and high voltage profiles may occur, which can impact the controls and operation of the distribution system. In many cases it would technically be possible for Independent Power Producers (IPPs) to reduce the capacity of their active power generation and instead participate in Volt-VAr control through the regulation of reactive power, but most of their attention is focused on maximum active power generation as a result of a lack of certain rules and regulations. (Zarghami, Kaviani, et al. 2014)

One of the project's goals is to demonstrate how photovoltaic systems can effectively reduce the total demand of the distribution network if they are allowed to regulate both active and reactive power. This process has been called Complex Power Optimization and implemented through the solution of a nonlinear optimization problem.

The DC/AC inverter is an essential part of power conversion in photovoltaic systems. Control of parallel inverters in distributed AC power systems has been addressed in the literature, where the focus is towards fair load share amongst multiple inverters, accounting for the effect of line impedance and other variations in the unit parameters. A method for controlling parallel inverters interfaced with distributed energy resources in a micro-grid to achieve high performance has been proposed, where the goal is to gain smooth control of the system in grid-connected and isolated modes of operation. A supervisory control and energy management system for inverter-based devices has been introduced with main control tasks over voltage and frequency with minimized communication requirements. In regards to the impact of large-scale integration of photovoltaic energy sources, a study has been carried out to determine how energy storage can limit the fast variation of power injection into the grid, which corresponds to the maximum allowed voltage variation in a certain AC grid.

The study does not look into detailed control of the power electronic infrastructure in PV systems. Its main contribution is to show how power injection from PV inverters can be optimized in steady-state conditions for providing maximum benefit to the utility provider. For this purpose, a supervisory control has been proposed for determining the active and reactive power set points in each inverter of the system. After defining the optimization problem and its constraints, application of the proposed scheme has been implemented on a modified IEEE 34 bus test system. Results of simulations show that by using the proposed approach, it is possible to considerably reduce the total demand of the distribution system, while keeping the voltage and power flow constraints of the system within their allowed range.

Test Results

Appendix A presents a proposed methodology for optimization of the generation amount of DGs. In this part of the report the mentioned methodology is tested on a sample system. In order to demonstrate the results of nonlinear optimization of photovoltaic systems, a modified version of the IEEE 34 bus test system as shown in Figure 27 was selected. This system includes two voltage levels of 24.9 kV and 4.16 kV with a total peak load of 2.1 MW. In the study, variations of load profile and solar irradiance for 5 different hours of a typical sunny summer day in San Francisco have been considered as shown in Table 13.

Figure 27: IEEE 34 Bus Test System with PV installation

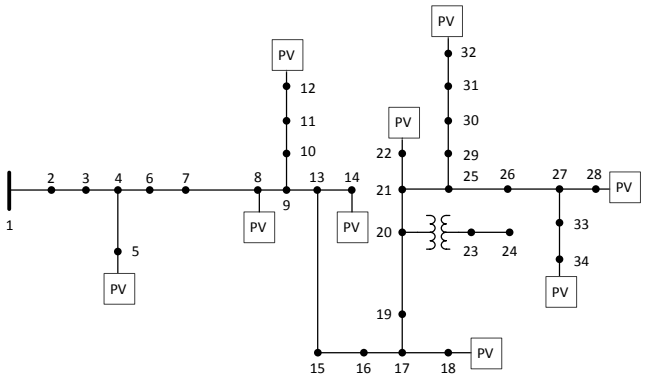

As seen from Table 13 the selected hours can demonstrate conditions such as low load-low irradiance (6 am), high load-high irradiance (9 am, 12 pm, 2 pm), and high load-medium irradiance (5 pm).

Table 13: Demand Reduction (%) by PVs in Different Operating Conditions

Operational Conditions / System and Optimization Conditions		Hour of the day				
		6am	9am	12pm	2pm	5pm
		Load (%)				
		64	89	89	92	100
		Irradiance (%)				
		6.25	80	100	87.5	50
Penetration Capacity 10%	Max. P generation	0.57	5.40	6.67	5.19	2.45
	Optimized PQ	0.58	6.70	8.35	6.78	3.41
Penetration Capacity 20%	Max. P generation	1.14	10.27	12.50	9.75	4.70
	Optimized PQ	1.42	13.29	16.58	13.56	6.75
Penetration Capacity 30%	Max. P generation	1.70	14.59	17.48	13.71	6.77
	Optimized PQ	2.15	19.85	24.71	20.23	10.20

The system was first simulated in the five mentioned hours with no solar generation. Then, nine similar PV installations were considered with total penetration level capacities of 10 percent, 20 percent, and 30 percent of the peak load, respectively. In each penetration level and each hour, simulations were conducted with *pure active power generation* and *optimized power generation* and the reduction in total demand was recorded and compared against the case with no PV in the same hour as shown. Reduction is always more effective in cases with optimized power generation. Specifically, the difference is more significant with higher penetration levels. To verify the results of optimization for each PV, generated reactive and active powers at each node and for each hour have been shown in Table 14. Negative Q numbers demonstrate that reactive powers have been absorbed by the PV systems.

To demonstrate the effect of reactive power absorption of PV inverters on node voltages, voltage profiles of the system for high load-high irradiance periods are shown in Figure 28-33. It can be seen that when maximum active power is acquired from PV systems, they can potentially take the voltage profile out of its allowed limits. Looking further into the voltage profile of bus 24 (which is a heavy-loaded node located near the end of the feeder) reveals that its voltage exceeds the upper limit even under medium penetration levels.

However, it was observed that optimized power generation by PV systems can effectively keep the voltage profile within the constraints, which is one of the constraints of the optimization problem.

Table 14: Active and Reactive Power Generation by PV with 30% Penetration Capacity

Node		Hour 6 am	9 am	12 pm	2 pm	5 pm
5	P(kW)	+4.1	+50.7	+63.6	+54.5	+31.4
	Q(kVAr)	-1.6	-24.6	-30.3	-28.7	-15.8
8	P(kW)	+3.7	+47.7	+59.0	+50.7	+28.4
	Q(kVAr)	-2.3	-29.9	-38.5	-35.0	-20.9
12	P(kW)	+3.7	+47.6	+59.3	+50.6	+27.8
	Q(kVAr)	-2.4	-30.0	-38.0	-35.1	-21.7
14	P(kW)	+3.7	+46.7	+57.6	+49.5	+27.4
	Q(kVAr)	-2.4	-31.5	-40.4	-36.6	-22.2
18	P(kW)	+3.7	+45.5	+56.3	+47.8	+25.8
	Q(kVAr)	-2.4	-33.3	-42.2	-38.9	-24.0
22	P(kW)	+3.9	+42.6	+52.0	+43.7	+22.8
	Q(kVAr)	-2.0	-36.9	-47.5	-43.4	-26.8
28	P(kW)	+3.5	+43.9	+52.7	+43.7	+23.3
	Q(kVAr)	-2.7	-35.3	-46.7	-43.4	-26.4
32	P(kW)	+3.7	+43.0	+51.8	+44.0	+23.1
	Q(kVAr)	-2.4	-37.6	-47.7	-43.1	-26.6
34	P(kW)	+3.9	+42.4	+51.9	+44.1	+22.9
	Q(kVAr)	-1.9	-37.0	-47.6	-48.0	-26.8

Figure 28: Voltage Profile of the System at 9 am with 30% Penetration Capacity

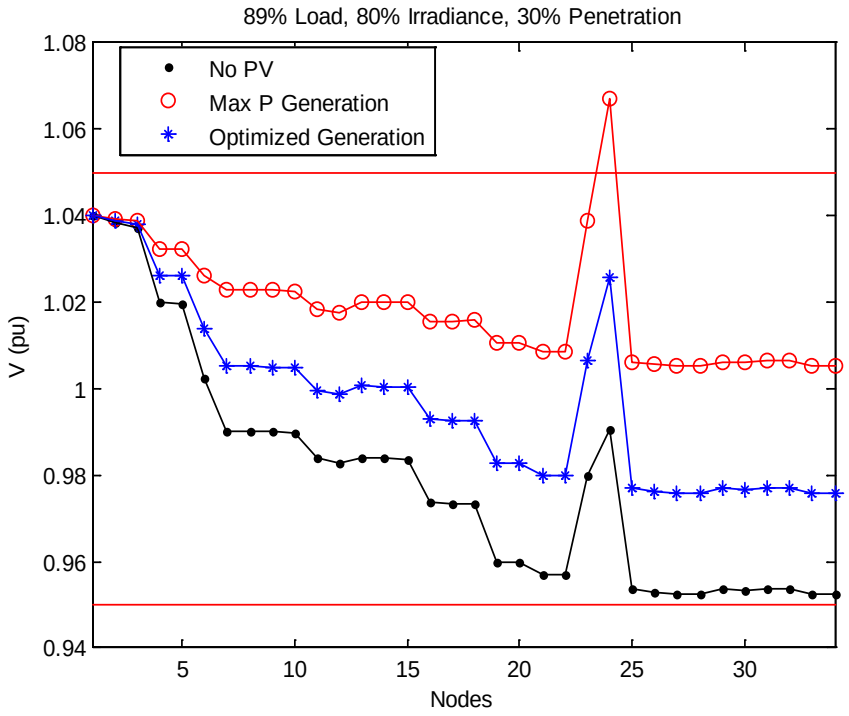

Figure 29: Voltage Profile of the System at 12 pm with 30% Penetration Capacity

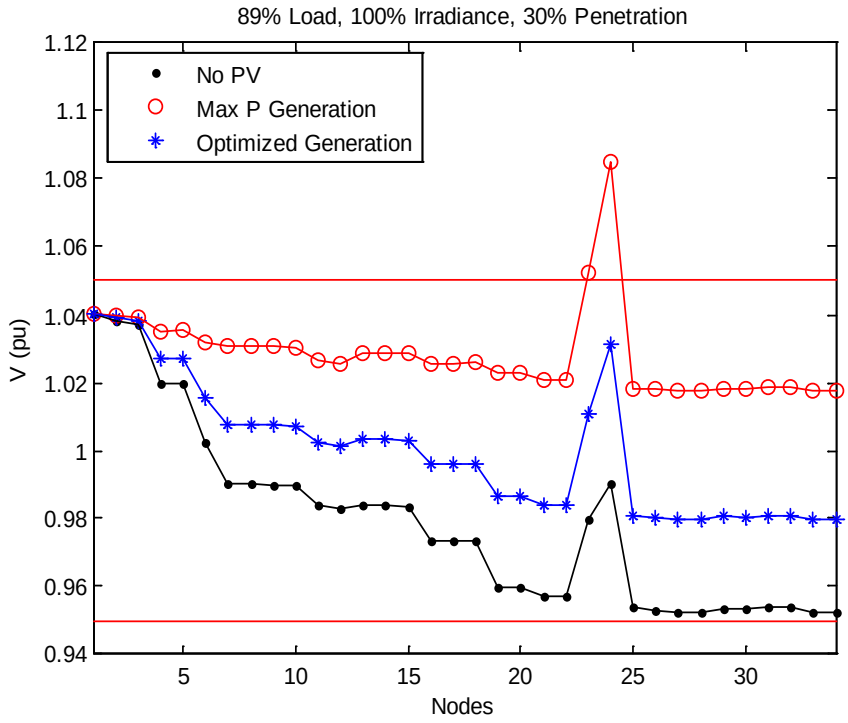

Figure 30: Voltage Profile of the System at 2 pm with 30% Penetration Capacity

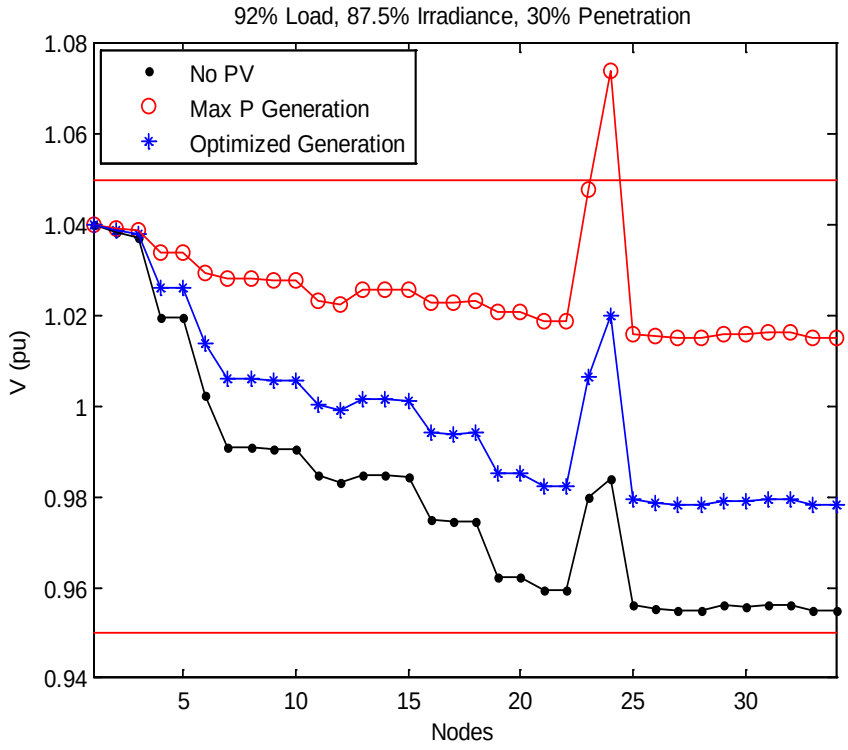

Figure 31: Hourly Voltage Profile of Bus 24 During Different Hours with 10% Penetration Capacity

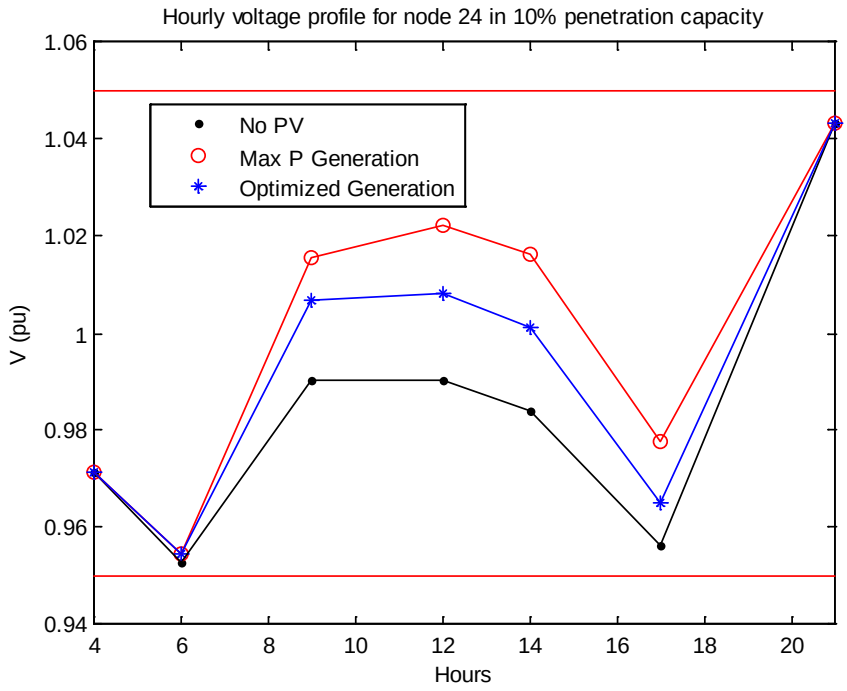

Figure 32: Hourly Voltage Profile of Bus 24 During Different Hours with 20% Penetration Capacity

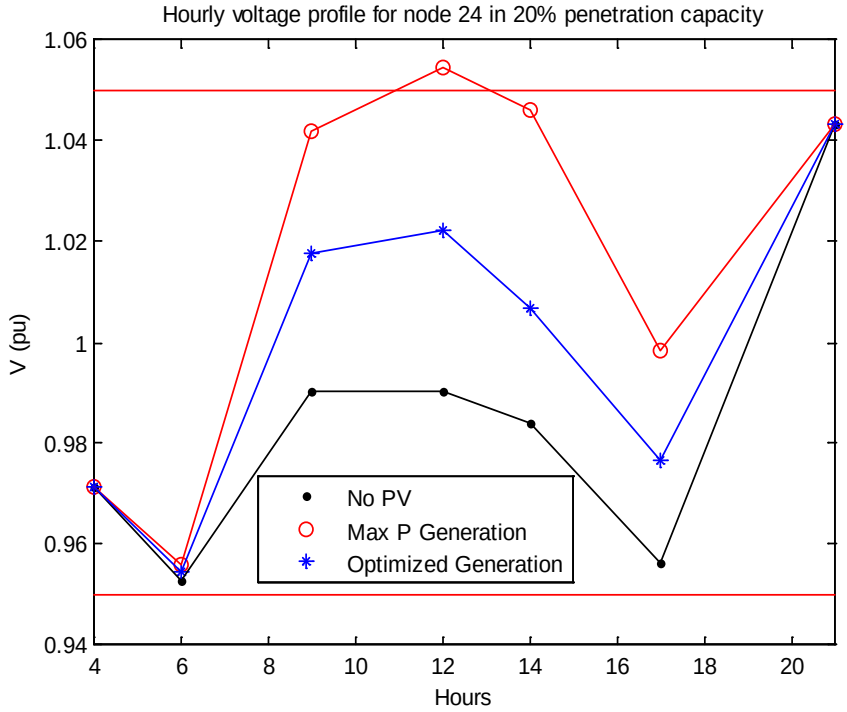

Figure 33: Hourly Voltage Profile of Bus 24 During Different Hours with 30% Penetration Capacity

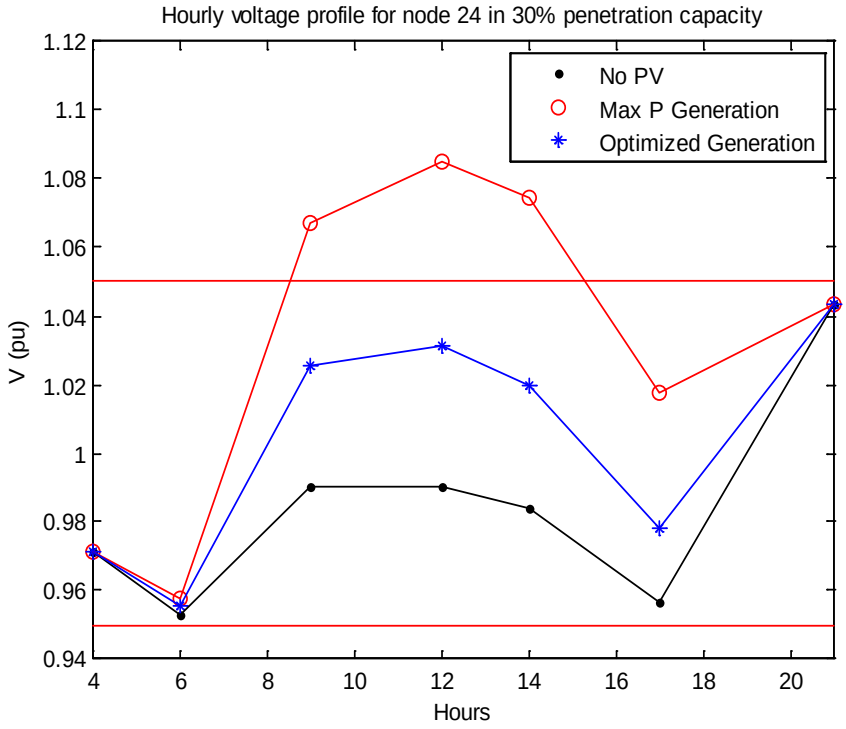

The current work shows only a preliminary study demonstrating the potential of PV devices participating in system optimization. In practice, optimization needs to be coordinated with other active and reactive power apparatus, such as energy storage and capacitor banks. In the optimization practice, certain barriers still exist. Some of these are:

- Lack of certain rules and regulations for reactive power control of inverters.
- Lack of certain metrics for measuring how independent power producers can be compensated through participation in system optimization.
- Coordination of the optimization algorithms with other operational modules such as load and solar forecasting.
- Integration of existing controls into the optimization algorithm.
- Lack of fast optimization algorithms in large-scale systems.

State Estimation Methodologies

Kalman-Filter Algorithm and PMUs for State Estimation of Distribution Networks

Introduction of a new type of generation in the distribution system requires advanced control and monitoring of the electric network, due to the issues mentioned before. State estimation of the power grid plays a significant role in the energy control center. The algorithm provides

complete and reliable near real-time information for analysis, control, and optimization of the system. Since power system state estimation was introduced in 1970, it has remained an extremely active and contentious area of research. Currently, state estimation plays an important role in modern Energy Management Systems (EMS) providing data for other functions of the EMS system, such as security monitoring, optimal power flow, security analysis, on-line power flow studies, supervisory control, automatic voltage control, and economic dispatch control.

Recently, the increased use of Phasor Measurement Units (PMUs) conforming to IEEE C37.118™-2005 for monitoring the grid has influenced operational uses for the acquired data from sources such as SE. The evolution of distribution grids from passive to active networks will lead to the additional use of PMU data in operational practices for these grids. SE is one of the more challenging tasks of operation and using PMU data may allow simplifications and improvements in the SE of these networks.

Various methods for SE have been introduced in the past. Among those methods, Weighted Least Square (WLS) and Kalman Filter (KF) are the most popular and applicable in many fields. One of the newest KF methods is the Iterated Kalman Filtering (IKF), which is characterized by an iterative application of the KF for the case of non-linear processes.

IKF, as a new method, has been implemented for SE of a test distribution system. In order to validate the simulation results, WLS method, as a common algorithm, has been simulated for the test grid. In this case study, the IEEE 13 bus network has been used as a test system. Furthermore, one Distributed Generation (DG) unit has been added to bus no. 9. Finally, the performance of the IKF algorithm has been evaluated based on the WLS method.

Test System Simulation

Figure 34 shows the IEEE 13–bus distribution test feeder that has been used to obtain the simulation results in this section. Bus 1 has been assumed to be the slack of the system as it represents the connection to the sub–transmission network. The test feeder has been considered symmetric with balanced loads. Therefore, the positive sequence was only referenced. Furthermore, the researchers considered only one DG on bus No. 9 with 358 kW of active power injection into the network.

Figure 34: IEEE 13 Bus Test System

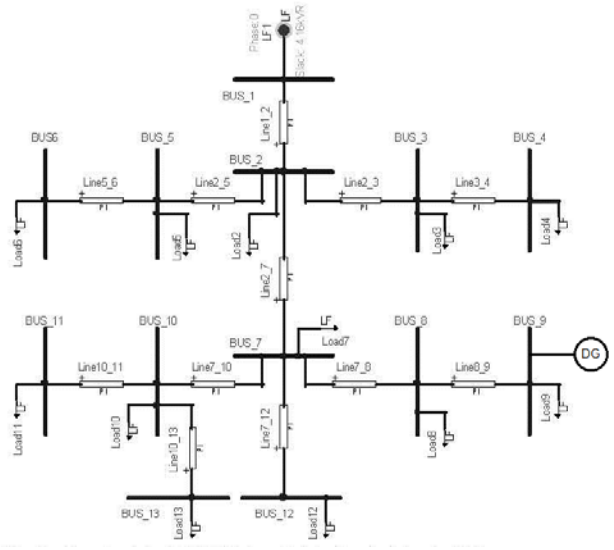

The configuration of the measurement points (measured phasors and active–reactive power injections) is reported in Table 15. The daily total active and reactive load profiles are shown inFigure 35. They are separated by 15 minutes time intervals. (Shabaninia, Vaziri and Vadhva, et al. 2012), (Shabaninia, Vaziri and Amini, et al. 2014)

Table 15: Type of Measurements in the Simulated Network

Bus Number	PMU measurements	PQ measurements
1	✓	✓
2		✓
3	✓	✓
4		✓
5	✓	✓
6		✓
7	✓	✓
8	✓	✓
9		✓
10	✓	✓
11		✓
12		✓
13		✓

Figure 35: Daily Total Active Load Profile (24 hours)

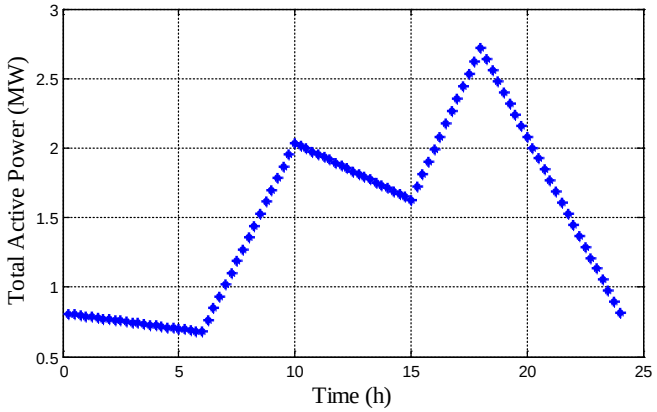

Validation of IKF State Estimation Method

In this section, validation of the IKF SE method has been done with reference to WLS SE algorithm.

IKF and WLS SE methods have been implemented to estimate the voltage magnitudes and angles at all buses. Using PMU data is the main difference between the traditional WLS methods and what has been proposed in this study.

To generate the required data, load flow has been performed for 96 sample loads (every 15 minutes in a day) and noise levels with normal probability distribution were added.

Two algorithms were compared for different measurements (R) and process covariance (Q) matrices in this network. As these two quantities have a large effect on the performances of the KF process, the above analysis has been performed for different R and Q matrices. In principle, R shows the confidence of measurements, whereas Q weights the certainty of estimated values.

Considering Table 16 and Table 17 for measurements and the process covariance matrices (R and Q respectively), the results of IKF and WLS estimation for node 9 of the test system are shown in Figure 36-43. (Shabaninia, Vaziri and Vadhva, et al. 2012), (Shabaninia, Vaziri and Amini, et al. 2014)

Table 16: Selected Values for R and Q Case 1

R	PMU RMS variance [p.u.]	$5.778 \cdot 10^{-5}$
	PMU phase variance [rad]	$6.561 \cdot 10^{-5}$
	Active power variance [p.u.]	$4.000 \cdot 10^{-5}$
	Reactive power variance [p.u.]	$4.000 \cdot 10^{-5}$
Q		10^{-7}

Table 17: Selected Values for R and Q Case 2

R	PMU RMS variance [p.u.]	$5.778 \cdot 10^{-6}$
	PMU phase variance [rad]	$6.561 \cdot 10^{-6}$
	Active power variance [p.u.]	$4.000 \cdot 10^{-6}$
	Reactive power variance [p.u.]	$4.000 \cdot 10^{-6}$
Q		10^{-7}

Figure 36: True and Estimated Values of Voltage Magnitude Related to Node 9 of the Test System for 24 Hours (Case1)

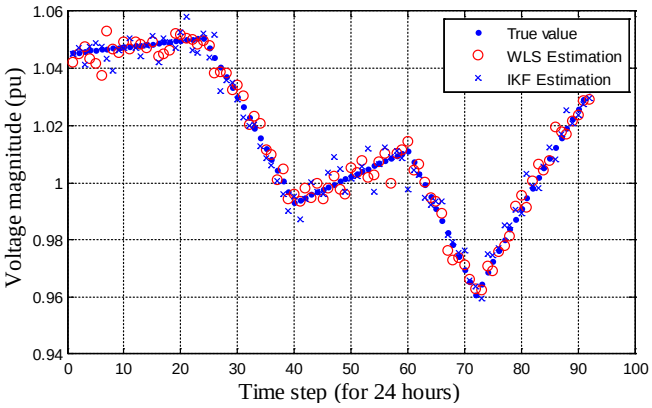

Figure 37: True and Estimated Values of Voltage Angle Related to Node 9 of the Test System for 24 Hours (Case1)

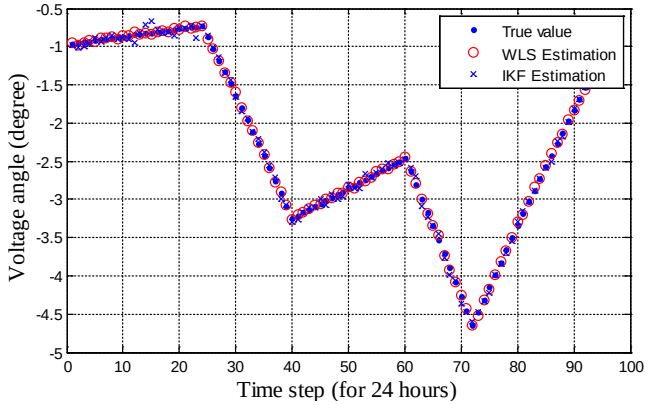

Figure 38: Voltage Magnitude Relative Error Related to Node 9 of the Test System for 24 Hours (Case1)

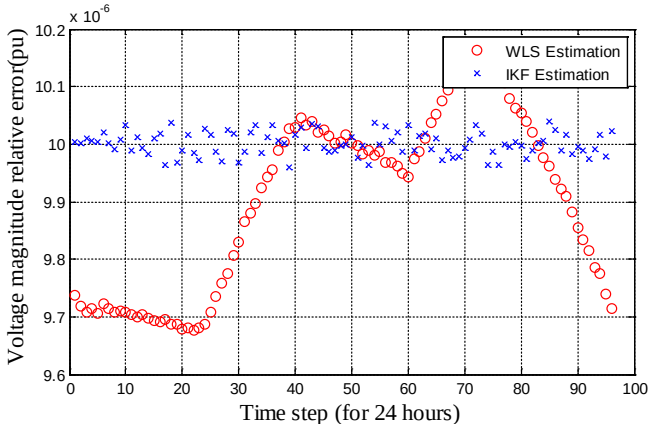

Figure 39: Voltage Angle Relative Error Related to Node 9 of the Test System for 24 Hours (Case1)

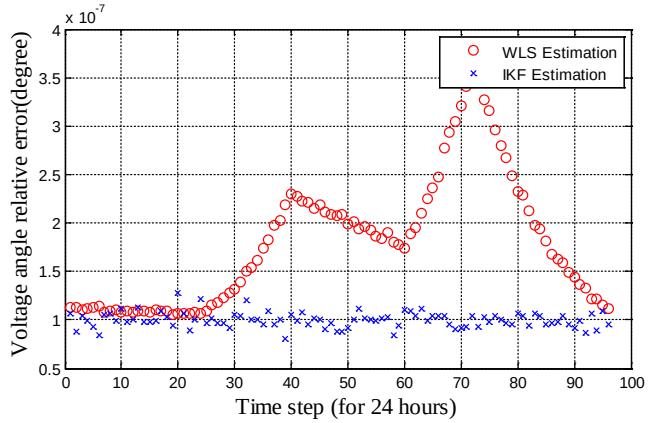

Figure 40: True and Estimated Values of Voltage Magnitude Related to Node 9 of the Test System for 24 Hours (Case2)

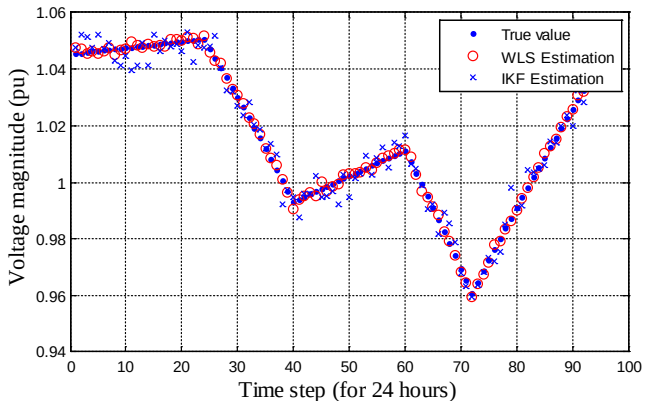

Figure 41: True and Estimated Values of Voltage Angle Related to Node 9 of the Test System for 24 Hours (Case2)

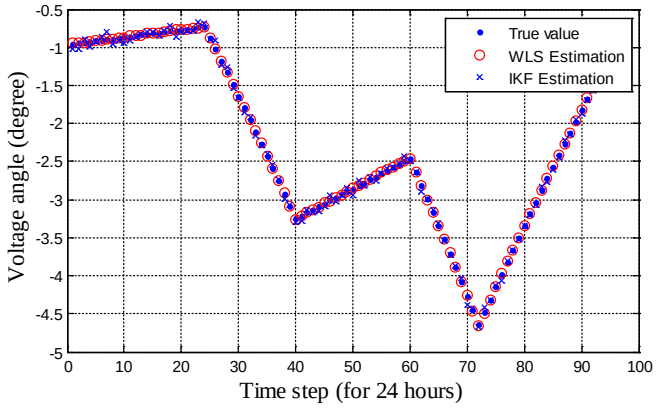

Figure 42: Voltage Magnitude Relative Error Related to Node 9 of the Test System for 24 hours (Case2)

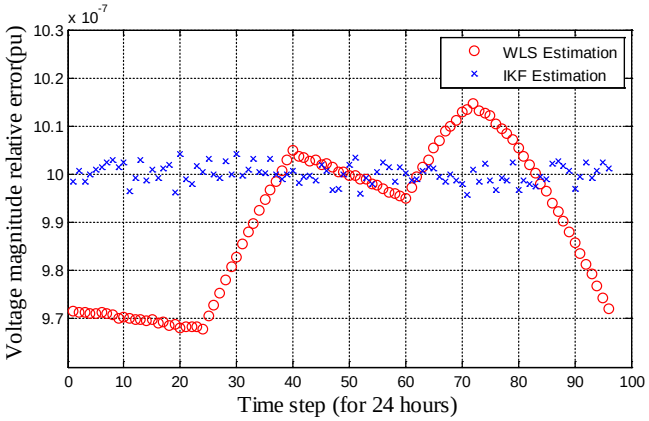

Figure 43: Voltage Angle Relative Error Related to Node 9 of the Test System for 24 hours (Case2)

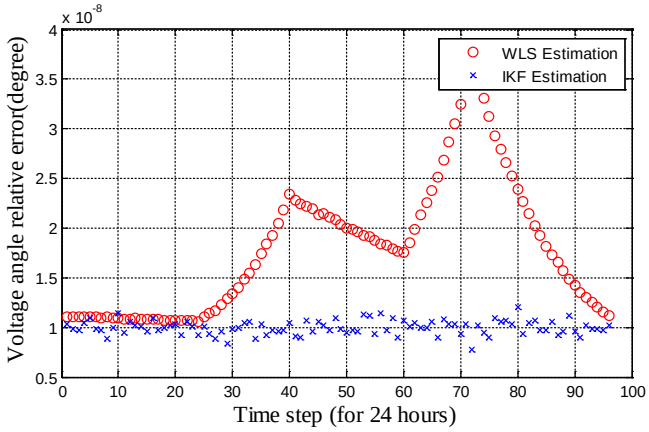

Simulation results considering Table 17 for measurements and the process covariance matrix (R and Q respectively) are shown in the previous figures. As illustrated, it is clear that WLS and IKF have a better performance in this case.

Iterated Kalman Filter (IKF) equations have been derived for power system State Estimation (SE). To validate the proposed algorithm, the Weighted Least Square (WLS) SE equations with proven results have been used as metrics. Based on the simulation results, the proposed method has a proper performance. The accuracy of the method in comparison with WLS depends on the process and measurements covariance matrix (Q and R respectively). Comparison of the values with the output from the CYME® Software show satisfactory results to be presented in future research. (Shabaninia, Vaziri and Vadhva, et al. 2012), (Shabaninia, Vaziri and Amini, et al. 2014)

Case Studies for Verification of Protection Concerns

Test System Simulation and Results

The IEEE 34-node test feeder was modified to obtain a 24-Bus system shown in

Figure 45. The step-up transformers T1 and T3 boost the voltage from 2.4 KV to 24.9 KV, while the step-down transformer T2 reduces the voltage from 24.9 KV to 4.16 KV. There are two DGs connected to the 24-bus system in the model. DG1 and DG2 are located on BUS812 and BUS826 respectively. The IEEE 34-Bus Test System is also known as IEEE 34 Node Test Feeder, which is supplied by the IEEE Distribution System Analysis Subcommittee. All line sections are assumed to be constructed with typical 4/O Aluminum conductors and have 5-feet spacing between center and outer conductors. (Nie, et al. 2016), (Fu, et al. 2015)

Table 18: Line Segment Data in IEEE 34-Node Test Feeder

Line Segment Data					
Node A	Node B	Length(ft.)	Node A	Node B	Length(ft.)
800	802	2580	824	828	840
802	806	1730	828	830	20440
806	808	32230	830	854	520
808	810	5804	832	858	4900
808	812	37500	834	860	2020
812	814	29730	852	832	10
816	818	1710	854	856	23330
816	824	10210	854	852	36830
818	820	48150	858	864	1620
820	822	13740	858	834	5830
824	826	3030	888	890	10560

Table 19: Impedance Data in IEEE 34-Node Test Feeder

Impedance / System	$R_1 = R_2$	$X_1 = X_2$	R_0	X_0
Substation (ohms)	0.00025	1.24002	0.00000	0.00620
Lines (ohms/mile)	0.44200	0.72010	0.72800	2.293850

Figure 44: Relay Desensitization Simulation Model for 25 Nodes Feeder

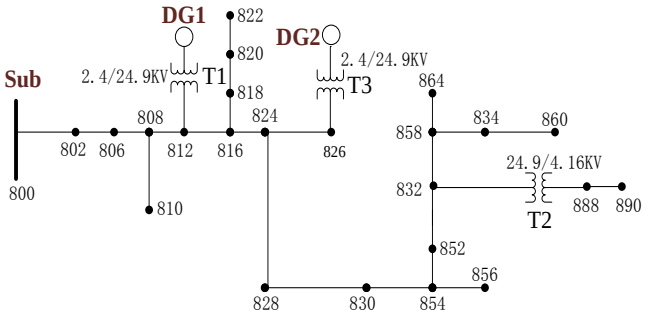

Case Studies and Simulations' Results

Three different case studies have been conducted here. Different fault and DG locations were considered for case studies 1 and 2. A special case was also considered to demonstrate the demand for new protection equipment.

Case 1-Fault at BUS822, Variable DG2

In simulations, the size of DG2 was increasing from 0 to 10 MW, in 1 MW increments, while DG1 was set at the constant size of 5 MW. A model of case 1 is shown in

Figure 45.

Figure 45: Relay Desensitization Simulation Model for Case 1

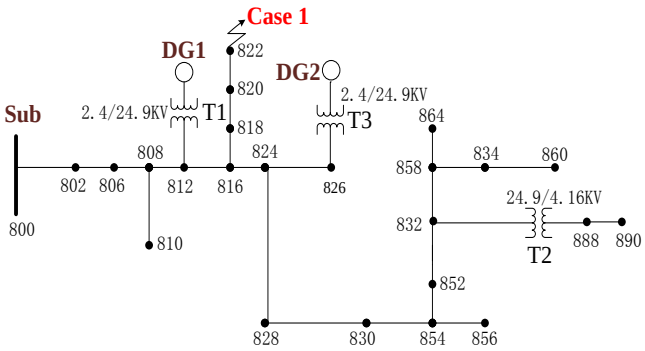

For case 1, simulation results are shown from Figure 46-49. The obtained results are shown in Tables 20-23. IT is the total fault current at the fault, while IS, IDG1, and IDG2 refer to the fault current's contributions from the substation, DG1, and DG2 respectively. The results were obtained from APSEN® and ETAP® softwares and are compared inside the tables. According to the data in the table, there's a small difference between ASPEN® and ETAP® because the fault current in ASPEN® is bigger than the one in ETAP®, but the error is less than 2 percent. In order to compare the results between ETAP® and ASPEN® on all figures, dotted lines indicate ETAP® results while solid lines show the results from ASPEN®. To distinguish the fault currents of DGs from total and substation, two axes with different scales were used in all figures. The left axis represents the fault currents from total and substation, while the right axis is for the DGs.

For all cases as indicated by the tables, the total fault current increases with the increased penetration of DG2, while the fault current contributions from the substation and the fixed DG1 decreases. After comparing four fault types, the dropping rates of fault current contributions of substation for the L-L-G case is greater than the rates for 3 phase, 1L-G and L-L cases, which indicate that the phenomenon of relay desensitization is more significant for L-L-G faults.

Table 20: L-L Fault on BUS822 in ETAP® and ASPEN®

	ASPEN®(White)				ETAP®(Yellow)			
DG2	**L-L (Amperes)**							
(MW)	I_T	I_S	I_{DG1}	I_{DG2}	I_T	I_S	I_{DG1}	I_{DG2}
0	3400	3210	200	0	3380	3164	229	0
1	3440	3200	199	56	3419	3152	228	56
2	3480	3190	198	111	3458	3140	227	112
3	3520	3170	197	165	3497	3129	226	167
4	3560	3150	197	219	3536	3117	225	221
5	3600	3150	196	273	3574	3105	224	275
6	3630	3140	195	326	3612	3094	223	328
7	3670	3130	195	378	3649	3082	222	381
8	3710	3120	194	430	3687	3071	222	433
9	3750	3100	193	481	3723	3060	221	485
10	3780	3090	192	532	3760	3048	220	536

Figure 46: L-L Fault on BUS822 versus Capacity of DG2

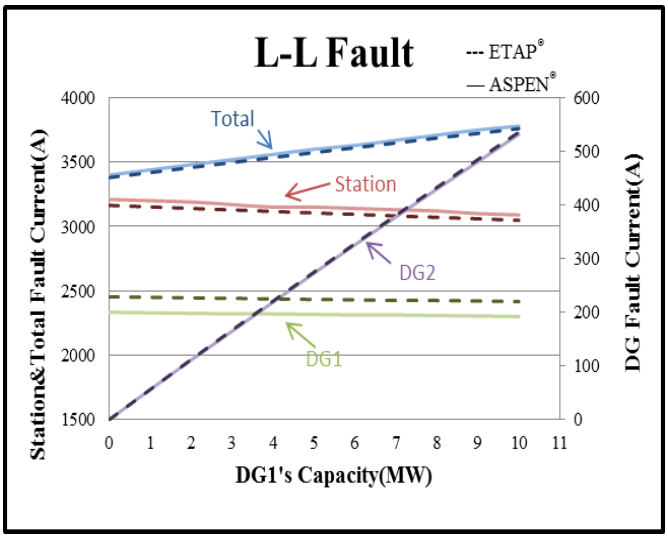

Table 21: 3 Phase Fault on BUS822 in ETAP® and ASPEN®

	ASPEN®(White)				ETAP®(Yellow)			
DG2	**3 Phase (Amperes)**							
(MW)	I_T	I_S	I_{DG1}	I_{DG2}	I_T	I_S	I_{DG1}	I_{DG2}
0	3930	3700	232	0	3882	3661	229	0
1	3970	3690	231	56	3922	3648	229	56
2	4010	3680	231	111	3962	3635	228	112
3	4050	3660	230	166	4001	3622	227	167
4	4090	3650	229	221	4040	3610	226	222
5	4120	3640	228	275	4079	3597	225	276
6	4160	3630	227	328	4117	3585	225	330
7	4200	3610	227	381	4155	3572	224	383
8	4240	3600	226	434	4193	3560	223	436
9	4280	3590	225	486	4231	3548	222	488
10	4310	3580	224	538	4268	3536	222	540

Figure 47: 3 Phase Fault on BUS822 versus Capacity of DG2

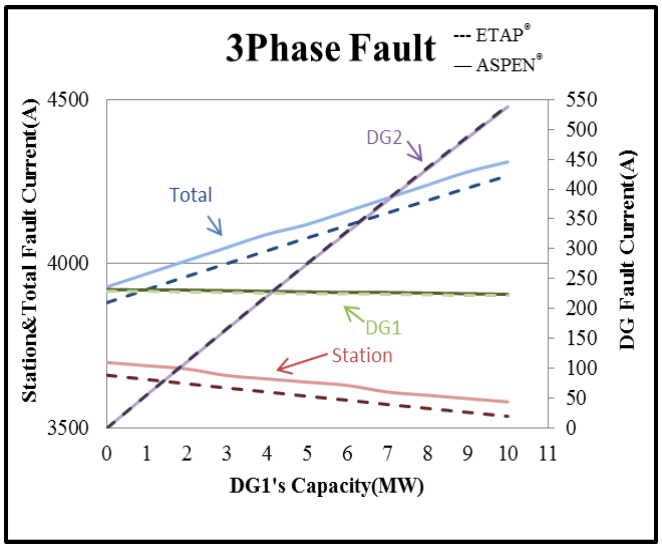

In 3 phase fault condition, when DG2's capacity increased from 0 to 10 MW, total fault current increased from 3930 A to 4310 A while current contributions declined significantly for substation and other DGs. For substation, the fault current decreased from 3700 A to 3580 A and the contribution from DG1 dropped 8 amperes.

Table 22: L-G Fault on BUS822 in ETAP® and ASPEN®

	ASPEN®(White)				ETAP®(Yellow)			
DG2	**1L-G (Amperes)**							
(MW)	I_T	I_S	I_{DG1}	I_{DG2}	I_T	I_S	I_{DG1}	I_{DG2}
0	2840	2350	500	0	2804	2305	508	0
1	2960	2350	471	149	2923	2303	479	151
2	3050	2340	447	276	3023	2298	456	280
3	3140	2330	428	389	3109	2291	437	394
4	3210	2320	411	490	3184	2283	420	495
5	3280	2310	397	581	3252	2273	406	587
6	3340	2300	385	665	3313	2262	394	671
7	3390	2290	374	743	3369	2251	384	749
8	3440	2280	365	815	3420	2239	374	822
9	3490	2260	357	884	3468	2227	366	891
10	3530	2250	349	949	3512	2215	359	956

Figure 48: L-G Fault on BUS822 versus Capacity of DG2

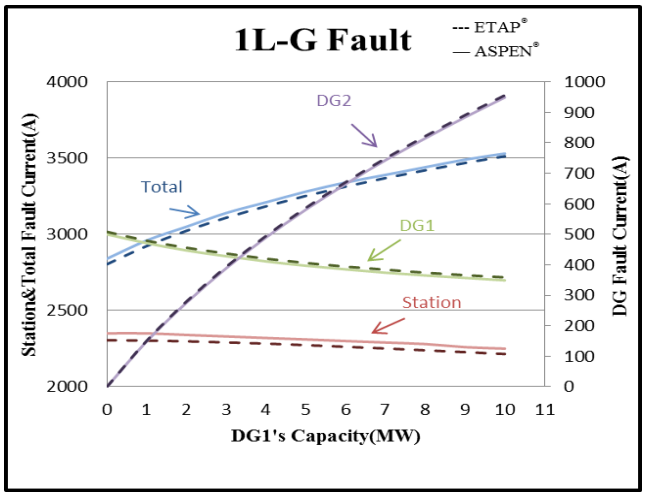

Table 23: L-L-G Fault on BUS822 in ETAP® and ASPEN®

	ASPEN®(White)				ETAP®(Yellow)			
DG2	**L-L-G(Amperes)**							
(MW)	I_T	I_S	I_{DG1}	I_{DG2}	I_T	I_S	I_{DG1}	I_{DG2}
0	3720	3370	389	0	3681	3326	384	0
1	3780	3350	370	110	3748	3308	366	111
2	3840	3330	355	206	3809	3292	351	207
3	3900	3320	342	291	3864	3276	339	292
4	3950	3300	331	368	3915	3261	329	369
5	3990	3290	322	439	3963	3246	320	440
6	4040	3270	314	505	4009	3232	313	506
7	4080	3260	307	567	4052	3218	306	568
8	4130	3250	301	626	4094	3205	301	627
9	4170	3230	296	683	4135	3192	296	683
10	4210	3220	291	738	4174	3179	291	737

Figure 49: L-L-G Fault on BUS822 versus Capacity of DG2

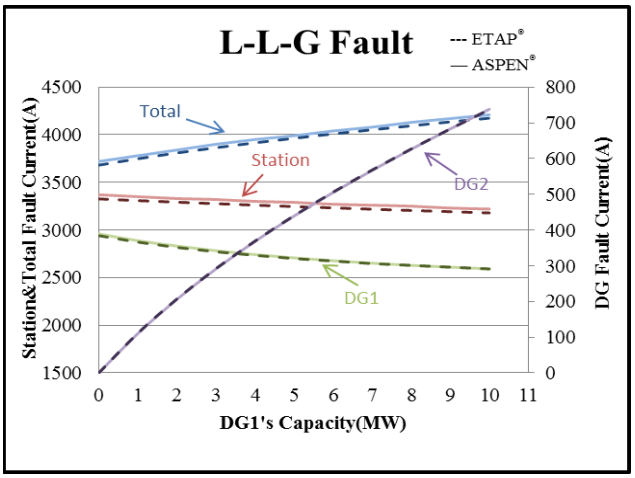

Case 2-Fault Location BUS856, Variable DG1

To prove the generality of this phenomenon, another case was modeled and simulated using the two programs. The model of case 2 is shown as Figure 50.

Figure 50: Relay Desensitization Simulation Model for Case 2

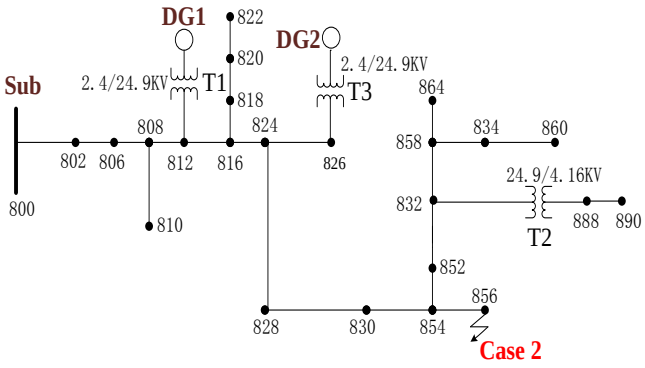

In case 2, DG1's capacity was chosen as the variable factor, while DG2's was kept fixed at 5 MW. Four types of faults were simulated at BUS856 instead of BUS822. Other parameters remained the same as in case 1.

DG from renewable resources is beneficial in providing clean power for the system. Increased penetration levels of DG can negatively impact protection of the system. Four types of faults were simulated at two different locations with increasing penetration of a DG using two different software programs to reconfirm relay desensitization. From the fault current data for substation in Tables 24-27 and Figures 51-54, it is obvious that the fault current on substation could drop from 3.2% to 15.4% as a sample DG capacity increases from 0 to 10MW for different

fault types. Among four fault types, the most severe case is a 15.4% drop for relay desensitization for a 1L-G fault on BUS856. The lower the fault current, the longer it will take for relay to trip. This confirms the phenomenon of relay desensitization, which was also identified by previous researchers.

Table 24: L-L on BUS856 in ETAP® and ASPEN®

	ASPEN®(White)				ETAP®(Yellow)			
DG1	**L-L (Amperes)**							
(MW)	I_T	I_S	I_{DG1}	I_{DG2}	I_T	I_S	I_{DG1}	I_{DG2}
0	1840	1700	0	155	1834	1689	0	157
1	1850	1690	21	154	1841	1674	24	156
2	1860	1670	42	153	1849	1660	48	155
3	1860	1660	62	152	1856	1646	71	154
4	1870	1650	82	152	1863	1632	94	153
5	1880	1640	102	151	1870	1618	117	152
6	1880	1620	121	150	1877	1605	139	151
7	1890	1610	140	149	1884	1592	161	151
8	1890	1600	159	149	1891	1579	182	150
9	1900	1590	178	148	1897	1566	203	149
10	1910	1580	196	147	1904	1553	224	148

Figure 51: L-L Fault on BUS856 versus Capacity of DG1

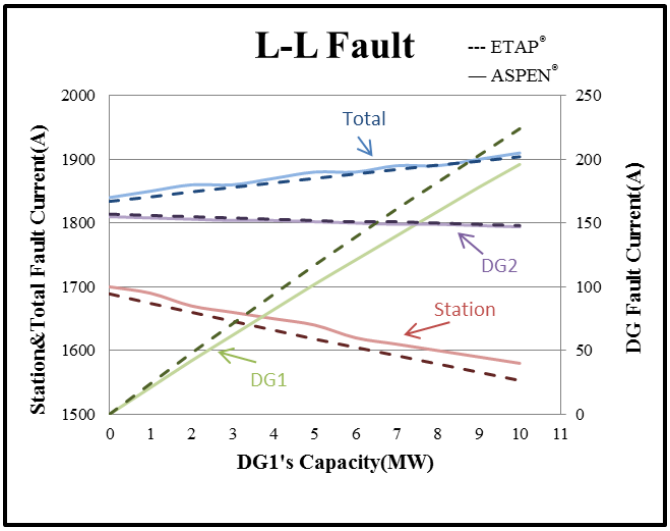

Table 25: 3 Phase Fault on BUS856 in ETAP® and ASPEN®

	ASPEN®(White)				ETAP®(Yellow)			
DG1	3 Phase (Amperes)							
(MW)	I_T	I_S	I_{DG1}	I_{DG2}	I_T	I_S	I_{DG1}	I_{DG2}
0	2120	1970	0	156	2108	1958	0	158
1	2130	1950	25	156	2116	1943	24	157
2	2140	1940	49	155	2123	1928	48	156
3	2140	1920	72	154	2131	1914	72	155
4	2150	1910	96	153	2138	1899	95	155
5	2160	1900	119	152	2145	1885	118	154
6	2160	1880	142	152	2153	1871	141	153
7	2170	1870	164	151	2160	1857	163	152
8	2180	1850	186	150	2167	1843	185	152
9	2190	1840	208	149	2173	1830	206	151
10	2190	1830	229	149	2180	1817	228	150

Figure 52: 3 Phase Fault on BUS856 versus Capacity of DG1

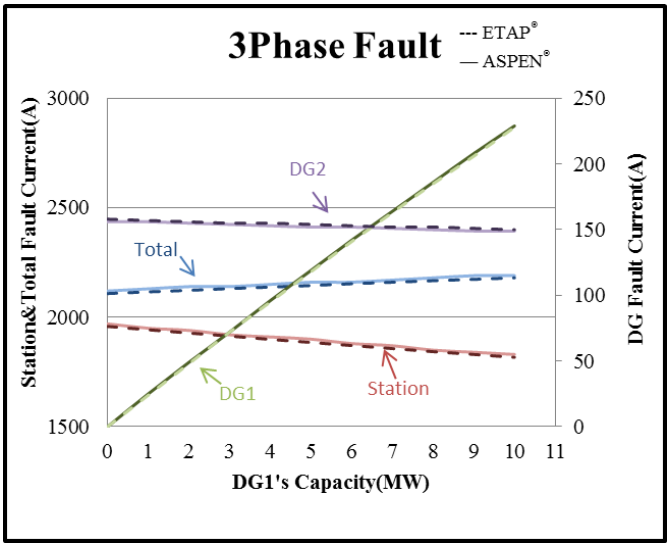

Table 26: 1L-G Fault on BUS856 in ETAP® and ASPEN®

	ASPEN®(White)				ETAP®(Yellow)			
DG1	1L-G (Amperes)							
(MW)	I_T	I_S	I_{DG1}	I_{DG2}	I_T	I_S	I_{DG1}	I_{DG2}
0	1380	1080	0	312	1379	1069	0	315
1	1390	1050	39	304	1387	1046	40	307
2	1400	1030	75	297	1395	1024	77	300
3	1410	1010	106	290	1401	1004	109	294
4	1410	997	135	285	1407	986	139	288
5	1420	981	161	280	1413	969	166	283
6	1420	966	186	276	1418	953	192	279
7	1430	952	209	272	1422	939	215	275
8	1430	939	230	268	1427	924	238	272
9	1430	926	250	265	1431	911	259	269
10	1440	914	269	262	1435	898	278	266

A comparison of the results obtained from the software programs for these two cases showed less than a 5% difference. This high degree of agreement tends to confirm the validity of the relay desensitization phenomenon due to the increased penetration levels of DG. (Nie, et al. 2016), (Fu, et al. 2015)

Figure 53: 1L-G Fault on BUS856 versus Capacity of DG1

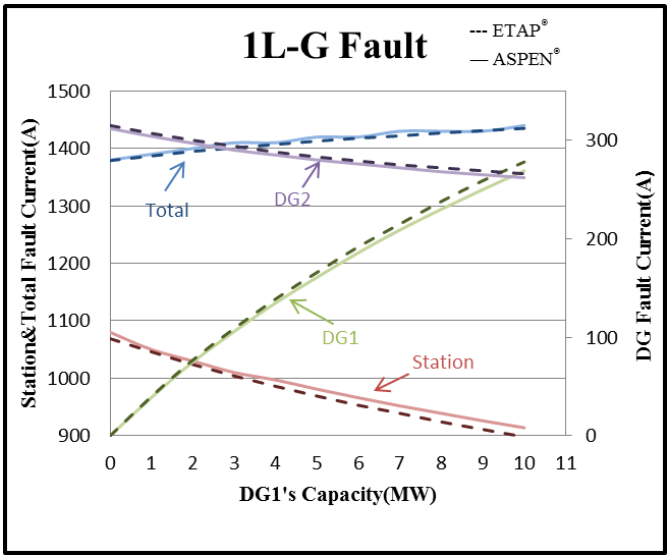

Table 27: L-L-G Fault on BUS856 in ETAP® and ASPEN®

	ASPEN®(White)				ETAP®(Yellow)			
DG1	L-L-G (Amperes)							
(MW)	I_T	I_S	I_{DG1}	I_{DG2}	I_T	I_S	I_{DG1}	I_{DG2}
0	2000	1780	0	237	1993	1767	0	237
1	2010	1760	33	232	2001	1747	33	232
2	2020	1740	63	227	2010	1729	64	228
3	2030	1730	90	224	2017	1712	92	224
4	2030	1710	116	220	2025	1695	119	221
5	2040	1700	141	217	2032	1679	145	218
6	2050	1680	164	215	2040	1664	169	216
7	2050	1670	186	212	2047	1649	193	214
8	2060	1650	208	210	2054	1635	216	211
9	2070	1640	229	208	2060	1621	238	210
10	2070	1630	249	207	2067	1607	259	208

Figure 54: L-L-G Fault on BUS856 versus Capacity of DG1

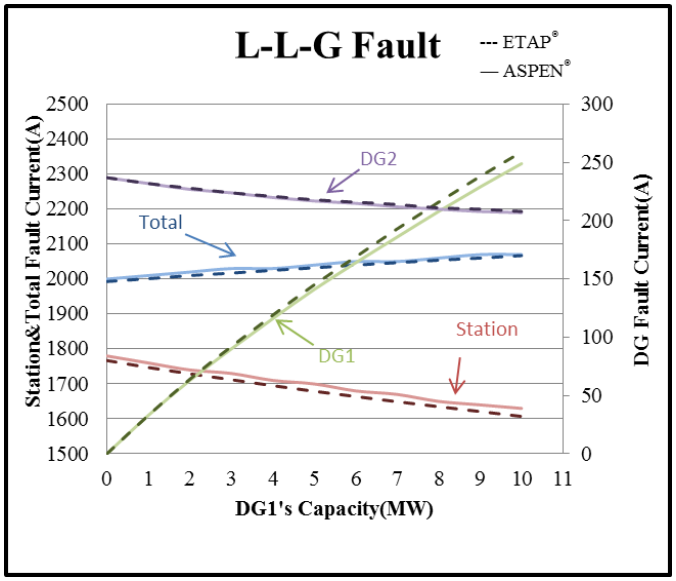

It is important to note that the small (less than 3 percent) difference between IT and the sum of all current contributions is due to slight angular differences in the fault current phases. More importantly, the total fault current increases with the increased penetration levels of DG1. In contrast, the fault currents contributed from other sources decreased as the capacity of DG1 increased. For instance, L-L-G fault current from substation decreased from 1780 A to 1630 A when DG1's capacity increased from 0 to 10 MW. Similar results can be obtained from three other types of fault conditions.

Special Case-Requiring Additional Protection

It is possible that the contribution from a source can fall below the pickup threshold of the relay for some remote fault location. For instance, when the distance between BUS834 and BUS860

increased to three miles, the fault contributions seen by the relay at DG1 fell below its pickup value. For example, the DG1 contribution to a 3 Phase fault on BUS860 is 272 A, which is below the rated current 288A and the pickup value of the overcurrent relay. The green circle in Figure 55 indicates the location for a future protection device that could be installed on the load side of BUS832. The 3-Phase fault contribution of DG1 for a fault at BUS832 is 472 A, which can be detected by the relay.

Figure 55: Relay Desensitization Simulation Model for Special Case

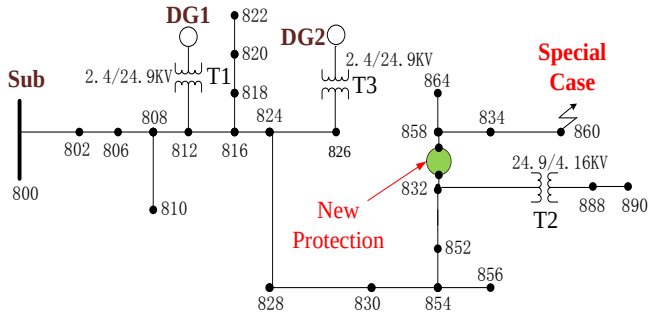

The results of both case studies obtained from ETAP® and ASPEN® programs showed over 95% agreement. When the capacity of the variable DG increased, contributions from existing DG and substation were decreased resulting in relay desensitization. This effect varies for different locations and could render the relay inoperable as stated in special case. For such cases, additional protection equipment should be installed at the proper location to establish an efficient and effective fault detection and clearing. For future research and analysis, effects of inverter-based generation should be considered. (Nie, et al. 2016), (Fu, et al. 2015)

I2t for Relay Desensitization

As mentioned in previous chapters, the increased level of DG generation will increase the stress level on the equipment along the distribution line. 3Phase, L-L-G, L-L and 1L-G that occur at Bus 860 are considered and I^2t calculations are conducted on the response times of DG's phase overcurrent relay on the 2.4kV for all faults. The results are obtained using ETAP® and ASPEN® software platforms.

In 3Phase fault case shown in Table 28, the total fault current, IT, increases by 6.7% in ASPEN® and 6.8% in ETAP® with the DG's size varying from 0MW to 10MW. By contrast, the fault current contribution from the substation IS decreases by 4.8% in ASPEN® and 4.8% in ETAP®, correspondingly. The fault current contribution from DG (I'DG) after the substation breaker has opened increases to almost double its initial value (IDG) before the substation breaker is opened in both programs.

Table 28: 3Phase Fault Currents in ETAP® and ASPEN®

	ETAP®(Yellow)				ASPEN®(White)			
S_{DG}	I_T(A)		I_S(A)		I_{DG}	I'_{DG}	I_{DG}	I'_{DG}
0	3486	3520	3486	3520	0	0	0	0
1	3511	3550	3469	3500	43	77	44	77
2	3535	3570	3451	3490	87	152	87	152
3	3559	3600	3434	3470	129	226	131	226
4	3582	3620	3417	3450	171	299	173	299
5	3606	3640	3400	3430	213	371	215	371
6	3629	3670	3383	3420	254	441	257	441
7	3652	3690	3366	3400	295	511	299	511
8	3675	3720	3350	3380	336	579	340	579
9	3697	3740	3333	3370	376	646	380	646
10	3720	3760	3317	3350	416	712	420	712

In L-L-G fault case, shown in Table 29, the total fault current, IT, increases by 9.6% in ASPEN® and 9.2% in ETAP® with the DG's size varying from 0MW to 10MW. Meanwhile, the fault current contribution from the substation, IS, decreases by 7.9% in ASPEN® and 7.6% in ETAP® respectively. The fault current contribution from DG (I'DG) after the substation breaker has opened dramatically rises as compared to its initial value (IDG) in both programs.

Table 29: L-L-G Fault Currents in ETAP® and ASPEN®

	ETAP®(Yellow)				ASPEN®(White)			
S_{DG}	I_T(A)		I_S(A)		I_{DG}	I'_{DG}	I_{DG}	I'_{DG}
0	3234	3270	3234	3270	0	0	0	0
1	3275	3310	3198	3230	86	104	87	105
2	3313	3340	3165	3200	162	200	164	206
3	3348	3380	3136	3170	230	290	233	293
4	3380	3410	3110	3150	292	375	295	377
5	3410	3440	3085	3120	349	455	352	457
6	3439	3470	3062	3100	402	531	405	533
7	3467	3490	3040	3080	452	604	455	605
8	3493	3520	3019	3060	500	675	502	674
9	3519	3540	2999	3040	545	743	546	741
10	3543	3570	2980	3020	589	809	589	805

In L-L fault case shown in Table 30, the total fault current, IT, rises by 7.7% in ASPEN® and 6.9% in ETAP® with DG's size ranging from 0MW to 10MW. However, the fault current

contribution from the substation, IS, decreases by 5.3% and 4.6% in ASPEN® and ETAP® respectively

Table 30: L-L Fault Currents in ETAP® and ASPEN®

	ETAP®(Yellow)				ASPEN®(White)			
S_{DG}	I_T(A)		I_S(A)		I_{DG}	I'_{DG}	I_{DG}	I'_{DG}
0	3019	3050	3019	3050	0	0	0	0
1	3043	3070	3002	3040	43	75	38	66
2	3067	3090	2986	3020	86	149	75	132
3	3091	3110	2970	3010	129	221	112	196
4	3115	3140	2953	2990	171	292	149	259
5	3138	3160	2937	2980	212	362	185	321
6	3161	3180	2921	2960	253	430	221	382
7	3183	3200	2905	2950	294	497	257	443
8	3206	3220	2890	2930	334	563	292	502
9	3228	3240	2874	2920	374	627	327	560
10	3250	3260	2859	2910	413	691	362	618

In 1L-G fault case shown in Table 31, the total fault current, IT, increases by 19.1 % in ASPEN® and 18.7% in ETAP® with DG's size ranging from 0MW to 10MW. However, the fault current contribution from the substation, IS, decreases by 13.5% and 12.6% in ASPEN® and ETAP® respectively.

Table 31: 1L-G Fault Currents in ETAP® and ASPEN®

	ETAP®(Yellow)				ASPEN®(White)			
S_{DG}	I_T(A)		I_S(A)		I_{DG}	I'_{DG}	I_{DG}	I'_{DG}
0	2268	2300	2268	2300	0	0	0	0
1	2339	2370	2225	2270	116	117	115	105
2	2399	2430	2186	2220	218	228	215	205
3	2452	2480	2151	2190	307	333	303	300
4	2499	2530	2119	2160	388	434	381	392
5	2541	2570	2088	2130	461	529	452	479
6	2579	2610	2060	2100	527	620	517	563
7	2613	2640	2033	2080	589	707	577	644
8	2645	2680	2008	2050	647	790	632	721
9	2674	2710	1984	2030	700	870	684	796
10	2702	2730	1961	2010	751	946	733	867

The tripping time for the relay at substation (tS) is much shorter than the one for the relay at DG (t'DG) for all four types of faults (Tables 32-33).

Table 32: Tripping Time for 3Phase and L-L-G Faults in ETAP® and ASPEN®

	3Phase Fault Case				L-L-G Fault Case			
	ASPEN®(White)		ETAP®(Yellow)		ASPEN®(White)		ETAP®(Yellow)	
S_{DG}	t_S(s)	t'_{DG}(s)	t_S(s)	t'_{DG}(s)	t_S(s)	t'_{DG}(s)	t_S(s)	t'_{DG}(s)
0	0.2458	0.0000	0.2450	0.0000	0.2532	0.0000	0.252	0.0000
1	0.2463	1.2909	0.2455	1.2909	0.2544	1.1920	0.2534	1.2909
2	0.2468	1.3125	0.2457	1.3075	0.2554	1.2029	0.254	1.3075
3	0.2472	1.3347	0.2463	1.3301	0.2564	1.2140	0.255	1.3301
4	0.2477	1.3565	0.2468	1.3592	0.2573	1.2267	0.256	1.3592
5	0.2481	1.3792	0.2473	1.3771	0.2582	1.2405	0.257	1.3771
6	0.2486	1.4021	0.2476	1.4015	0.2591	1.2555	0.258	1.4015
7	0.2492	1.4258	0.2481	1.4248	0.2599	1.2714	0.258	1.4248
8	0.2496	1.4489	0.2487	1.4475	0.2607	1.2880	0.259	1.4475
9	0.2502	1.4726	0.2490	1.4699	0.2615	1.3056	0.26	1.4699
10	0.2506	1.4979	0.2496	1.4975	0.2623	1.3233	0.261	1.4975

Table 33: Tripping Time for L-L and 1L-G Faults in ETAP® and ASPEN®

	L-L Fault Case				1L-G Fault Case			
	ASPEN®(White)		ETAP®(Yellow)		ASPEN®(White)		ETAP®(Yellow)	
S_{DG}	t_S(s)	t'_{DG}(s)	t_S(s)	t'_{DG}(s)	t_S(s)	t'_{DG}(s)	t_S(s)	t'_{DG}(s)
0	0.2607	0.0000	0.26	0.0000	0.3023	0.0000	0.3	0.0000
1	0.2614	1.0223	0.26	1.2909	0.3057	1.6839	0.302	2.1741
2	0.2620	1.0384	0.261	1.3075	0.3089	1.7816	0.306	2.2692
3	0.2627	1.0573	0.261	1.3301	0.3120	1.8859	0.309	2.4135
4	0.2633	1.0759	0.262	1.3592	0.3150	1.9968	0.311	2.5439
5	0.2640	1.0948	0.262	1.3771	0.3180	2.1106	0.314	2.6959
6	0.2646	1.1138	0.263	1.4015	0.3207	2.2297	0.317	2.8514
7	0.2653	1.1330	0.263	1.4248	0.3235	2.3612	0.319	2.9962
8	0.2659	1.1526	0.264	1.4475	0.3260	2.4971	0.322	3.17
9	0.2666	1.1726	0.265	1.4699	0.3286	2.6394	0.324	3.3337
10	0.2672	1.1925	0.265	1.4931	0.3313	2.7851	0.326	3.5091

The increased trend of the tripping times for relays at substation (tS) as well as at DG (t'DG) as functions of total fault current (IT) for the 3Phase fault case is shown in Figure 56. The L-L-G, L-L, and 1L-G fault cases have similar trends. This clearly indicates that the total I^2t increases as the DG penetration rises.

Figure 56: Tripping Time versus Total Fault Current

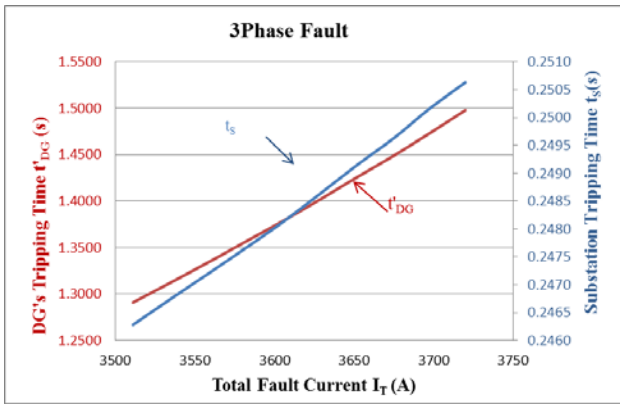

The closeness and agreement of values determined by ASPEN® and ETAP® for all fault types indicate a high degree of confidence in the correctness of the results. The total fault current and fault current contribution from DG rise with the increased penetration of DG, while the fault contribution from substation declined in all four cases simulated by both programs. Total I^2t and contributions from substation and DG are calculated and compared as shown in previous tables. For a more visualized comparison, dotted and solid lines represent I^2t results from ETAP® and ASPEN® in Tables 34-37 and Figures 57-60.

Table 34: Stress Values for 3Phase Fault

	3Phase Fault(×10³ A²s)					
	ASPEN®(White)			ETAP®(Yellow)		
S_{DG}	I^2t_S	I^2t_DG	I^2t_T	I^2t_S	I^2t_DG	I^2t_T
0	2987	0	2987	3035	0	3035
1	2964	7	3042	3007	7	3100
2	2939	26	3108	2993	26	3156
3	2915	60	3187	2965	60	3247
4	2892	106	3277	2937	107	3333
5	2868	167	3382	2910	167	3432
6	2846	240	3499	2896	241	3559
7	2823	329	3630	2868	329	3686
8	2801	430	3773	2842	431	3844
9	2779	545	3929	2828	545	3993
10	2758	676	4101	2801	677	4162

Figure 57: 3Phase Fault Case for I^2t Values

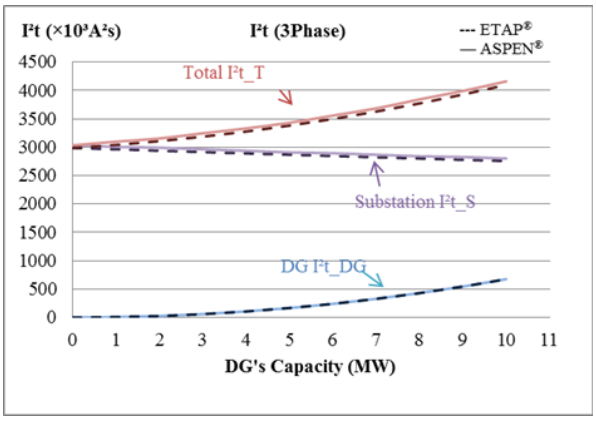

The total I^2t _T values are increased to 137.3% and 137.1% in ASPEN® and ETAP® respectively as the size of DG varies from 0MW to 10MW. However, the I^2t contribution from the substation, I^2t _S, reduced by 7.7% and 7.7% in ASPEN® and ETAP® respectively.

Table 35: I^2t Values for L-L-G Fault

	L-L-G Fault(×10³ A²s)					
	ASPEN®(White)			ETAP®(Yellow)		
S_{DG}	I^2t_S	I^2t_DG	I^2t_T	I^2t_S	I^2t_DG	I^2t_T
0	2648	0	2648	2696	0	2696
1	2601	12	2738	2643	13	2787
2	2559	45	2842	2604	52	2882
3	2522	94	2955	2565	106	3009
4	2488	158	3076	2540	179	3133
5	2458	235	3206	2501	266	3274
6	2429	323	3345	2476	367	3427
7	2402	422	3493	2451	480	3574
8	2376	533	3649	2427	605	3751
9	2352	654	3815	2402	742	3922
10	2329	785	3987	2378	892	4124

Figure 58: L-L-G Fault Case for I^2t Values

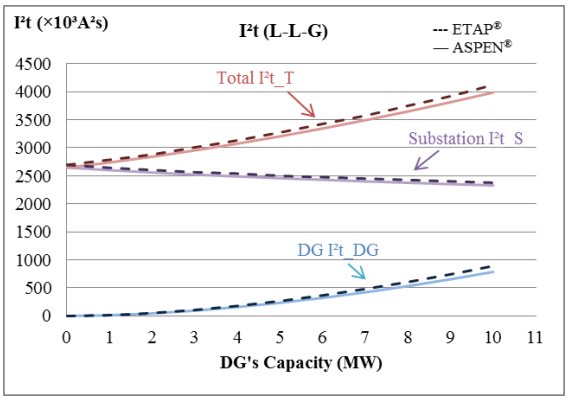

For L-L-G fault case, the total I^2t _T values are increased to 150.5% and 153.0% in ASPEN® and ETAP® respectively as the size of DG varies from 0MW to 10MW. However, the I^2t contribution from the substation, I^2t _S, reduced by 12.1% and 11.8% in ASPEN® and ETAP® respectively.

Table 36: I^2t Values for L-L Fault

	L-L Fault(×10³ A²s)					
	ASPEN®(White)			ETAP®(Yellow)		
S_{DG}	I^2t_S	I^2t_DG	I^2t_T	I^2t_S	I^2t_DG	I^2t_T
0	2376	0	2376	2414	0	2414
1	2356	5	2425	2402	5	2454
2	2336	19	2482	2378	20	2507
3	2317	43	2548	2366	44	2566
4	2296	77	2625	2341	79	2656
5	2277	121	2708	2329	124	2734
6	2258	174	2801	2305	179	2826
7	2239	237	2902	2293	245	2926
8	2221	311	3014	2269	321	3038
9	2202	393	3134	2257	406	3156
10	2184	487	3264	2245	504	3286

Figure 59: L-L Fault Case for I^2t Values

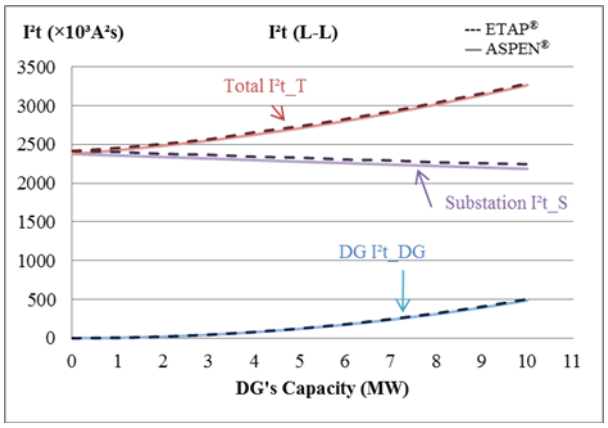

The total I²t _T values are increased to 137.4% and 136.1% in ASPEN® and ETAP® respectively as the size of DG varies from 0MW to 10MW. However, the I²t contribution from the substation, I²t _S, is reduced by 8.1% and 7.0% in ASPEN® and ETAP® respectively.

Table 37: I^2t Values for 1L-G Fault

	1L-G Fault(×10³ A²s)					
	ASPEN®(White)			ETAP®(Yellow)		
S_{DG}	I²t_S	I²t_DG	I²t_T	I²t_S	I²t_DG	I²t_T
0	1555	0	1555	1586	0	1586
1	1514	23	1691	1557	25	1718
2	1476	91	1854	1509	97	1890
3	1444	204	2050	1480	218	2087
4	1414	364	2284	1452	388	2335
5	1386	569	2555	1424	611	2620
6	1361	823	2867	1397	888	2962
7	1337	1131	3227	1379	1217	3332
8	1315	1491	3636	1352	1609	3792
9	1293	1910	4098	1334	2059	4285
10	1274	2383	4614	1316	2568	4821

Figure 60: 1L-G Fault Case for I2t Values

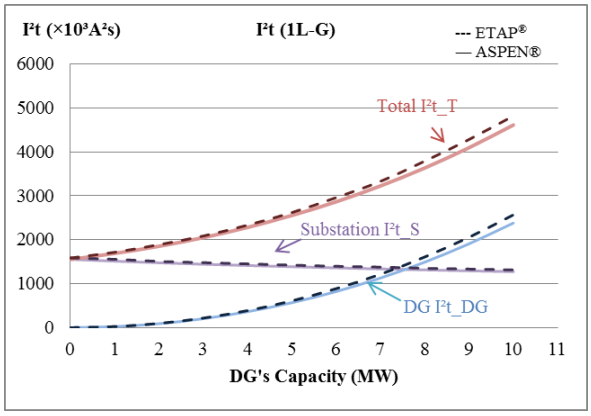

For 1L-G fault case, the total I^2t _T values are increased to 296.7% and 304.0% in ASPEN® and ETAP® respectively as the size of DG varies from 0MW to 10MW. However, the I^2t contribution from the substation, I^2t _S, is reduced by 18.1% and 17.0% in ASPEN® and ETAP® respectively.

I^2t _DG values at DG will increase as the capacity of DG grows. By contrast, I^2t _S values from substation exhibit a gradually descending trend. The decreasing trend of I^2t _S from substation contradicts the given, which indicated a growing trend for I^2t _S. The fault current factor is more prominent in impacting I^2t. As the tripping time of the relay at substation increases, the value of I^2t _S also shows a decreasing trend.

For all simulated cases, I^2t results closely follow the same trend in both programs. Additionally, the total (I^2t _T) and DG's contribution (I^2t _DG) of four types of fault are very similar. Simulations in both programs yield the same results with minimal differences. (Nie, et al. 2016), (Fu, et al. 2015)

Conservation Voltage Reduction Case Studies

To investigate the achievable savings through implementing CVR, an actual distribution feeder was adopted. The feeder consisted of numerous spot loads of different load classes and compositions. The distribution feeder was connected to the upper network through an 115kV/12.47kV main substation transformer, with an impedance of 12.5% pu. A tap changer was added to the secondary side of the substation transformer as a means for controlling voltage. During normal operations, the voltage at the main substation was maintained at 1.05 pu. For simplicity, the secondary networks were not modeled; instead they were aggregated as spot loads fed by the primary feeder. To keep the voltage within ANSI standards during normal operations, one fixed capacitor and five voltage-controlled capacitors were installed throughout the system. The system was tested under 30% and 50% penetration of photovoltaic generation. The PV arrays were distributed throughout the system, with a large concentration located near the end of the feeder. The rating and output of each photovoltaic array varied based on location, customer type, climate, and time. Furthermore, to analyze potential savings, the corresponding Locational Marginal Pricing (LMP) for the area was adopted.

As mentioned previously, the savings from CVR are highly dependent on the load composition, its model, climate, and time of day. In the current work, a week of peak demand during the summer was chosen to demonstrate maximum effects of the photovoltaic systems. Therefore, accurate load profiles for residential, industrial, and commercial loads were adopted to capture the demand and load composition at different hours of the days in the chosen week. It was assumed that within each hour, the demand and composition of the loads remained almost constant, and the ZIP parameters were assigned to the loads accordingly. In the duration of the week, the ZIP parameters for certain types of loads, such as residential, were more volatile and shifted considerably from one hour to the next. Furthermore, the ZIP parameters deviated greatly from the morning peak to the afternoon peak.

To determine the effectiveness of CVR, three distinct test cases were simulated. In all cases, CVR factor density was found using simulated data. In the first test case, no photovoltaic generation was considered. In the second and third cases, PV penetration levels of 30% and 50% were implemented, respectively.

In all three cases, the necessary data for calculation of the aggregated ZIP load parameters based on LS method were collected by simulating the system at various substation voltages, changing from 11.8465kV (0.95pu) to 13.0935 (1.05pu) in steps of 0.1247 kV (0.01pu). The line-to-neutral voltages and active and reactive powers were measured at the secondary of the substation and were used for finding the aggregated ZIP load parameters. Next, estimated CVR factor densities were calculated with respect to the nominal tap position. The error between actual and estimated CVR factor densities was found to be very small in all cases. As an example, Figure 61 shows the relative error between the estimated and actual CVR factor densities during the simulated week for the case with 30 percent PV penetration. As seen, the maximum error is less than 0.03%.

Figure 61: Relative Error Between Estimated and Actual CVR Factor Densities (30% PV penetration)

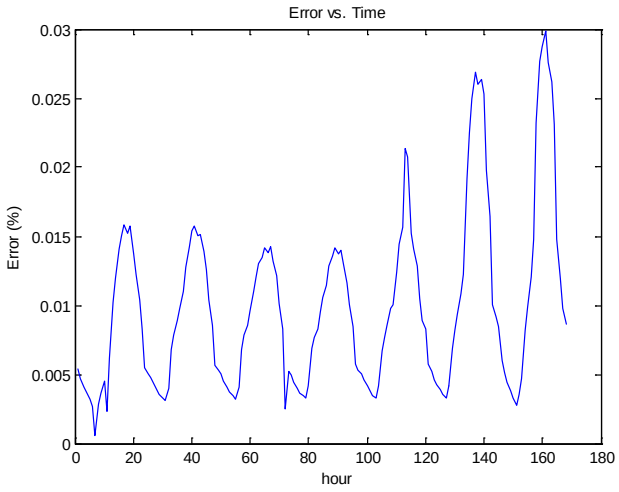

Figure 62 shows variations of the estimated CVR factor density during time for the three studied cases. The CVR factor density shifts throughout the day due to variations in load values and load types. As observed, during hours with high solar irradiance, the CVR factor density improves with the increase in PV output generation.

Figure 62: CVR Factor Density versus. Time

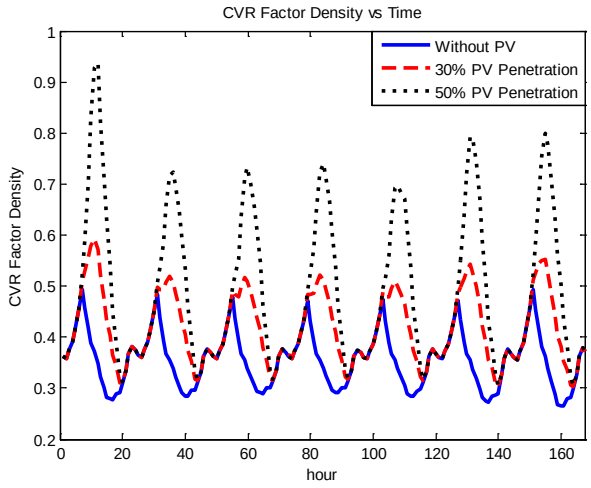

For system operators, the estimated CVR factor density can provide a guideline for predicting the potential reduction in the demand of the distribution system through CVR. While the increase in CVR factor density implies the possibility of energy savings, but reducing the voltage at the substation to its extreme lowest level may not always result in best CVR practices, particularly when downstream reactive power compensation is not enough. As a result, depending on specific situations of a system, operators may use the estimated CVR factor density for implementation of appropriate rules in Volt-VAr control. In the studied cases, the set of rules previously shown was found to result in the best practice of CVR. Using the recommended taps shown in Table 38, no violation of voltage constraints was observed throughout the system.[1]

Figure 63 demonstrates the voltage profile of the system in different cases during peak load conditions. As can be seen from the profiles, with implementation of the control methodology, there are no voltage violations in the system. On the other hand, without implementation of the control methodology, 606 voltage violations were found in the case without PV, 67 violations were observed in the case with 30 percent PV penetration, and 15 violations were found with 50 percent PV penetration. Figure 64 demonstrates tap changer settings in the peak 24 hour period using the rules previously stated. [2] (Rahimi, et al. 2014)

Table 38: Volt-VAr Control Methodology Using CVR Factor Density

Condition	Tap Position
$CVR_{fd,est}(t) \geq 0.365$	$V_{tap} = 0.95\ pu$
$0.31 \leq CVR_{fd,est}(t) < 0.365$	$V_{tap} = 0.96\ pu$
$CVR_{fd,est}(t) < 0.31$	$V_{tap} = 0.97\ pu$

[1] Seen in Table 1

[2] Seen in Table 1

Figure 63: Voltage Profile During Peak Load Conditions

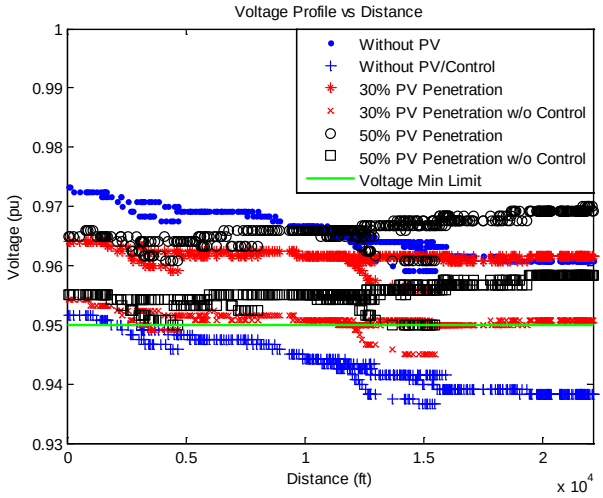

Table 39 demonstrates the benefits of implementing CVR in the main substation of the system in the three different studied cases. These benefits have been expressed in terms of average weekly demand reduction as well as cost savings using the corresponding LMP data. The demand and cost reductions in Table 39 are based on lowering the taps from $V_{tap} = 1.05$ to the recommended taps suggested by Table 38. (Rahimi, et al. 2014)

Figure 64: Tap Changer Settings in the Peak 24-hour Period

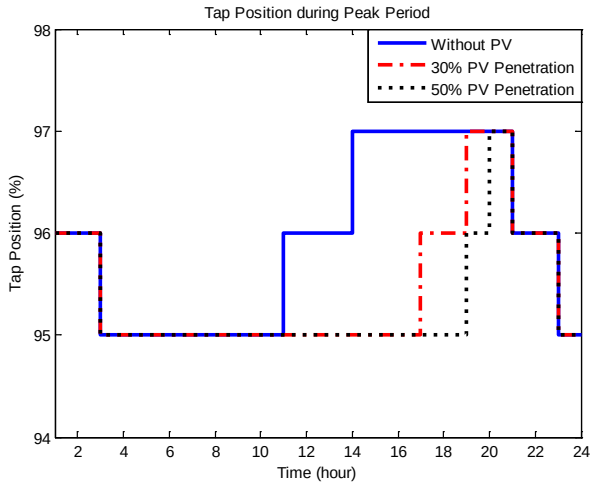

Table 39: Demand Reduction Compared toV_tap=1.05

	PV Penetration		
	0%	30%	50%
Weekly Demand Reduction (kW)	7059.5	7861.4	7945.7
Weekly Demand Reduction (%)	1.8	2.3	2.6

Cost Savings (%)	1.7	2.3	2.6

Figure 65 demonstrates the changes in the ZIP load parameters during the studied week. From this figure, the cause for variations of the CVR factor density with the changes of PV penetration in the system can be explained. (Rahimi, et al. 2014)

Figure 65: Variations of the ZIP Parameters versus Time in Different PV Penetration Levels

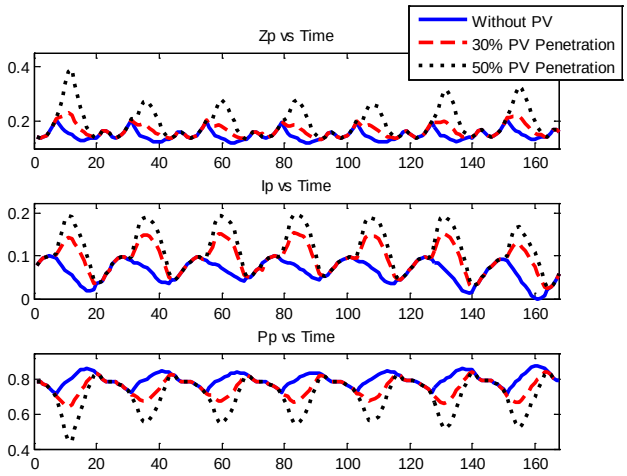

With the increase in the penetration level of PVs, the constant impedance and constant current components of the active power load in the ZIP model increase, while its constant power component decreases (see equations 13-15). For example, during hour 11, the shift in the ZIP parameters are: $\Delta Zp = 142\%$, $\Delta Ip = 214\%$ and $\Delta Pp = -76.7\%$. This means that the aggregated load viewed from the main substation of the system leans more towards becoming constant impedance and constant current. As a result, reducing the voltage at the substation level can result in the reduction of the overall active power demand of the system.

This study shows the effectiveness of CVR in an actual distribution circuit with varying levels of PV penetration using real world data and operating conditions. Through simulations, the aggregated ZIP load parameters at the main substation of an actual system were found during a high demand week in the summer, and the CVR factor density was estimated using these parameters. Based on the estimated CVR factor densities and their variations throughout the mentioned week, a Volt-VAr control methodology was suggested for reducing the demand of the system without violating the voltage constraints mandated by ANSI standards.

Through this study, it was shown that the increased penetration of PV in a distribution circuit can improve the effectiveness of CVRas it weakens the constant power component of the aggregated load, thus increasing the CVR factor density and reducing the total demand of the system.

For analyzing the effectiveness of CVR in extreme cases, this study looked into the summer peak period of the system. However, to fully realize the benefits of CVR, the study should be further extended to analyze all days of the year including winter, spring, and fall seasons. This is due to the fact that during certain periods, ZIP parameters are dependent on the location, climate, weather, and load compositions. Therefore, during other seasons the practice of CVR in the presence of photovoltaic systems may not be as beneficial as observed in the summer peak. (Rahimi, et al. 2014)

Furthermore, in this work, PV systems have been simulated at unity power factor. However, due to the possibility of the changes in regulations regarding the interconnection of distribution generations, the effectiveness of CVR in the presence of photovoltaic systems should also include the cases when PV systems can inject/absorb reactive power to the system. (Rahimi, et al. 2014)

Conclusions – Steady State and Flicker Impacts of DG Penetration on Distribution Systems

Integration of renewable power generation systems using distributed generation has gained increasing popularity in the past few years. Advantages of renewable power generation include emission free power generation, relief of congestion in lines by providing local generation to high load areas, load frequency control, and ancillary services. Although renewable energy sources come with numerous advantages, many problems associated with their integration also need to be addressed. Most importantly, the intermittent nature of renewable power generation, stability issues, and consistency of the source must be questioned, since production of energy is not consistently available due to outside factors.

The current distribution network was not designed for integration of renewable distributed generation (DG) at high penetration levels. This report illustrates a series of studies that have been carried out to improve the operation of distribution networks with high penetration of renewable distributed generation. Major concerns for integration of renewable distributed generation are identified as: voltage fluctuation, and the improper operation of utility distribution system protection equipment. The concerns include deviations from conservation voltage reduction levels set by current operational standards. Furthermore, several mitigation measures that would alleviate the impacts of distributed generation are considered and proposed.

Massive proliferation of renewable energy will impact the operation, controls, and protection of the grids. One of these issues is related to the extra injection of power during daytime hours due to levels of high irradiation, which results in the backflow of power and system over-voltages. Current regulations do not allow photovoltaic inverters to participate in voltage or reactive power control. Hence, photovoltaic inverters are only allowed to inject active power to ensure maximum profits for investors. From the system's perspective, however, this type of operation may not result in the best practices. A coordinated active/reactive power control of the PV inverters can resolve the issues associated with voltage profile, while reducing the total demand of the system from the utility's perspective. For this purpose, a nonlinear optimization problem has been defined in which total demand of the system is minimized while considering system constraints, such as voltage profile and line flows.

Ultimately, implementation of renewable energy resources at higher penetration levels is challenging the system by requiring the accommodation of more accurate monitoring and controls. One proposed approach is a theoretical formulation of state estimation for distribution grids with Renewable Energy Sources (RES). Precisely estimated system states can also be beneficial in optimal scheduling, security assessment, and real-time transactions. Along with

the attempt for state estimation, the availability of Phasor Measurement Units (PMU) has been considered with the fact that PMU data will simplify the state estimation problem.

Despite the issues and concerns, some research has also shown that strategic investments in enabling technologies can greatly increase the DN's ability to utilize an increasing level of DG. National Standard IEEE 1547 is a stepping stone to furthering the possibilities of DG integration, as separate standards focusing specifically on high DG penetration are needed. Optimization of generation location is currently a tedious process and further research involving the rapid analysis of multiple generators and locations would be beneficial. Voltage control, despite how widely it has been studied, needs further research and investigation due to the fact that multiple solutions to other problems alter the existing topology. Mesh topology offers solutions to many problems and introduces a host of new scenarios to study. Investigations will include transitioning from radial to mesh topology, the cost, maintenance, short circuit studies, voltage control, and system protection.

The addition of DG to a radial distribution system will affect the feeder in several ways. For example, the DG can alter the direction of power flow in the distribution system, causing protection and control related issues. Some adverse effects include fluctuation in voltage levels, voltage flicker, power quality issues, degradation in system reliability, system protection, and harmonic distortion. The presence of DG in distribution systems affects voltages and reactive power at locations close to the DG installation. These changes in voltages and reactive power can be controlled locally. The operating voltage profile of the feeder can be optimized by considering the load, DG power output, and its mode of operation. The changes in loading condition or DG penetration level will directly influence the operating voltage. The voltage and reactive power control in distribution systems is typically done using On Load Tap Changers (OLTC) operations, shunt capacitors, and voltage regulators.

Battery storage is one of the industry-approved devices used to support systems with high penetration of renewable energy. Applications and benefits of distributed storage devices on the performance of distribution power systems are discussed in this report. Particularly, this includes the implementation of the Battery Energy Storage System (BESS) for system improvement. An overview of predominant battery types are covered with their benefits and advantages. Diverse applications for BESS are described, such as peak load shaving, power quality improvement, load/frequency control, system balancing, and congestion management. As a side matter to the active distribution network, the impacts of plug-in electric vehicles and problems regarding the dispatch of BESS units are introduced.

This report discussed the integration of renewable energy in distribution systems and presents the newly introduced challenges that are faced. It also provided some proposed solutions, such as changes in operation of the system, utilization of accurate measurements, and diligent algorithms like state estimation. Finally, application of the industry-approved mitigating device (energy storage) is illustrated. The material contains case studies to show the impacts as well as testing the proposed mitigation measures.

Objectively, the series of studies illustrate the integration of renewable energy in distribution systems and presents the newly introduced challenges that are faced. It will also provide solutions, such as changes in operation of the system, utilization of accurate measurements, and diligent algorithms like state estimation. Finally, application of the industry-approved mitigating device (energy storage) is illustrated. The material contains case studies to show the impacts as well as testing the proposed mitigation measures.

CHAPTER 2:
Grid Cyber Security Issue Identification

Introduction

The goal is to provide cyber security enhancements that support smart grid technologies in California's transmission and distribution systems. There are two main questions that need to be answered: "Is the utility industry adequately preparing California rate payers for the risks and consequences associated with enabling the smart meters?" and "Is the next generation of power professionals being provided with adequate tools to understand cyber security within the context of an energy utility?" By looking at the recent advances in cyber security, including currently active research, real facts can be placed into the hands of decision makers in the Investor Owned Utilities (IOU). Additionally, consumers can be armed with awareness of the risks and areas of concern, and give them the right tools and knowledge to minimize those risks and maximize the benefits of harnessing the data supplied by the IOU's.

Purpose

This research focuses on the infrastructure of the Customer Premise Network (CPN) and its cyber security risks and regulations. The researchers closely examined the current implementations of the industrial communication standard called ZigBee Smart Energy Profile (SEP) version 1.x and the future implementation of the ZigBee SEP version 2.0. The research team analyzed the CPN technology for cyber security issues and attempted to quantify the risk to consumers when they use the energy information gathered from the CPN energy management system (or related technology). Additionally, the team considered the policies and enforcement likely to come from regulatory agencies, such as the North American Electric Reliability Corporation (NERC) in the critical infrastructure protection policies.

News headlines like Stuxnet, Duqu, and DragonFly, or the 2013 "Metcalf Incident" in San Jose, have increased public and political pressure to secure the energy ecosystem. There is also increasing demand to reduce U.S. dependency on foreign oil as well as an increasing awareness that energy use affects the environment. The United States has recognized that responding to these demands requires renovating the existing electric power system and upgrading the aging electric grid infrastructure. Modernizing the electric grid by implementing Smart Grid related technologies—"smart" systems of two-way communication between utilities and consumers—will transform the energy industry into a new age of reliability, availability, and efficiency that will contribute to the economy and environmental health.

As the deployment of Smart Grid technologies is increasing throughout the electric infrastructure, the need to secure the electric grid and the challenges of doing so have been gaining speed. California has seen the near universal rollout of the Advanced Metering Infrastructure from the major IOU's in California, which means now is the time to highlight the changing landscape with the Smart Grid and how that infrastructure reaches into the homes of California ratepayers.

The increasing prevalence of the Internet-of-Things and connected devices has come hand in hand with the rise of the Smart Grid. Time-of-Use (TOU) pricing, where electricity prices vary depending on when the energy is consumed, is yet another developing reality for the consumer. (California Energy Comission 2014) The increase in TOU pricing schemes for consumers has created a need to optimize the electricity use in the home. This is a need that the Smart Grid is able to fill using smart devices that communicate with the electric grid and optimize the use of electricity for the consumer.

Upgrading and replacing the aging energy infrastructure is a national priority, and modernizing the electric grid creates benefits as well as new risks and challenges. (Office of Electricity Delivery and Energy Reliability 2014) The infrastructure of connected utilities, consumers, distribution providers, and market participants makes the grid an attractive target for attacks by criminals and nation-states alike. Keeping the electric grid efficient and safe from the growing cybersecurity concerns and the potential for widespread disruption demands attention and has resulted in numerous pieces of cybersecurity legislation as well as mandates from all levels of government – Federal, State, and Local.

Would-be attackers of the Smart Grid see the energy sector as an attractive target and are actively exploiting flaws in the systems in order to infiltrate and sabotage America's infrastructure. A cyber attack on the Smart Grid could easily affect more than just utilities though; the Internet-of-Things connecting the world, individuals, and businesses are also potential targets and potential victims. Recovering from the impact of a cyber attack and preventing further attacks may cost untold millions of dollars. The challenge is that cyber threats are quick to evolve, becoming increasingly complex and sophisticated, requiring increasing time and resources that are difficult to justify in difficult economic circumstances. The unfortunate reality is that changes prompting improvements often come on the heels of an incident.

Federal agencies such as the U.S. Department of Homeland Security (DHS), Department of Energy (DOE), National Institute of Standards and Technology (NIST) and other Smart Grid working panels, as well as energy firms, research institutions, and academia are collaborating to prevent cyber attacks and protect the critical infrastructure. The government has also established infrastructure protection standards and policies to further strengthen and secure the critical infrastructure sectors of North America. Federal regulations and compliance standards are in the midst of being overhauled and updated to ensure they are appropriately addressing the real risks as they exist today, as well as the emerging trends and threats in the years to come.

With the Smart Grid and smart devices, utilities and consumers are able to control and adjust the flow of energy. Unlike the current grid, which was designed with the only goal of bringing electricity from the utility to its consumers, the Smart Grid's two-way dialogue allows for the more reliable and efficient exchange of electricity and information between the utility and consumer. The Smart Grid also allows the incorporation of newer technologies such as solar and wind energy productions as well as plug-in electric vehicles. As envisioned, this

infrastructure would replace the aging electric infrastructure in order to reach and manage the electricity needs of the 21st century.

One of the goals for the Smart Grid is to change the paradigm of how electricity is generated and how the end user consumes it. The Smart Grid integrates new technologies that improve energy efficiency and reduce greenhouse gas emissions. It also helps lower the consumption of foreign oil through the use of renewable energy sources, benefitting the environment and combatting climate change. Traditionally, two-thirds of all electricity generated in the U.S. came from burning some type of fossil fuel like coal or natural gas; however, with the exception of solar power, all Smart Grid electric power comes from rotating some form of turbine to produce electricity.

One of the first steps in creating the Smart Grid is to connect devices and enable communications for increased efficiency. The *NIST Framework and Roadmap* lays out the logical domains for smart grid communications. (Office of the National Coordinator for Smart Grid Interoperability 2010)

Figure 66 shows the closely integrated data flows that allow markets to share data with transmission, distribution, and generation; in fact, in a nearly complete star topology, it allows communications to flow between all of the actors in the Smart Grid. In this way, efficiencies can be achieved and stability can be introduced to offset the unpredictability of renewable generation sources. These technologies also allow consumers to actively participate in controlling energy usage by allowing them to view near real-time energy usage data. Research shows that consumers reduce their use by 5 to 10 percent when they know how much energy they are using. (Ghansah 2014)

At the same time, these communication channels open up attack vectors for malicious actors to disrupt communications, affect operations, and breach customer privacy and security. This report focuses on the particular technologies within the Smart Grid domain, the inherent risks and best practices, and what regulations and initiatives are being and have been introduced to mitigate these threats.

Figure 66: Smart Grid Communication Domains

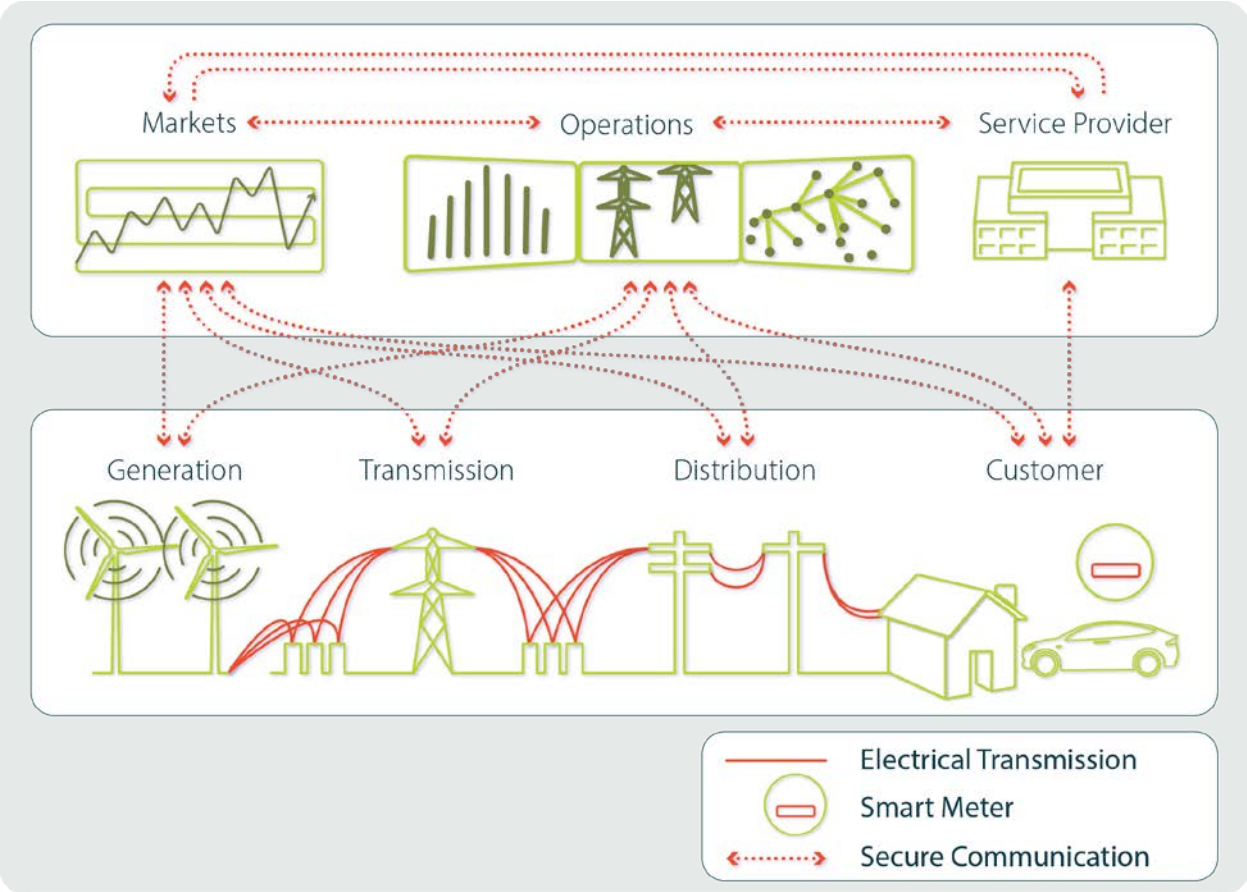

Figure by: CSGC – Deborah Frost and Shanna Rossi

Customer Domain

The customer's domain—sometimes referred to as the Customer Premise Network—can be thought of as all of the technology and resources used at the customer site to enable the communication and consumption of energy related data. This encompasses (among other potential devices):

- Customer Gateways
- Customer PCs
- Smart energy appliances
- Smart thermostats
- Smart Meters
- Energy Displays

- Energy Storage
- Plug-in Electric Vehicles

Figure 67 shows the various devices and how they relate to each other. The main communication hub between the utility and the consumer will be at the Smart Meter, which will communicate over 802.15.4, usually through a ZigBee compliant interface, to a Customer gateway.

Figure 67: Customer Communication Domains

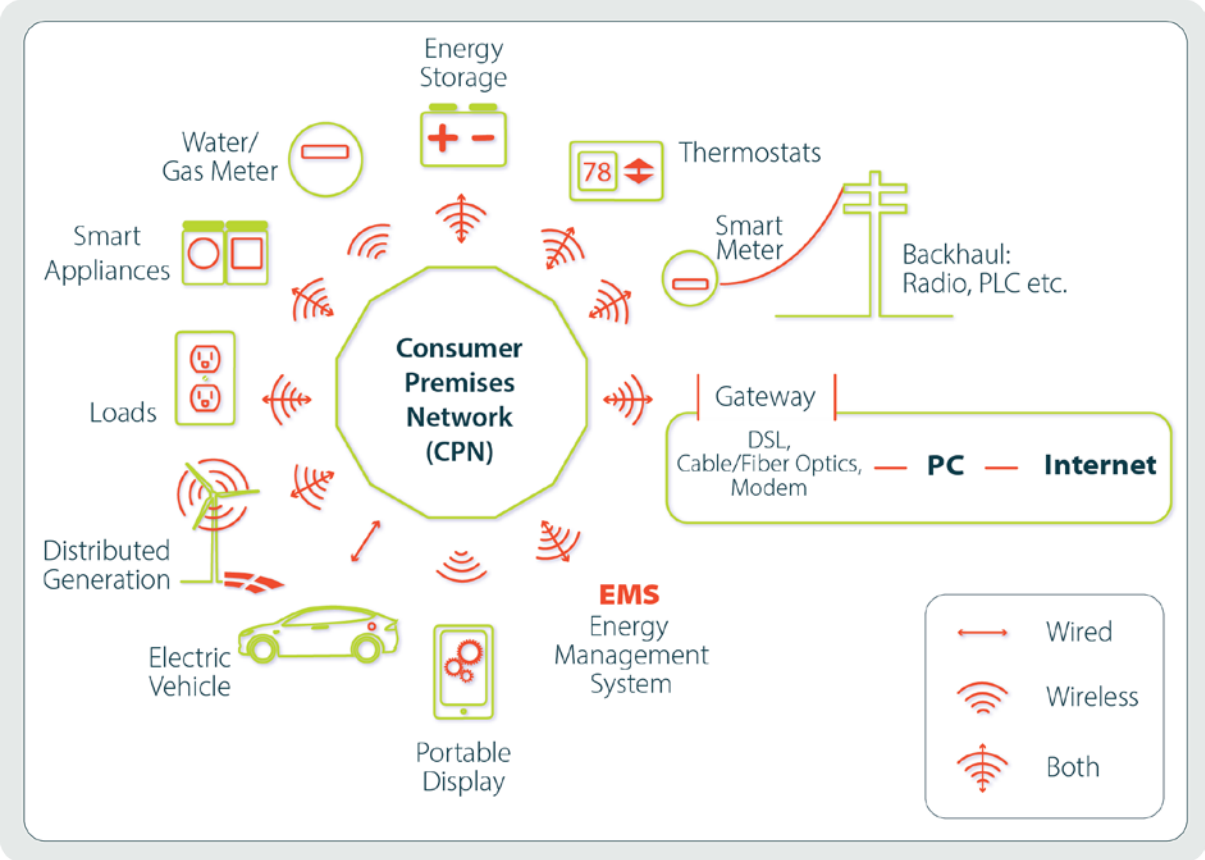

Figure by: CSGC – Deborah Frost and Shanna Rossi

Customer Gateway

The customer gateway acts as an interface interconnecting the AMI network and customer's systems and appliances within the customer's premise. For example, the integrated system, ZigBee wireless technology, acts as an interface that lets the devices from the utility's end and the customer's end communicate and work with each other. ZigBee operates on the 802.15.4 specification and was designed with security in mind, but even it is susceptible to physical attacks, key attacks where hackers obtain encryption keys, and replay and injection attacks where the ZigBee device is tricked into performing unauthorized actions. (Bowers 2012)

Home Area Networks (HANs):

Home Area Networks connect "smart" home appliances and electronic products to the Smart Grid for remote monitoring, metering, and controls. For example, smart appliances such as an air conditioner, refrigerator, or smart dishwater could be controlled based on tariff pricing or utilized in the demand response capabilities of the utility. Utilities can send out signals to the appliances, connected to the HAN, telling them to respond accordingly to reduce the load on the power grid.

ZigBee Networks

The three IOUs of California have all installed smart meters that operate on the ZigBee Secure Energy Profile 1.0 and 1.x. (Loria, Tatro, et al. 2014) This allows consumers to connect devices that consume energy data. As depicted in Figure 68, there are many devices that could potentially be a part of this ZigBee network.

Figure 68: ZigBee Networks

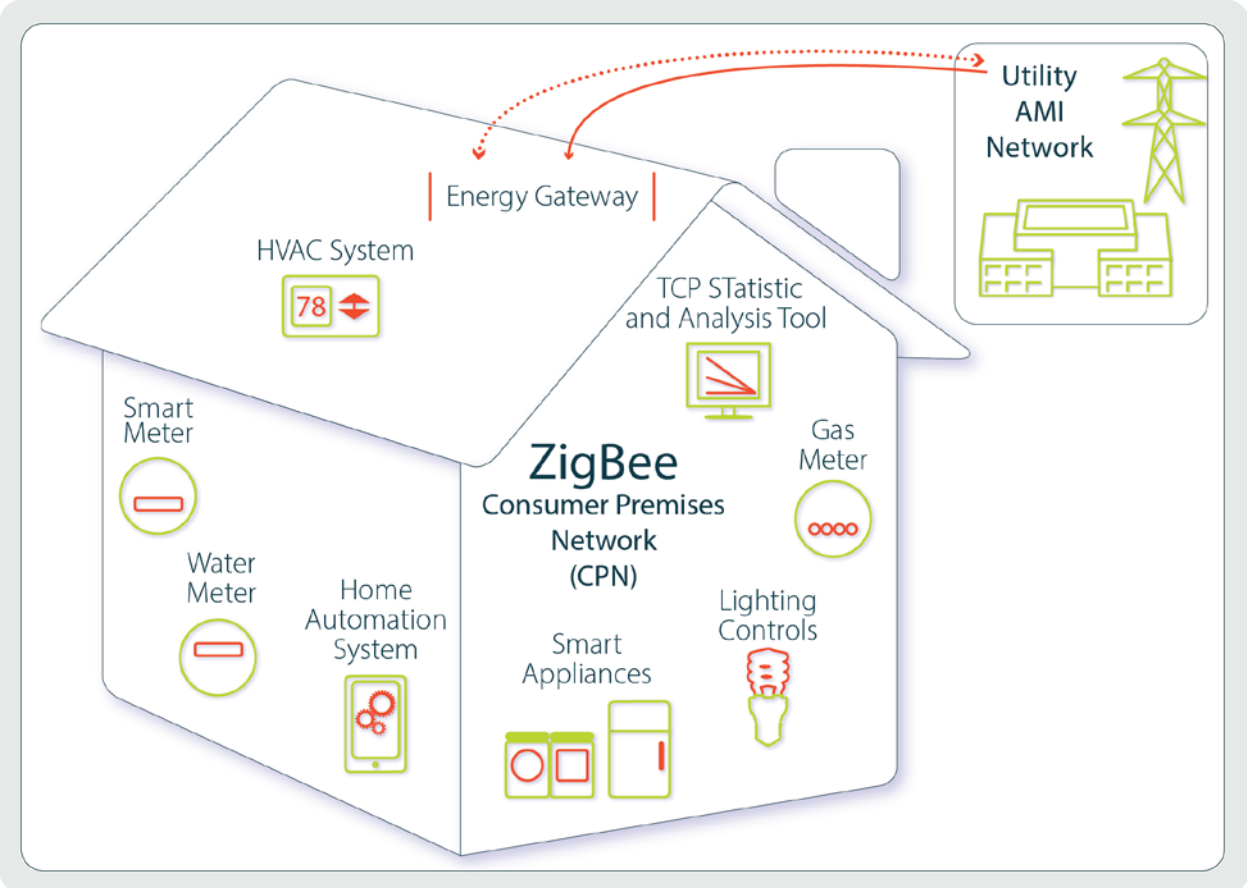

Figure by: CSGC – Deborah Frost and Shanna Rossi

Security Concerns and Response Efforts

The communication model of the Smart Grid is where the fundamental concerns for cyber security are generated. In the traditional model of the electric grid, these end devices didn't communicate with one another, nor did they share near real-time information to the consumer. There are so many different communication paths and so many elements, even with the utility itself, that provide a communication interface, that the proliferation of attack points has skyrocketed as the implementation of Smart Grid technologies increased. Table 40 is a listing of the actors and their domains where security needs to be addressed.

Table 40: Domains and Actors in the Smart Grid – Source NISTIR7628

Actor Number	Domain	Actor	Acronym	Description
1	Generation	Plant Control System – Distributed Control System	DCS	A local control system at a bulk generation plant. This is sometimes called a Distributed Control System (DCS).
2	Customer	Customer		An entity that pays for electrical goods or services. A customer of a utility, including customers who provide more power than they consume.
3	Customer	Customer Appliances and Equipment		A device or instrument designed to perform a specific function, especially an electrical device, such as a toaster, for household use. An electric appliance or machinery that may have the ability to be monitored, controlled, and/or displayed.
4	Customer	Customer Distributed Energy Resources: Generation and Storage	DER	Energy generation resources, such as solar or wind, used to generate and store energy (located on a customer site) to interface to the controller (home area network/business area network (HAN/BAN)) to perform an energy-related activity.
5	Customer	Customer Energy Management System	EMS	An application service or device that communicates with devices in the home. The application service or device may have interfaces to the meter to read usage data or to the operations domain to get pricing or other information to make automated or manual decisions to control energy consumption more efficiently. The EMS may be a utility subscription service, a third party-offered service, a consumer-specified policy, a consumer-owned device, or a manual control by the utility or consumer.
6	Customer	Plug-in Electric Vehicle/ Electric Vehicle Service Element	PEV/ EVSE	A PEV is a vehicle propelled by an electric motor and powered by a rechargeable battery. It can be recharged using an external power source. When the external power source is the power grid, the EV is connected through the EVSE that provides power and communication.

7	Customer	Home Area Network Gateway	HAN Gateway	An interface between the distribution, operations, service provider, and customer domains and the devices within the customer domain.
8	Customer	Meter		Point of sale device used for the transfer of product and measuring usage from one domain/system to another.
9	Customer	Customer Premise Display		A device that displays usage and cost data to the customer on location.
10	Customer	Sub-Meter – Energy Usage Metering Device	EUMD	A meter connected after the main billing meter. It may or may not be a billing meter and is typically used for information-monitoring purposes.
11	Customer	Water/Gas Metering		A point of sale device used for the transfer of product (water and gas) and measuring usage from one domain/system to another.
12	Distribution	Distribution Data Collector		A data concentrator collecting data from multiple sources and modifying/transforming it. .
13	Distribution	Distributed Intelligence Capabilities		Advanced automated/intelligence application that operates in a normally autonomous mode from the centralized control system to increase reliability and responsiveness.
15	Distribution	Distribution Remote Terminal Unit/Intelligent Electronic Device	RTUs or IEDs	Receives data from sensors and power equipment, and can issue control commands, such as tripping circuit breakers, if voltage, current, or frequency anomalies are identified, RTUs and/or IEDs can raise/lower voltage levels to maintain the desired voltage range.
16	Distribution	Field Crew Tools		A field engineering and maintenance tool set that includes mobile computing and handheld devices.
17	Distribution	Geographic Information System	GIS	A spatial asset management system that provides utilities with asset information and network connectivity for advanced applications.
18	Distribution	Distribution Sensor		A device that measures a physical quantity and converts it into a signal that can be read by an observer or by an instrument.
19	Markets	Energy Market Clearinghouse		Wide area energy market operation system providing high-level market signals for distribution companies (ISO/RTO and Utility Operations).
20	Markets	Independent System Operator/Regional Transmission Organization Wholesale Market	ISO/RTO	An ISO/RTO control center that participates in the market and does not operate the market.
21	Operations	Advanced Metering Infrastructure Headend	AMI	This system manages the information exchanges between third party systems or systems not considered headend, such as the Meter Data Management System

				(MDMS) and the AMI network.
22	Operations	Bulk Storage Management		Provides management for energy storage connected to the bulk power system.
23	Operations	Customer Information System	CIS	Enterprise-wide software applications that allow companies to manage aspects of their relationship with a customer.
24	Operations	Customer Service Representative	CSR	Customer service provided by a person (e.g., sales and service representative) or by automated means called self-service (e.g., Interactive Voice Response [IVR]).
25	Operations	Distributed Generation and Storage Management		Distributed generation is the process of generating electricity from many small, local energy sources. Storage management enables the efficient integration of distributed generation sources into the grid.
26	Operations	Distribution Engineering		A technical function of planning or managing the design or upgrade of the distribution system. For example: • The addition of new customers, • The build out for new load, • The configuration and/or capital investments for improving system reliability.
27	Operations	Distribution Management Systems	DMA	A suite of application software that supports electric system operations. Example applications include topology processor, online three-phase unbalanced distribution power flow, contingency analysis, study mode analysis, switch order management, short-circuit analysis, volt/VAR management, and loss analysis. These applications provide operations staff and engineering personnel additional information and tools to help accomplish their objectives.
28	Operations	Distribution Operator		Person operating the distribution system.
29	Operations	Distribution Supervisory Control and Data Acquisition	SCADA	A supervisory computerized system that gathers and processes data and applies operational controls for distribution- side systems used to control dispersed assets.
30	Operations	Energy Management System	EMS	A system used by electric grid operators to monitor, control, and optimize the performance of the generation and/or transmission system.
31	Operations	ISO/RTO Operations		Wide area power system control center providing high-level load management and security analysis for the transmission grid, typically using an EMS with generation applications and network analysis applications.
32	Operations	Load Management Systems/Demand Response Management	LMS/DRMS	An LMS issues load management commands to appliances or equipment at customer locations in order to decrease load during peak or emergency situations. The DRMS issues pricing or other signals to

		System		appliances and equipment at customer locations in order to request customers (or their preprogrammed systems) to decrease or increase their loads in response to the signals.
33	Operations	Meter Data Management System	MDMS	System that stores meter data (e.g., energy usage, energy generation, meter logs, meter test results) and makes data available to authorized systems. This system is a component of the customer communication system. This may also be referred to as a 'billing meter.'
34	Operations	Metering/Billing/ Utility Back Office		Back office utility systems for metering and billing.
35	Operations	Outage Management System	OMS	An OMS is a computer system used by operators of electric distribution systems to assist in outage identification and restoration of power. Major functions usually found in an OMS include: • Listing all customers who have outages. • Predicting location of fuse or breaker that opened upon failure. • Prioritizing restoration efforts and managing resources based upon criteria such as location of emergency facilities, size of outages, and duration of outages. • Providing information on extent of outages and number of customers impacted to management, media, and regulators. • Estimating restoration time. • Managing crews assisting in restoration. • Calculating crews required for restoration.
36	Operations	Transmission SCADA		A supervisory computerized system that gathers and processes data (e.g., transmitting device status) and applies operational controls (e.g., manages energy consumption by controlling compliant devices) for transmission-side systems used to control dispersed assets.
37	Operations	Customer Portal		The online interface through which a customer can interact with the energy service provider. Typical services may include: customer viewing of their energy and cost information online, enrollment in prepayment electric services, and enablement of third party monitoring and control of customer equipment.
38	Operations	Wide Area Measurement System	WAMS	Communication system that monitors all phase measurements and substation equipment over a large geographical base that can use visual modeling and other techniques to provide system information to power system operators.

39	Operations	Work Management System	WMS	A system that provides project details and schedules for work crews to construct and maintain the power system infrastructure.
40	Operations	Work Management System	WMS	A system that provides project details and schedules for work crews to construct and maintain the power system infrastructure.
41	Service Provider	Aggregator/Retail Energy Provider		Any marketer, broker, public agency, city, county, or special district that combines the loads of multiple end-use customers in facilitating the sale and purchase of electric energy, transmission, and other services on behalf of these customers.
42	Service Provider	Billing		An entity that performs the function of generating an invoice to obtain payment from the customer.
43	Service Provider	Energy Service Provider	ESP	Provides retail electricity, natural gas, and clean energy options, along with energy efficiency products and services.
44	Service Provider	Third Party		A third party providing a business function outside of the utility.
45	Transmission	Phasor Measurement Unit	PMU	A device that measures the electrical parameters of an electricity grid with respect to universal time (UTC) such as phase angle, amplitude, and frequency to determine the state of the system.
46	Transmission	Transmission Intelligent Electronic Device (IED)		A device that receives data from sensors on the power network and power equipment and can issue control commands, such as tripping circuit breakers if they sense voltage, current, or frequency anomalies, or raise/lower voltage levels in order to maintain the desired level. A device that sends data to a data concentrator for potential reformatting.
47	Transmission	Transmission Remote Terminal Unit (RTU)		A remote terminal unit passes status and measurement information from a transmission substation or feeder equipment to a SCADA system and transmits control commands sent from the SCADA system to the field equipment.
48	Operations	Security/Network / System Management		An entity that monitors and configures the security, network, and system devices.
49	Operations	Transmission Engineering		A technical function of planning or managing the design or upgrade of the transmission system (e.g., equipment designed for more than 345,000 volts between conductors).

Source: NISTIR 7628 Rev.1 Vol.1

Given the scope of actors, it becomes important to understand who or what the potential threats are and where they are coming from. Throughout this report, it is common in the cyber security world to refer to actors with NIST's term "Adversary." This vocabulary is highlighted to avoid confusion as this report progresses and refers to documents such as NIST Special Publications

where the term actor will not necessarily have the same definition as it does in various industry publications or guides. Table 41 is a brief synopsis of the potential threat actors.

Table 41: Categories of Adversaries to Information Systems

Adversary	Description
Nation States	State-run, well organized, and financed. Use foreign service agents to gather classified or critical information from countries viewed as hostile or as having an economic, military, or a political advantage.
Hackers	A group of individuals (e.g., hackers, phreakers, crackers, trashers, and pirates) who attack networks and systems seeking to exploit the vulnerabilities in operating systems or other flaws.
Terrorists/ Cyberterrorists	Individuals or groups operating domestically or internationally who represent various terrorist or extremist groups that use violence or the threat of violence to incite fear with the intention of coercing or intimidating governments or societies into succumbing to their demands.
Organized Crime	Coordinated criminal activities including gambling, racketeering, narcotics trafficking, and many others. An organized and well-financed criminal organization.
Other Criminal Elements	Another facet of the criminal community, which is normally not well organized or financed. Normally consists of few individuals, or of one individual acting alone.
Industrial Competitors	Foreign and domestic corporations operating in a competitive market and often engaged in the illegal gathering of information from competitors or foreign governments in the form of corporate espionage.
Disgruntled Employees	Angry, dissatisfied individuals with the potential to inflict harm on the smart grid network or related systems. This can represent an insider threat depending on the current state of the individual's employment and access to the systems.
Careless or Poorly Trained Employees	Those users who, either through lack of training, lack of concern, or lack of attentiveness pose a threat to smart grid systems. This is another example of an insider threat or adversary.

Cybersecurity's primary directive is risk identification and risk mitigation – perfectly secure computing does not exist. However, by recognizing areas of concern and vulnerability, and following the best practices discussed later, it is possible to lower the value of the information and raise the cost of compromise such that the information no longer holds any value to the attacker. As the penetration of smart technologies onto the electric grid and into consumer's homes continues to grow, so does the risk and so do the potential attack vectors, and therefore the areas of concern that need to be considered. The concepts behind Smart Grid cyber security – whether it is in the NIST publications, the Critical Infrastructure Protection regulations, or the information sharing initiatives brought about by different agencies – is all about understanding those risks and minimizing the likelihood and potential impact. It is up to the consumer, who likely will not have a background in the types of risk management meant to keep them safe, to learn and understand those risks and rewards associated with participating in the Smart Grid. It is not an insurmountable task, and this next section intends to examine the current risks. Much of the Smart Grid's architectures and frameworks have been standardized by various agencies such as the NIST publications, the standards governing bodies such as IEEE, or the various industry alliances such as the ZigBee alliance.

The U.S. Department of Homeland Security's Industrial Control Systems Cyber Emergency Response Team (ICS-CERT) responded to more than 200 security incidents between October 2012 and May 2013, which is twice the number they responded to in 2012. Of those incidents, 53 percent were from the energy sector, an increase of 40 percent in the previous year. (St. John 2014) This is largely due to grid devices becoming more reliant on communication and being networked, making them vulnerable to attacks. A survey conducted by ThreatTrack found that about 72 percent of energy and financial industry respondents said that they are certain their business would be the target of cyber threats. Of the respondents, 34 percent reported that their endpoints had been infected within the last 12 months, and of energy firm respondents, 61 percent identified that email poses the biggest threat. Twelve percent of the energy industry respondents fear attacks may be from foreign governments, while less than 10% fear it may be an insider threat. (Smart Grid Today 2014)

The US government has been performing and replicating real cyber attacks to find possible vulnerabilities in the electric system so that they can predict and prevent potential cyber threats. They tested a self-destruction of an electrical generator motor triggered by a cyber attack. On May 22, 2014, CNN reported that hackers attacked an American public utility's control system where they successfully breached into the utility's computer network. (Todd, Brian; CNN News n.d.) The specifics, like most of these incidents tend to be, was withheld as sensitive information. According to Julian Waits of ThreatTrack Security, energy firms "often work with many small contractors, who potentially have inconsistent, incongruous or poor security practices." (Waits, Julian, ThreatTrack Security 2014) He explained that a lot of energy companies still have systems that are out-of-date and connected over unsecure networks, which creates opportunities for malicious actors. However, modernizing these systems often means connecting them to routable networks (IP) networks, and this creates inherent vulnerabilities due to the expanding scope of the attack surface. Again, the advantages outweigh the risk in most cases, but understanding the attack surface is the first step to minimizing the value of the target. (Waits, Julian, ThreatTrack Security 2014)

Demand Response

For the consumers in California who participate in Demand Response (DR) schemes, the security concerns around the DR are closely tied to the security concerns around ZigBee and the AMI due the communication channels that the utility has to communicate with. The issues of concern include load-shedding, integrity of pricing signals coming from Automated DR systems, Time-Of-Use price, among others. A compromise of the integrity or the confidentiality of the systems could expose consumer information, or result in the disruption or modification of their electric service.

Smart Grid Communications Platforms

What makes the Smart Grid vulnerable to increased attack is the proliferation of communication channels and information paths. The key concept of the Smart Grid, shown in Figure 69, is that devices are able to communicate with each other to increase efficiency, resiliency, and integration of renewable resources.

Figure 69: Communication Domain

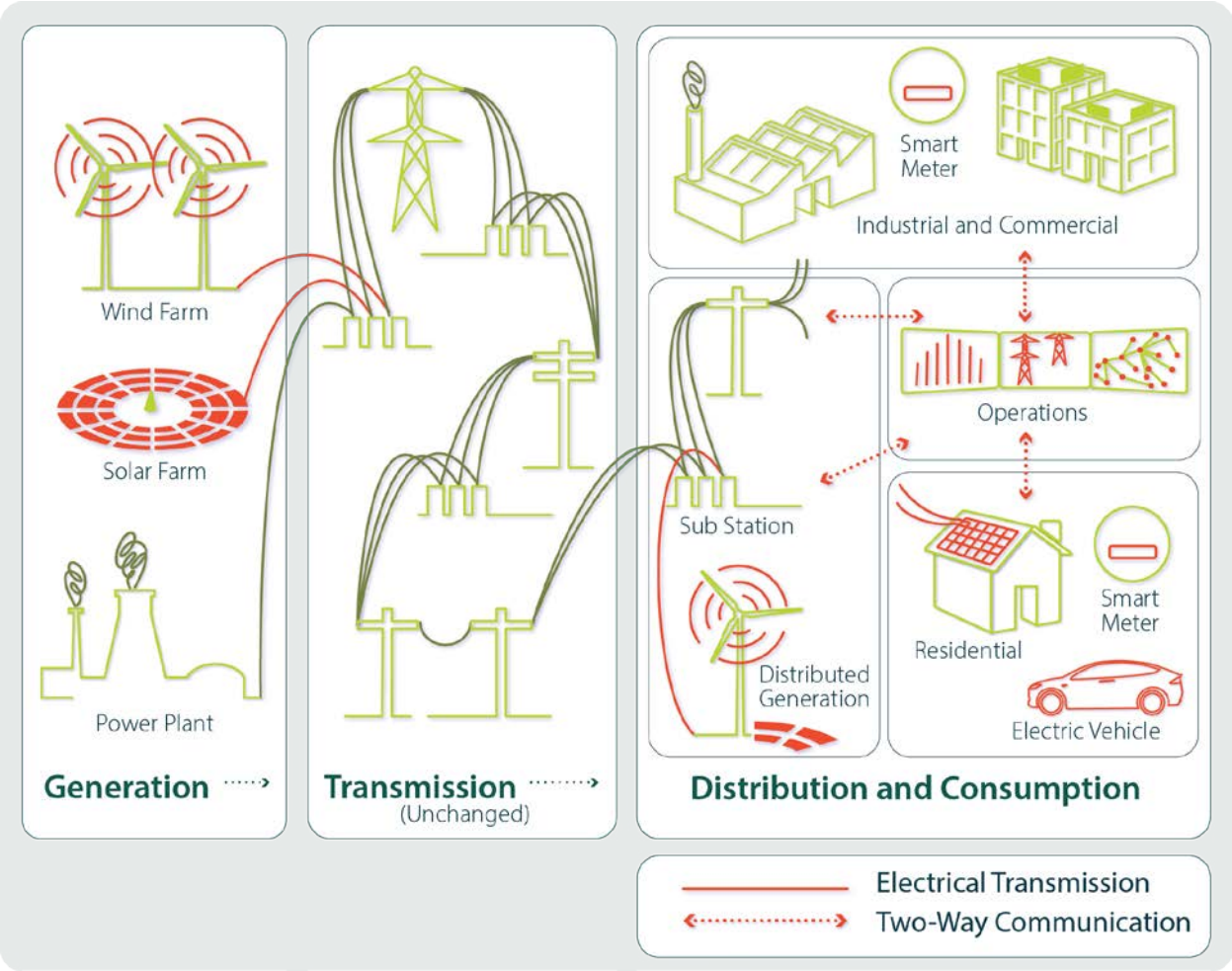

Figure by: CSGC – Deborah Frost and Shanna Rossi

With each new communication channel or data point, the attack surface grows and the more complex the risk management structure becomes.

Each of the Smart Grid domains has their own characteristics.

- SCADA

  These devices usually have some form of traditional operating system, such as Windows or Linux, and they communicate over traditional IP networks, encapsulating control systems protocols such as serial data, ICCP, ModBus, and DNP3.

- Demand Response
- AMI
- Customer Domain

- Gateway
- Home Area Network (HAN)

  Because data and information are sent through the wireless network, hackers could potentially breach into the wireless network and redirect traffic or steal private information, which is why there should be some consideration of the technological impacts of NANs, often called Wireless Neighborhood Area Networks (WNAN).

- Neighborhood Area Network (NAN)

Enhancing Smart Grid Cyber Security

Not surprisingly, there is a great deal of cooperation and information initiatives around Smart Grid cyber security. Private vendors, suppliers, researchers, and academia have all taken part in confronting the challenges, many of them collaborating with government agencies to further the research. For instance, the Energy Sector Control Systems Working Group (ESCSWG), Pacific Northwest National Laboratory (PNNL), and Energetic Incorporated joined forces for research on improving the energy delivery system. The DOE Office of Electricity Delivery and Energy Reliability Cybersecurity for Energy Delivery Systems (CEDS) program funded this group's effort. In this program they worked with energy providers, national laboratories, universities, and other federal agencies to ensure a more secure and resilient power grid. The scope of the collaboration was significant, including:

- U.S. Department of Homeland Security (DHS) Industrial Control Systems Cyber Emergency Response Team (ICS-CERT)
- Duke Energy
- Edison Electric Institute (EEI)
- Electric Power Research Institute (EPRI)
- Federal Energy Regulatory Commission (FERC)
- Independent Electric System Operator (IESO)
- Utilities Telecom Council (UTC)

Along with contributions from the American Public Power Association (APPA), American Gas Association (AGA), and Idaho National Laboratory (INL), the ESCSWG, PNNL, and Energetic Incorporated researched and established a new guidance for the energy industry to implement cybersecurity protections into power delivery systems.

Published in April 2014, the guidance "Cybersecurity Procurement Language for Energy Delivery Systems" provides strategies as well as suggested language that energy suppliers can use during contract and vendor negotiations in product design and manufacturing to enhance cybersecurity protections for a stronger and securer electric grid. The document was created as

a guideline for companies to reduce security risks by ensuring proper wording and understanding between entities and vendors.

Another major association guiding Smart Grid interoperability standardization is the Institute of Electrical and Electronic Engineers (IEEE). IEEE is the world's largest technical professional society dedicated to advancing technology. IEEE has more than 100 standards related to Smart Grid and more than 20 IEEE standards have been identified in the NIST Framework and Roadmap for Smart Grid Interoperability Standards, Release 1.0. (National Institute of Standards and Technology, U.S. Department of Commerce 2012) The standards currently in progress include: (Charlton, W.C., IEEE SMART GRID n.d.)

- IEEE P2030 Draft Guide for Smart Grid Interoperability of Energy Technology and Information Technology Operation with the Electric Power System (EPS), and End-Use Applications and Loads
- IEEE 802 LAN/MAN Standards Series
- IEEE SCC21 1547 Standards for Interconnecting Distributed Resources with Electric Power Systems
- IEEE Standard 1159 for Monitoring Electric Power Quality
- IEEE Standard 762: Standard Definitions for Use in Reporting Electric Generating Unit Reliability, Availability, and Productivity, and
- IEEE SCC 31 Automatic Meter Reading and Related Services.

Another industry alliance focused on improving the Smart Grid infrastructure and standardizing Smart Grid related technology is ZigBee Alliance. They are working towards standardizing Smart Grid Neighborhood Area Networks to improve interoperability between utilities and product manufacturers. In January 2014 they announced that a "group of leading smart metering and Smart Grid member companies are developing a communication profile aimed at achieving true plug-and-play interoperability between the member's wireless Smart Grid Neighborhood Area Network (NAN) products and solutions." (CHW Staff, Connected Home World 2014) Moreover, ZigBee standards have been integrated into Smart Grid's system to monitor, control, inform, and automate the transfer and use of energy. Other ZigBee standards include:

- ZigBee Building Automation (Efficient commercial spaces)
- ZigBee Remote Control (Advanced remote controls)
- ZigBee Smart Energy (Home energy savings)
- Smart Energy Profile 2 (IP-based home energy management)
- ZigBee Home Automation (Smart homes)

Perhaps the most salient standard to come out of the ZigBee Alliance has been the release of SEP 2.0. This standard decouples the energy profile from the transport mechanism, making the

energy management features of the protocol stack transportable between different communication methods, such as 802.15.4, WiFi, WiMax, or IPv6 and Ethernet. Unfortunately for California, the IOU's have installed meters that are ZigBee SEP 1.x compatible and aren't likely to be upgraded any time soon. (Loria, Tatro, et al. 2014)

Universities have also been called on to assist utilities, government, policy makers, technology providers, and other critical organizations with exploring solutions and developing tools to support industry. They provide a unique capability in researching essential topics related to improving Smart Grid cybersecurity, and the US government has funded a number of universities. Several key organizations recognized as research centers for the Smart Grid:

- California State University, Sacramento (CSUS):

  California State University, Sacramento (CSUS) focuses on encouraging consumption of renewable energy sources in order to improve the electricity delivery systems. The CSUS's focuses of research are grid cyber security, sensors and home area networks, and electrical energy transmission and distribution. (California State University, Sacramento 2015)

- University of California, Los Angeles (UCLA):

  The UCLA Smart Grid Energy Research Center (SMERC) "performs research, creates innovations, and demonstrates advanced wireless/communications, Internet and sense-and-control technologies to enable the development of the next generation of the electric utility grid – The Smart Grid." SMERC's current focuses are Automated Demand Response, Electric Vehicle integration (G2V and V2G), Microgrids, Distributed and renewable integration, and Cybersecurity. (University of California, Los Angeles 2015)

- Carnegie Mellon University (CMU):

  The Energy Research Initiative (ERI) at CMU will be addressing the need for smart alternative energy sources. Managed by the Semiconductor Research Corporation (SRC), the ERI will address efficient generation and distribution of renewable energy sources: photovoltaics and systems engineering, and technologies to enable and optimize Smart Grids. (Carnegie Mellon University 2015)

- The University of Texas at Austin:

  The Center for Electromechanics (CEM) at the University of Texas at Austin is collaborating with Austin Energy and Pecan Street, Inc., to anticipate the challenges of Smart Grids. (University of Texas, Austin 2015)

- Purdue University:

  Purdue University, in partnership with Ivy Tech Community College, was funded by the Department of Energy to create an education and training program that will minimize the gap between education and workforce in the electric energy sector. (Purdue University, Discovery Park 2015)

Conclusions – Grid Cyber Security Issue Identification

Smart Grid, a somewhat nebulous term, identifies a collection of concepts and services rather than a defined collection of assets. These services—delivered by many independent devices capable of communicating with multiple partners, in multiple ways—are what the Federal Title XIII calls the Smart Grid. It is also important to remember that the term "Smart Grid" is defined by different concepts depending on a user's perspective. To the consumer, it is the smart devices that help reduce energy usage through smart thermostats and home gateways that report on Time-of-Day pricing. To the utilities, it is the demand response infrastructure that helps stabilize the distribution grid as islands of microgeneration are brought on line. What these devices are capable of doing and how they are helping shape the energy future is what defines the Smart Grid.

In many ways, the security concerns of the Smart Grid are analogous to the security concerns shared by traditional Information Technology (IT) and the concerns shared by the end consumer. From the utility point of view, there is a separation of duties between IT and Operations Technology (OT), but much of that can be boiled down to operational availability and the requirements for support and safety, and the basic approaches to security can be shared across all three domains – consumer, IT, and OT. Another key difference, and area of concern for the Smart Grid and its associated devices, is the class of devices that don't fall specifically into the traditional IT model – i.e., devices that present attack vectors but tend to be embedded in nature such as smart meters, demand response devices, and home gateways. These devices don't always lend themselves to security updating and vulnerability patching. Some of these issues tend to be self-mitigating, such as the ZigBee protocol used by the smart meters and the inherent security it employs, while others, such as the customer premise network gateway, tend to rely more on the measures employed by the consumer.

The commonality between the different environments, primarily utility entities and consumers, is a concept of risk mitigation through protection, detection, and response. The end user should follow some form of information security best practices for the home, of which there are many sources of basic practices. The website OnguardOnline.gov presents many useful and practical solutions that are written at a level the average consumer can digest without having a highly technical background. For the utility, the story is somewhat more complex. As mentioned, there are numerous NIST publications that are relevant – NIST SP800-82 "Guide to Industrial Control Systems Cybersecurity," NISTIR 7628 "Guidelines for Smart Grid Cybersecurity," and many, if not all, of the standard IT best practice approaches that any organization should incorporate as part of their Defense-in-Depth approach.

Researchers expect these approaches and guidelines to continue to evolve as more and more devices connect to the Smart Grid and industry develops approaches for handling them. The Federal Cybersecurity framework released by NIST last year is completely new and is still being assimilated by the various entities. While cybersecurity has been a growing field within IT, it is still nascent in the Industrial Control Systems world, more so in the Smart Grid. This report has only laid a foundation for what is a continually evolving field that requires constant monitoring and the dedicated individuals helping to secure the grid and California's future.

It cannot be overstated that the responsibility for customer data in the customer area network belongs to the customer. Following best practices from websites such as OnguardOnline.gov can help to mitigate that risk. These include using strong encryption on wireless networks, using firewalls and anti-malware, applying security patches, and using strong password techniques as discussed in the body of the report. Above all, it is recommended that customers become actively engaged in the security of the data and their privacy.

Going forward, the final recommendations are for the utilities to consider the possibility of upgrading their smart meters to ZigBee SEP 2.0 compliant hardware and firmware. ZigBee SEP 2.0 offers the possibility of stronger encryption and more robust communication channels. While metering infrastructures typically have lifespans measured in decades, the planning process for the next generation of smartmeters and AMI to support the full implementation of the Smart Grid should begin now. In addition, the standards imposed on utilities as part of the critical infrastructure protection program should be seen as the bare minimum of "due care," and utilities should continually strive to set the bar as high as possible, thereby raising the overall cost for an attacker.

With the due diligence of consumers, utilities, and the supply chain system, a structure of risk mitigation, detection, and deterrence can take the Smart Grid to the next level of security. If the guidelines published by NIST, DOE, etc. are properly implemented, they can give the public the confidence in the Smart Grid that is needed to support the growth and implementation of these technologies. It's through these endeavors that the U.S. and California will continue to strive for, and reach, the goals of maximum renewable penetration in the electric grid, sustainable electric resources, and independence from fossil fuel resources.

CHAPTER 3:
Customer Premise Network Design and Testing

Introduction

This activity examined both the current status of consumer energy management and evaluated some of the potential energy management methodologies applicable to energy consumers. As of the writing of this report in Spring 2015, California IOU's have recently finished installing an estimated 12.5 million smart meters, both electric and gas, throughout their service areas. All of these smart meter models appear to meet or exceed the 2002 CPUC minimum functional requirements; however, with the exception of a limited number of pilot programs, it does not seem that the utilities are yet positioned to maximize the full capabilities of the smart meters primarily due to cyber security concerns. Thus, unfortunately, the important real-time dynamic (TOU, CPP) pricing communication, and demand response signals which can feed compatible applications that educate customers and allow for flexible energy data management, and flexible load control communication are usually missing. While the utilities are aggressively studying the cyber security issues, the smart meters have yet to have their downstream wireless abilities turned on in some cases. This status was confirmed by the IOU's response to the late 2013 telephone survey. Bringing the information possible with the AMI meters to the consumer in a real-time manner is still largely being deferred to the future.

Purpose

Energy use and pricing data that the AMI system can communicate to the consumer is critical feedback to the consumer. Most utilities have some form of delayed energy data with up to a 24-hour lag time, but movement to real-time information is still cautiously being studied by the utilities. With the delayed and, more effectively, with the real-time information, consumers can consciously reduce their energy consumption which results in carbon reduction. Economic studies have shown that with real-time energy usage and pricing being communicated, consumers could reduce 7 percent of their energy use with just real-time usage data. The savings increased to a maximum of 24 percent when real-time-of-use pricing was also included.

The goal was to design and test Customer Premise Networks (CPNs) specifically for residential and commercial buildings. The authors believed that as renewable energy sources are deployed across the various levels of energy users and energy producers, a shift in energy management will be desired. The shift envisioned is to encourage local energy generation (often called DG for distributed generation). Thus, consumers must install a local renewable energy resource and be able to maximize the generation of energy from that resource. At the most simple view, this means that the consumer must have (or have access from) the distributed energy source, information on the current capacity of the energy source which is providing energy to the consumer, a control system that manages this energy for the consumer, and most likely local energy storage that is separate from the power grid for at least some part of the consumer's energy needs.

Central to this need to robustly manage energy at levels not anticipated in the original construction of the power grid, is the need for methods to monitor energy, for channels that communicate the various bits of information needed to act, for systems that can perform these functions on a daily basis with limited user input, and for systems that can optimize the renewable source and not the historic revenue stream of energy from the utility. This is a very energy consumer centric viewpoint that seems to best fit the increasing reliance on distributed generation.

The research approach was to create a laboratory on the campus of CSU, Sacramento (Sac State) in Riverside Hall. This laboratory was equipped with test equipment and staffed with both faculty and student researchers. Research was then performed that examined the information, control, and energy flow aspects of consumer management of energy. Heating and cooling (HVAC) is a large fraction of a consumer's energy use and the researchers devoted a large portion of the effort in determining how distributed generation will impact HVAC. Lighting and plug level loads used by appliances were also considered and examined in the laboratory. One major aspect that was not tested was energy storage. There are two factors that deprioritize energy storage. First, the need for consumer based energy storage seems to be some years off. Second, the cost of energy storage needs to come down to competitive levels versus just using the utility as the alternate source when the consumer's DG is not available.

The activities centered on the laboratory based design and test. Researchers designed and tested sensor systems that harvested ambient light and thus never needed external power. They also created sensor systems (light level, temperature, humidity and occupancy detection) that could communicate these values to a central processing unit. Data from a utility (SMUD) provided insolation (sunlight energy measurements) and weather data device located on the roof of Riverside Hall. This outside data was then fed into an energy model based on Matlab's Simulink software that provided information on the likely ability to harvest information from a local photovoltaic source.

Conclusions - Customer Premise Network Design and Testing

California IOU's have recently finished installing an estimated 12.5 million electric and gas smart meters throughout their service areas. All of these smart meter models appear to meet or exceed the 2002 CPUC minimum functional requirements; however, with the exception of a limited number of pilot programs, it does not seem that the utilities are yet positioned to maximize the full capabilities of the smart meters primarily due to cyber security concerns. Thus, unfortunately, the important real-time dynamic (TOU, CPP) pricing communication, and demand response signals which can feed compatible applications that educate customers and allow for flexible energy data management, and flexible load control communication are usually missing. While the utilities are aggressively studying the cyber security issues, the smart meters have yet to have their downstream wireless abilities turned on in some cases. This status was confirmed by the IOU's response to the late 2013 telephone survey. Bringing the information possible with the AMI meters to the consumer in a real-time manner is still largely being deferred to the future.

Energy use and pricing data that the AMI can communicate is critical feedback to the consumer. Most utilities have some form of delayed energy data with usually a 24 hours lag time. But moment to real-time information is still cautiously being studied by the utilities. With both the delayed and, more effectively, with the real-time information, the consumer can consciously reduce their energy consumption which results in carbon reduction. Economic studies have shown that with real-time energy usage and pricing being communicated, consumers could reduce 7 percent of their energy usage with just real-time usage data. The savings increased to a maximum of 24 percent when real-time-of-use pricing was also included.

This real time data communication is also paramount to renewable integration. Real-time data allows for advanced monitoring of utility generation equipment and, when combined with HAN tools, can be used to control the instability that renewable energy generation might cause on the grid. On the consumer side, the real-time data communication forms the backbone of an automated robust energy management system for the residential home when combined with the proper HAN devices.

Whether the tool set available to consumers is called *Customer Premise Networks* (CPN) or *Home Area Networks* (HAN), it is the ability to manage local energy generation and local energy consumption that holds the largest promise from the emerging tool set. In the author's opinion, real time data communication is paramount to renewable integration. Real-time data allows for advanced monitoring of utility generation equipment and, when combined with CPN/HAN tools, can be used to control the instability that renewable energy generation might cause on the grid. On the consumer side, the real-time data communication forms the backbone of an automated robust energy management system for the residential home when combined with the proper CPN/HAN devices.

Industry partners have begun to roll out CPN/HAN devices that are Zigbee enabled and are available for purchase by consumers. As of now, these devices fall into one of three categories: In Home Display, Programmable Communicating Thermostats, or Load Control Devices. Currently, some of these devices have been vetted by the IOU utility companies and validated to work with the IOUs specific AMI smart meter for their region. By creating smart sensors and robust data managements CPN/HAN tools systems integrated with this current grid technology, the i4Energy group has conducted many studies and test experiments that show promising results of consumers saving up to 29 percent in energy consumption with automated control systems fed by real-time energy usage and pricing data.

CHAPTER 4:
Conclusions

Distributed Generation Impacts

In the area of distributed generation impacts, this report discussed the integration of renewable energy in distribution systems and presented the newly introduced challenges of distributed generation impacts. Case studies utilizing typical utility feeders as well as standardized feeders were conducted to display and/or verify the perceived concerns.

Integration of DG from renewable resources promotes a clean and hazard free type of energy. Interconnection of DG at higher levels accelerates meeting the Renewable Portfolio Standard (RPS) goals set by the California legislature. This higher penetration level of renewable energy resources will challenge the system and require more accurate control devices and algorithms.

The project's researchers verified the adverse impacts of the renewable energy integration and proposed possible mitigation measures to alleviate the effects. Operational, protection, and control impacts have been analyzed and results have been documented and publicized. Conceptual studies and formulations for advanced technics such as state estimation have also been considered and documented. The studied cases and possible recommendations are beneficial to the utilities' day-to-day operation and will enhance the quality of the energy being delivered to the end customers. Despite the issues and concerns, research has shown that strategic investments in enabling technologies can greatly increase the distribution network's ability to utilize an increasing level of DG. National Standard IEEE 1547 is a stepping stone to furthering the possibilities of DG integration, along with the IEEE 2030 standards.

Cyber Security Issues

Researchers explained the consumer's cyber security and privacy risks and recommended best practices when using various smart devices around the home. The final recommendations are for the utilities to consider the possibility of upgrading their smart meters to ZigBee SEP 2.0 compliant hardware and firmware. ZigBee SEP 2.0 offers the possibility of stronger encryption and more robust communication channels.

It is expected these approaches and guidelines to continue to evolve as more and more devices connect to the Smart Grid and industry develops approaches for handling them. The Federal Cybersecurity framework released by NIST last year is completely new and is still being assimilated by the various entities. While cybersecurity has been a growing field within IT, it is still nascent in the Industrial Control Systems world, more so in the Smart Grid. This report has only laid a foundation for what is a continually evolving field that requires constant monitoring and the dedicated individuals helping to secure the grid and California's future.

It cannot be overstated that the responsibility for customer data in the customer area network belongs to the customer. Following best practices from websites such as OnguardOnline.gov can help to mitigate that risk. These include using strong encryption on wireless networks, using firewalls and anti-malware, applying security patches, and using strong password

techniques as discussed in the body of the report. Above all, it is recommended that customers become actively engaged in the security of the data and their privacy.

Going forward, the final recommendations are for the utilities to consider upgrading their smart meters to ZigBee SEP 2.0 compliant hardware and firmware. ZigBee SEP 2.0 offers the possibility of stronger encryption and more robust communication channels. While metering infrastructures typically have lifespans measured in decades, the planning process for the next generation of smartmeters and AMI to support the full implementation of the Smart Grid should begin now. In addition, the standards imposed on utilities as part of the critical infrastructure protection program should be seen as the bare minimum of "due care," and utilities should continually strive to set the bar as high as possible, thereby raising the overall cost for an attacker.

Customer Premise Network(CPN)/Home Area Network (HAN)

In the Customer Premise Network(CPN)/Home Area Network (HAN) research, industry partners have rolled out HAN devices that are Zigbee enabled and are available for purchase by consumers. These devices fall into one of three categories: In Home Display, Programmable Communicating Thermostats, or Load Control Devices. Currently, some of these devices have been tested by the utility companies and validated to work with the utilities specific smart meter for their region. Studies and test experiments show promising results of consumers saving up to 29 percent in energy consumption with automated CPN/HAN control systems fed by real-time energy usage and pricing data.

Energy use and pricing data communicated by the AMI is critical feedback to the consumer. Most utilities have some form of delayed energy data with usually a 24 hours lag time. But moment to real-time information is still cautiously being studied by the utilities. With both the delayed and, more effectively, with the real-time information, the consumer can consciously reduce their energy consumption which results in carbon reduction. Economic studies have shown that with real-time energy usage and pricing being communicated, consumers could reduce 7 percent of their energy use with just real-time use data. The savings increased to a maximum of 24 percent when real-time-of-use pricing was also included. (Foster and Mazur-Stommen 2012)

This real time data communication is also paramount to renewable integration. Real-time data allows for advanced monitoring of utility generation equipment and, when combined with HAN tools, can be used to control the instability that renewable energy generation might cause on the grid. On the consumer side, the real-time data communication forms the backbone of an automated robust energy management system for the residential home when combined with the proper HAN devices.

GLOSSARY

Term	Definition
Advanced Metering Infrastructure	A set of technologies that extend automatic meter reading with two-way communication. Among other capabilities, allows for consumer-informed time variant pricing.
Backhaul	In a network, the data link between a remote device or a subnetwork and the core of the network. In the context of smart grid communications, refers to the channel by which automatic meter reading or advanced metering infrastructure equipment communicates usage information from the consumer to the utility.
California Public Utilities Commission	The California government agency responsible for regulating common carriers and public utilities.
California Smart Grid Center (CSGC)	A research facility hosted by the College of Engineering and Computer Science at the California State University, Sacramento. The CSGC is chartered by the California Energy Commission to research and develop technologies to enable the adoption of renewable energy.
Compact Fluorescent Lamp (CFL)	A lighting technology that incorporates a narrow, folded fluorescent tube and electronic ballast in the form factor of a traditional incandescent bulb.
Concentrated Solar Power (CSP)	A system that produces electrical power by focusing sunlight to create heat, which is used to drive turbines. Contrasts with photovoltaic (PV) power.
Critical Peak Pricing (CPP)	A time variant pricing mechanism in which the rate assessed for electrical power increases to a large extent during announced periods of power grid stress. Used to encourage load shedding.
Customer Premises Network (CPN)	The set of locally networked technologies that relate to energy production, use, control, and monitoring.
Energy Service Provider Interface (ESPI)	A standard data format for customer meter data, designed and promoted by the North American Energy Standards Board.
Energy Storage	In the context of power generation systems, any technology, appliance, or device which allows time displacement between power generation and power usage. Obvious examples include general-purpose electrical storage like batteries and flywheel storage. Nonobvious examples include electric water heaters, which use electrical energy, store that energy as heat, and provide that heat energy at a later time.

EPIC	Electric Program Investment Charge
Extensible Markup Language (XML)	A standard for expressing arbitrary data in a structured format, using plain text for communication.
Flat Rate Pricing	The tariff structure under which electrical power is assessed at the same rate, regardless of the circumstances of use. In practice, this structure has been displaced by tiered pricing.
Heating, Ventilation, and Air Conditioning (HVAC)	The set of technologies, also known as climate *control*, which are used to regulate interior air quality for occupant health and comfort. In residential locations, HVAC is most often the largest use of energy.
In-Home Display (IHD)	A smart energy device that presents energy usage data, billing information, rate structures, and notifications to the residential user.
Light emitting diode (LED)	A solid-state device that produces light directly from the flow of electricity. Now used in high-efficiency residential and commercial lighting.
Load shedding	The removal of load from the power grid during times of high demand or during emergencies. May be implemented by demand response, critical peak pricing, or real-time pricing. See also peak shaving.
Load shifting	The scheduling of load usage away from times of peak overall usage, especially in favor of times of peak renewable generation. See also peak shaving.
Open Automatic Data Exchange (OpenADE)	A task force of the Open Smart Grid User's Group which works to promote sharing of data between utilities, consumers, and third parties. Promotes the ESPI standard.
Peak shaving	Any of a variety of measures taken to reduce overall usage during times of peak pricing. Includes both load shedding and load shifting strategies.
Photovoltaic (PV)	A system that produces electrical power directly from sunlight. Derives from the photovoltaic effect that converts electromagnetic energy directly to electromotive potential. Contrasts with concentrated solar power (CSP).
Real time pricing (RTP)	A time variant pricing structure under which the rate assessed for electrical power varies according the actual market price for power at the time of use. Used to encourage both load shifting and load shedding.
Smart Grid	Smart Grid is the thoughtful integration of intelligent technologies and innovative services that produce a more efficient, sustainable,

	economic, and secure electrical supply for California communities.
Tiered pricing	Also tiered rate pricing or tiered structure pricing. The tariff structure for electrical power in which the rate assessed varies between discrete values according to the amount of energy used during an invoice period or according to the peak power used. May encourage load shifting to reduce peak power. Contrasts with, but may be implemented concurrently with, time variant pricing.
Time of use (TOU)	A time variant pricing structure under which the rate assessed for electrical power varies according to published schedules which model the market price for power. Used to encourage load shifting.
Time variant pricing	Any of a variety of tariff structures for electrical power in which the rate assessed varies with the time at which the power is used. Used to encourage load shifting. Contrasts with, but may be implemented concurrently with, tiered pricing.
Universal Smart Network Access Port (USNAP)	A standard for interfacing smart energy devices with varying networks. Jointly published as ANSI/CEA-2045.

COMMONLY USED ACRONYMS

Acronym	Definition
AMI	Advanced Metering Infrastructure
ANSI	American National Standards Institute
BES	Bulk Electric System
BESS	Battery Energy Storage System
BEV	Battery [powered] Electric Vehicle
BPL	Broadband over Power Lines
BTU	British Thermal Unit
CCTF	California Cybersecurity Task Force
CFL	Compact Fluorescent Lamp
CHP	California Highway Patrol
CIA	Confidentiality, Integrity and Availability [hierarchy]
CIEE	California Institute for Energy and Environment
CIP	Critical Infrastructure Protection [Standards]
CIS	Customer Information System
CITRIS	Center for Information Technology Research in the Interest of Society
CPN	Customer Premises Network
CPP	Critical Peak Pricing
CPUC	California Public Utilities Commission
CSGC	California Smart Grid Center
CSI	California Solar Initiative
CSP	Concentrated Solar Power
CSR	Customer Service Representative
CSU	California State University
CSWG	[NIST] Cyber Security Working Group

CVE	Common Vulnerabilities and Exploits
DCS	Distributed Control System
DER	Distributed Energy Resources
DG	Distributed Generation
DHS	U.S. Department of Homeland Security
DMA	Distribution Management Systems
DMZ	Demilitarized Zone [as part of computer security]
DOE	U.S. Department of Energy
DR	Demand Response
DRMS	Demand Response Management System
EIA	[U.S.] Energy Information Administration
EISA	Energy Independence and Security Act [of 2007]
EMS	Energy Management Systems
ESCSWG	Energy Sector Control Systems Working Group
ESP	Energy Service Provider
ESPI	Energy Service Provider Interface
EUMD	Energy Usage Metering Device
EVSE	Electric Vehicle Service Element
GIS	Geographic Information System
HAN	Home Area Network
HVAC	Heating, Ventilation, and Air Conditioning
ICS-CERT	Industrial Control Systems Cyber Emergency Response Team
IED	Intelligent Electronic Device
IEEE	Institute of Electrical and Electronics Engineers
IHD	In-Home Display
IoT	Internet of Things
IOU	Investor Owned Utility

IP	Internet Protocol
ISO	Independent System Operator
IT	Information Technology
kW	kilo Watt [kilo = thousand]
LBNL	Lawrence Berkeley National Laboratory
LCS	Load Control Services
LED	Light Emitting Diode
LMS	Load Management Systems
MDMS	Meter Data Management System
MPPT	Maximum Power Point Tracking
MW	Mega Watt [Mega = Million]
NAN	Neighborhood Area Network
NAS	National Academy of Sciences
NDA	Non-Disclosure Agreement
NERC	North American Electric Reliability Corporation
NIST	National Institute of Standards and Technology
NISTIR	NIST Interagency or Internal Report
NSHP	New Solar Home Partnership
OMS	Outage Management System
OT	Operational Technology
P&O	Perturb and Observe
PCT	Programmable Communication Thermostats
PCT	Programmable Communicating Thermostat
PEV	Plug-in Electric Vehicles
PG&E	Pacific Gas & Electric
PH&EV	Plug-in Hybrid and Electric Vehicles
PII	Personally Identifiable Information

PLC	Programmable Logic Controller
PMU	Phasor Measurement Unit
PPA	Power Purchase Agreement
PV	Photovoltaic
RECS	Residential Engery Consumption Survey
REG	Residential Energy Gateway
RF	Radio Frequency
ROI	Return on Investment
RPS	[California] Renewables Portfolio Standard
RTO	Regional Transmission Organization
RTP	Real Time Pricing
RTU	Remote Terminal Unit
SCADA	Supervisory Control and Data Acquisition
SCE	Southern California Edison
SDG&E	San Diego Gas & Electric
SEP	Smart Energy Profile
SIMM	[California] Statewide Information Management Manual
SMUD	Sacramento Municipal Utility District
SSL	Secure Sockets Layer
T&D	[Electrical Power] Transmission and Distribution
TCP	Transmission Control Protocol
TOD	Time of Day
TOU	Time of Use
TPO	Third Party Operators
UC	University of California
US	United State [of America]
USNAP	Universal Smart Network Access Port

VRT	Voltage Ride-Through
WAL	Wireless Adaptive Lighting
WAMS	Wide Area Measurement System
Wi-Fi	[Trademarked name] for local area wireless technology
WLAN	Wireless Local Area Network
WMS	Work Management System
WPA	Wi-Fi Protected Access
XML	Extensible Markup Language

REFERENCES

Afzal, M., M. Zarghami, and A. Yazdani. "Voltage Impacts of DG on Distribution Grid with Voltage Regulators and SVCs." *2013 Annual IEEE Green Technologies Conference.* 2013. 322-329.

AlRuwaili, M. O., M. Y. Vaziri, S. Vadhva, and S. Vaziri. "Impact of Wind Generation Variability on Voltage Profile of Radial Power Systems." *Proceedings of the IEEE Green Technologies Conference.* Denver, 2013.

Bowers, Brad. "ZigBee Wireless Security: A New Age Penetration Tester's ToolKit." Cisco. January 9, 2012. http://www.ciscopress.com/articles/article.asp?p=1823368&seqNum=4.

California Energy Comission. "www.energy.ca.gov." 2014. http://www.energy.ca.gov/glossary/glossary-t.html.

California State University, Sacramento. "California Smart Grid Center." 2015. http://www.ecs.csus.edu/csgc/index.html.

Carnegie Mellon University. "[Smart Grid] Center to be Housed at CMU." 2015. http://www.cmu.edu/homepage/environment/2010/summer/smart-grid-research.shtml.

Charlton, W.C., IEEE SMART GRID. "IEEE has the expertise to make smart grid a reality." n.d. http://smartgrid.ieee.org/ieee-smart-grid (accessed 2015).

Chee Wie Tan, T.C. Green, and C.A. Hernandez-Aramburo. "Analysis of perturb and observe maximum power point tracking algorithm for photovoltaic applications." *2nd IEEE International Conference on Power and Energy (PECon 08).* 2008.

CHW Staff, Connected Home World. "ZigBee Wants To Standardize Smart Grid Neighborhood Area Networks (NAN)." January 27 2014. http://www.connectedhomeworld.com/content/zigbee-smart-grid-nan.

Foster, B., and Susan Mazur-Stommen. "Results from Real-Time Feedback Studies." February 2012. http://www.aceee.org/sites/default/files/publications/researchreports/b122.pdf.

Fu, W., L. Nie, M. Vaziri, and M. Zarghami. *Relay Desensitization Due to Increased Penetration of Distributed Generation, Master's Thesis.* California State University, Sacramento, 2015.

Ghansah, Isaac. "CATEGORIZING RESEARCH AND DEVELOPMENT ISSUES FOR CYBER SECURITY IN THE SMART GRID INTO CONFIDENTIAL AND NON-CONFIDENTIAL." May 2014. http://www.energy.ca.gov/2014publications/CEC-500-2014-051/CEC-500-2014-051.pdf.

Loria, William. *Energy Flow System.* Sacramento: California Smart Grid Center, 2014.

Loria, William, Russ Tatro, Suresh Vadhva, and Emir Macari. *Report on the use of CPN Tools.* Sacramento: California Energy Comission, 2014.

National Institute of Standards and Technology, U.S. Department of Commerce. "NIST Framework and Roadmap for Smart Grid Interoperability Standards Release 2.0." February 2012. http://www.nist.gov/smartgrid/upload/NIST_Framework_Release_2-0_corr.pdf.

Nie, L., W. Fu, M. Vaziri, and M. Zarghami. "Higher I-2t Stress on Equipment Due to Increased Penetration of Distributed Generation." *IEEE – PES 2016 General Meeting Conference.* Denver, 2016.

Office of Electricity Delivery and Energy Reliability. "www.energy.gov." 2014. http://energy.gov/oe/technology-development/smart-grid/recovery-act-smart-grid-investment-grants.

Office of the National Coordinator for Smart Grid Interoperability. "NIST Framework and Roadmap for Smart Grid Interoperability Stands, Release 1.0." January 2010. http://www.nist.gov/public_affairs/releases/upload/smartgrid_interoperability_final.pdf.

Purdue University, Discovery Park. "Purdue Smart Grid Initiative." 2015. http://www.purdue.edu/discoverypark/energy/research/efficiency/smart-grid.php.

Rahimi, A., M. Zarghami, M. Vaziri, and S. Vadhva. "A Simple and Effective Approach for Peak Load Shaving Using Battery Storage Systems." *North American Power Symposium (NAPS).* 2013. 1-5.

Rahimi, Ali, Ana Cloninger, M. Zarghami, and M. Vaziri. "Investigation on Volt-VAr control using CVR at various photovoltaic penetration levels." *North American Power Symposium (NAPS).* 2014. 1-5.

Shabaninia, F., M. Vaziri, M. Amini, and M. Zarghami. "Kalman-Filter Algorithm and PMUs for State Estimation of Distribution Networks." *2014 IEEE 15th International Conference on Information Reuse and Integration (IRI).* 2014. 868-873.

Shabaninia, F., M. Vaziri, S. Vadhva, and J. Vaziri. "A Novel State Estimation Formulation for Distribution Grids with Renewable Energy Sources." 2012. 1-5.

Smart Grid Today. "Survey finds energy firms taking cyber threat seriously." May 20, 2014. http://www.smartgridtoday.com/public/Survey-finds-energy-firms-taking-cyber-threat-seriously.cfm.

St. John, Jeff. "5 Tips to Cybersecure the Power Grid." April 25, 2014. http://theenergycollective.com/jeffstjohn/371656/5-tips-cybersecure-power-grid.

Todd, Brian; CNN News. "Utilities hack may affect your power." n.d. http://www.cnn.com/video/data/2.0/video/us/2014/05/22/tsr-dnt-todd-public-utility-hacked.cnn.html (accessed 2015).

University of California, Los Angeles. "Smart Grid Energy Research Center." 2015. http://smartgrid.ucla.edu/about.html.

University of Texas, Austin. "Center for Electromechanics." 2015. http://www.utexas.edu/research/cem/smartgrid.html.

Vaziri, Mohammad, Mahyar Zarghami, and Atousa Yazdani. "Review of Concepts to Increase Distributed Generation into the Distribution Network." *2014 Sixth Annual IEEE Green Technologies Conference.* 2014. 118-125.

Waits, Julian, ThreatTrack Security. "Two immediate steps to improve your Smart Grid cybersecurity (from an expert)." April 29, 2014. http://www.smartgridnews.com/artman/publish/Technologies_Security/Two-immediate-steps-to-improve-your-smart-grid-cybersecurity-from-an-expert-6500.html#.U7HCofldVqU.

Zarghami, M., B. Kaviani, F. Tavatli, and M. Vaziri. "Complex power optimization of photovoltaic systems." *2014 IEEE PES General Meeting, Conference & Exposition*, 2014: 1-5.

Zarghami, M., M. Y. Vaziri, A. Rahimi, and S. Vadhva. "Applications of Battery Storage to Improve Performance of Distribution Systems." *IEEE Green Technologies Conference.* 2013. 345-350.

—. "Applications of Battery Storage to Improve Performance of Distribution Systems." *Proceedings of the IEEE Green Technologies Conference.* Denver, 2013.

Appendix A:
DG Sizing Optimization

In this section, a simple formulation of the optimization problem is introduced. In this formulation, only PV inverters participate in the optimization process. This is a simplistic approach, but our goal is to show how changing the settings of PV inverters through a supervisory management system can effectively reduce the total demand of a utility. In the distribution system, depending on the time of the day and irradiance level of the sun, each PV system is capable of injecting a certain amount of active power. Under most circumstances, the practice is to generate as much active power as possible using Maximum Power-Point Tracking (MPPT) techniques. In the Complex Power Optimization problem however, it is desired to share the total capacity of power generation between active and reactive powers. This practice can be implemented through modulation of the inverters. By proper modulation, it is possible to create a phase shift between voltage and current waveforms on the AC side. As a result of this phase-shift, reactive power can be absorbed or injected by the inverter. However, since there is a limitation on the maximum current that can be tolerated by the switches in the inverter, active power generation needs to be reduced from its maximum value. A simple, yet practical approach is to equalize the maximum possible active power generation with the maximum apparent power at the inverter, which means that the trajectory of the complex power injected will be on the circumference of the semicircle as shown in Figure 1.

Figure 70: Schematics of the share between active and reactive powers

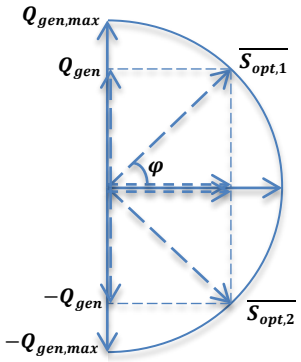

As seen in Figure 1, if maximum active power P_{max} is generated, no reactive power can be generated or absorbed. Alternatively, if maximum reactive power is generated or absorbed, no active power can be generated by the inverter. Through complex power optimization, it is desired to find the optimum value of active and/or reactive power for each PV during each period such that the total demand of the system viewed from the main substation is minimized. Based on optimization, a PV system may work in the first quarter of Figure (17) ($\overline{S_{opt,1}}$) where reactive power is generated, or in the fourth quarter ($\overline{S_{opt,2}}$) where reactive power is absorbed.

In this work, the focus is on complex power optimization for PV distributed generations, although a similar approach can be implemented for other types of controllable DGs. In a certain period, it is assumed that all load values, as well as other operational conditions of the system, such as values of capacitors and settings of voltage regulating devices are known and fixed. Moreover, the apparent power for each PV system is assumed to be known. Under these circumstances, the total apparent power demand of the distribution system can be written as a function of the power factor angles of the inverters as shown below:

$$S_{demand} = f(\varphi_1, \varphi_2, \dots, \varphi_{nPV})$$

The n_{PV} is the number of PV systems and φ_i represents their power factor angle.
Constraints of the optimization problem can be defined as:

$$P_i \geq 0 \qquad for\ i = 1, 2, \dots, n_{PV}$$

$$V_{min} \leq V_i \leq V_{max} \qquad for\ i = 1, 2, \dots, n$$

$$I_i \leq I_{i,max} \qquad for\ i = 1, 2, \dots, m$$

Constraint ($P_i \geq 0$ for $i = 1, 2, \dots, n_{PV}$) indicates that all PV systems must generate active power. Constraint ($V_{min} \leq V_i \leq V_{max}$ for $i = 1, 2, \dots, n$ 7) dictates that voltages in all system buses must be within their minimum and maximum limits. Constraint ($I_i \leq I_{i,max}$ for $i = 1, 2, \dots, m$) requires that the currents (I_i) in all system branch currents must be smaller than their maximum limits ($I_{i,max}$). In the above equations, n and m are the number of system buses and branches, respectively.

The cost function in ($S_{demand} = f(\varphi_1, \varphi_2, \dots, \varphi_{nPV})$) is nonlinear. One of the methods for estimating this equation is through B-coefficients, which provide a means for finding a loss function based on generator active power inputs. This method can be extended for estimating reactive power losses for further evaluation of the total apparent power demand. The loss coefficients found in this method, however, depend on the working conditions of the system and can vary with different generations. As a result, in this work it was decided to utilize an implicit method for evaluation of ($S_{demand} = f(\varphi_1, \varphi_2, \dots, \varphi_{nPV})$) through repetitive power flow solutions conducted inside a nonlinear optimization engine. The engine used for this purpose is named *fmincon*, which finds the minimum of a constrained nonlinear multivariable function in MATLAB. *Fmincon* uses one of four algorithms: *active-set*, *interior-point*, *sequential quadratic programming (sqp)*, or *trust-region-reflective*. Among these algorithms, *trust-region-reflective* and *interior-point* are large-scale algorithms, i.e., they deploy sparse matrices, whereas the other two, *sqp* and *active-set* are medium-scale. In this work, the default *trust-region-reflective* cannot be used, since it needs to be supplied with the gradient of objective function (which is not explicitly known). In our work, *interior-point* method was used because it can potentially handle bigger systems due to its large-scale structure. Among existing options for calculation of the Hessian matrix, the default option was chosen which evaluates the Hessian by a dense quasi-Newton approximation. This option is appropriate for an implicit cost

function, since the Hessian matrix does not need to be explicitly provided in the optimization problem.

APPENDIX B:
Distribution State Estimation Including Renewable Energy Sources

From a mathematical point of view, the DSE problem is an optimization problem with equality and inequality constraints. The objective function to be minimized is the summation of differences between the measured and calculated values. DSE including the RES can be formulated as follows:

$$Min \quad f(X) = \sum_{i=1}^{m} \omega_i (z_i - h_i(X))^2$$

$$X = [\overline{P_G}, \overline{P_{Load}}]_{1 \times n}$$

$$\overline{P_G} = [P_G{}^1, P_G{}^2, ..., P_G{}^{Ng}]$$

$$\overline{P_L} = [P_{Load}^1, P_{Load}^2, ..., P_{Load}^{N_L}]$$

$$n = N_g + N_L$$

Where:

X is the state variable's vector including the loads' and RES' outputs.

z_i is the measured values.

ω_i is the weighting factor of the i^{th} measured variable.

h_i is the state equation of the i^{th} measured variable.

m is the number of measurements.

N_g is the number of RES with variable outputs.

N_L is the number of loads with variable outputs.

$P_G{}^i$ is the active power of the i^{th} RES.

P^i_{Load} is the active power of the i^{th} load.

N is the number of state variables.

Constraints

Constraints are defined as follows:

- Active power constraints of RES:

$$P^{i}_{G,min} \le P^{i}_{G} \le P^{i}_{G,max} \qquad i = 1,2,3,...N_g$$

$P^{i}_{G,max}$ and $P^{i}_{G,min}$ are the maximum and minimum active power of the i^{th} RES, respectively

- Distribution line limits:

$$\left|P_{ij}^{Line}\right| < P_{ij,\max}^{Line}$$

$\left|P_{ij}^{Line}\right|$ and $P_{ij,\max}^{Line}$ are the absolute power flowing over distribution lines and the maximum transmission power between the nodes *i* and *j,* respectively

- Tap on voltage regulating transformers:

$$Tap_i^{\min} < Tap_i < Tap_i^{\max} \quad i = 1, 2, \ldots, N_t$$

$Tap_i^{\min}$, $Tap_i^{\max}$ and Tap_i are the minimum, maximum and current tap positions of the i^{th} transformer, respectively. N_t is the number of voltage regulating transformers installed along feeder

- Bus voltage magnitude

$$V_{\min} \le V_i \le V_{\max} \qquad \mathrm{i} = 1,2,3,\ldots,\mathrm{N_b}$$

V_i , V_{max}, V_{min} are the actual voltage magnitude of the i^{th} bus, the maximum and the minimum values of voltage magnitudes, respectively. N_b, is the number of buses.

- Active power constraints of loads:

$$P^{i}_{Load,min} \le P^{i}_{Load} \le P^{i}_{Load,max} \quad i = 1,2,3,...N_L$$

$P^{i}_{Load,max}$ and $P^{i}_{Load,min}$ are the maximum and minimum active power of the i^{th} load, respectively.

- Reactive power constraint of capacitors

$$0 \le Q_c^{\,i} \le Q^{i}_{c,max} \quad i = 1,2,3,\ldots,N_C$$

$Q_c{}^i$, $Q^i_{c,max}$ are the reactive power and maximum reactive power of the i^{th} capacitor, respectively. N_c is the number of capacitors installed along feeder.

APPENDIX C:
Peak Shaving and BESS Utilization

As stated above, the peak-shaving algorithm does not depend on system topology or its impedances. Assuming a sliding window, the method re-calculates the average of the aggregated load profile (*Pav*) after each time interval (τ) for the next utilization period (*up*). Then the fair share of each individual battery for charge/discharge will be based on its own capacity compared to the total capacity of BESS devices. This calculation estimates the charging/discharging of the batteries for the next eligible time interval (τ) determined by the utilization factor (*uf*). Utilization factor ($0 \leq uf \leq 1$) is defined as the area designated by energy bars (which is the area to be shaved) over the total area above (or below) the average power line, as shown in Fig. 1. The sliding window gives the system a futuristic approach for peak-shaving, i.e. through repeated calculation of (*Pav*) in each time interval, thus the effects of erroneous load forecasting in peak-shaving will be minimized. In Figure 1, a schematic of the method is depicted, in which the utilization period, energy bars and time intervals are shown. In Fig. 1, P is the aggregated load seen from the main substation. If $uf = 1$, the batteries will be utilized (charged or discharged) all the time. If $uf = 0$, the batteries will not be utilized at all. When *uf* is between these two margins, charge or discharge will only take place in specific time intervals shown by the energy bars. The amount of charged or discharged energy for battery m is found by:

$$\left|E_{bat,m}\right| = \left(SOC_{max,m} - SOC_{min,m}\right) \times \frac{|E_1|}{\sum_{i \in S}|E_i|}$$

Where in above S is the set of all energy bars determined by *uf*.

Based on (1), the absolute charged or discharged power of battery m at the grid side is:

$$\left|P_{bat,m}\right| = \eta_m . \left|E_{bat,m}\right| / \tau$$

The power value in (2) needs to be constrained based on two conditions. The first condition, as shown in (3), limits the power of the BESS to its maximum rate of charge/discharge.

$$\left|E_{bat,m}\right| / \tau \leq P_{max,bat,m}$$

The second condition, as shown in Figure 1 limits the state of charge of the BESS to its minimum (during discharge) or maximum (during charge) intervals, respectively.

$$SOC_{min,m} \leq SOC_m \leq SOC_{max,m}$$

Figure 1: Schematic description of the peak-shaving algorithm

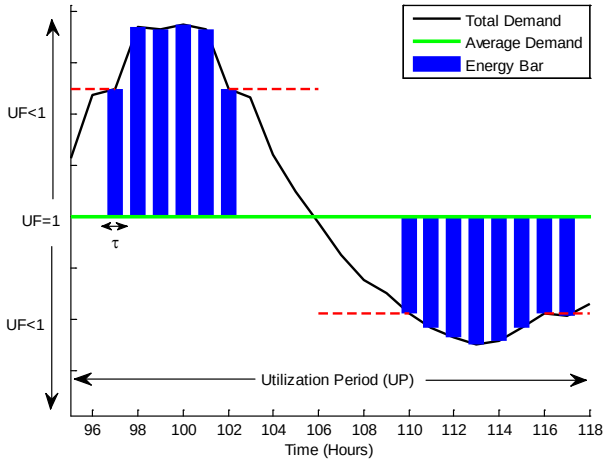

Figure 1 shows an instant of the intersection of the dotted line with the load profile which determines the energy bars used for calculations in the above formula. The dotted line is determined based on the utilization factor.

APPENDIX D:
Design of the Controller for Battery Storage Peak Shaving Functionality

Battery Discharge:

In the discharge mode, as shown in Figure 1, S_1 is kept open at all times, and S_2 is switched by the duty ratio of d. Assuming T to be the period of switching, when $0 < t < d.T$, S_2 is closed, and we have [2]:

$-v_{bat} = L_{dc}.pi_{bat}$
where $p = d/dt$ is the time derivative operator.

When $d.T < t < T$, S_2 is opened, and as a result:
$v_{dc} - v_{bat} = L_{dc}.pi_{bat}$

By averaging the behavior of the converter through weighting factors of d and $1\text{-}d$, we get:
$L_{dc}.pi_{bat} = (1-d)v_{dc} - v_{bat}$

Figure 71: Schematic diagram of the DC/DC converter in discharge mode

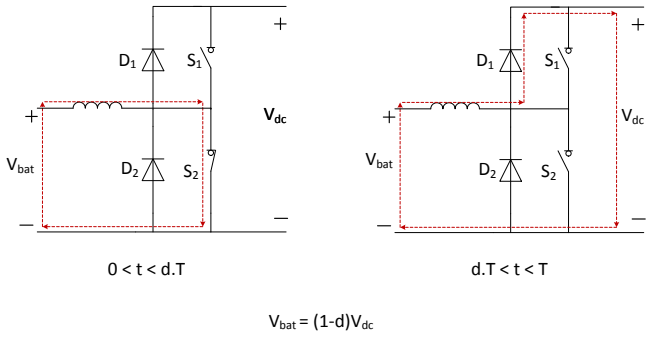

Assuming that the inductor L conducts through the whole cycle of T, its current at the beginning and the end of the cycle should be the same. As a result:
it can be found that in steady-state:

$v_{bat} = (1-d).v_{dc}$

Battery Charge:

In this mode, as shown in Figure 2, S_2 is always opened. When $0 < t < d'.T$, S_1 is closed, while $d'.T < t < T$, S_1 is opened. By averaging the behavior of the converter through weighting factors of d' and $1\text{-}d'$ we get:

$$L_{dc}.pi_{bat} = d'.v_{dc} - v_{bat}$$

It can be found that in steady-state:

$$v_{bat} = d'v_{dc}$$

$$d = 1 - d'$$

Assuming the DC/DC converter to be lossless, the relationship between i_{dc} and i_L in steady-state can be written as:

$$i_{dc} = (1 - d).i_{bat}$$

Figure 72: Schematic diagram of the DC/DC converter in charge mode

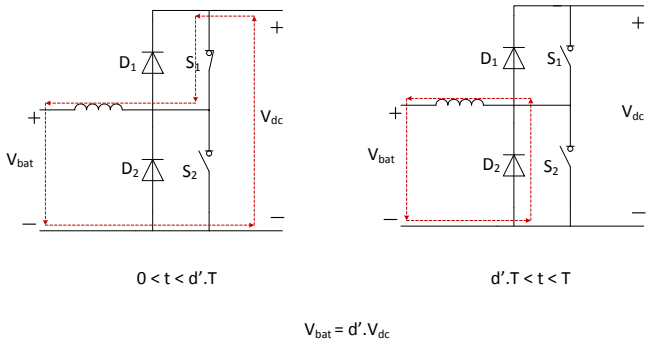

Active AC/DC Rectifier:

On the ac side, differential equations of the active rectifier can be written as [2]:

$$-v_{abc} + L_{ac}.pi_{abc} + e_{abc} = 0$$

Assuming no power loss, the following equation can be written for AC/DC conversion in the rectifier:

$$-v_a i_a - v_b i_b - v_c i_c = C_{dc}.v_{dc}.pv_{dc} + {v_{dc}}^2/R_{dc} + v_{dc} i_{dc}$$

Also, through the power balance in the DC/DC converter, i_{dc} in (10) can be substituted with the following:

$$i_{dc} = v_{bat}.i_{bat}/v_{dc}$$

The following equations are written in the *abc* stationary reference frame. Assuming balanced operation, and in order to simplify the controller design, these equations can be written in a rotating *dq* reference frame.

$$L_{ac}.pi_d = +L_{ac}.\omega.i_q + v_{dc}.u_d - e_d$$

$$L_{ac}.pi_q = -L_{ac}.\omega.i_d + v_{dc}.u_q - e_q$$

$$C_{dc}.pv_{dc} = -1.5 i_d.u_d - 1.5 i_q.u_q - \frac{v_{dc}}{R_{dc}} - (1-d) i_{bat}$$

where the *dq* reference frame rotates with angular frequency ω, and $0 \le k \le 1$ and $0 \le \alpha < 2\pi$ are the modulation amplitude and angle, respectively. The *abc* to *dq* transformation is based on:

$$\begin{bmatrix} x_d \\ x_q \end{bmatrix} = \begin{bmatrix} sin(\theta + 60^\circ) & sin\theta \\ cos(\theta + 60^\circ) & cos\theta \end{bmatrix} \begin{bmatrix} x_a \\ x_b \end{bmatrix}$$

where $\theta = \omega t + \theta_0$.

In summary, the state-space equations of the BESS can be described based on the following affine nonlinear set of differential equations:

$$\dot{X} = F(X) + G(X)U$$

where:
$X = [i_{bat} \quad v_{dc} \quad i_d \quad i_q\ ]^T$

$$F(X) = \begin{bmatrix} \frac{v_{dc} - v_{bat}}{L_{dc}} \\ -\frac{i_{bat}}{C_{dc}} - \frac{v_{dc}}{R_{dc}.C_{dc}} \\ +\omega i_q - \frac{e_d}{L_{ac}} \\ -\omega i_d - \frac{e_q}{L_{ac}} \end{bmatrix}$$

$$G(X) = \begin{bmatrix} -\frac{v_{dc}}{L_{dc}} & 0 & 0 \\ i_{bat} & -\frac{3}{2}.\frac{i_d}{C_{dc}} & -\frac{3}{2}.\frac{i_q}{C_{dc}} \\ 0 & \frac{v_{dc}}{L_{ac}} & 0 \\ 0 & 0 & \frac{v_{dc}}{L_{ac}} \end{bmatrix}$$

$U = [\, d \quad u_d \quad u_q \,]^T$

$u_d = 0.5k\cos(\theta_0 + \alpha)$

$u_q = 0.5k\sin(\theta_0 + \alpha)$

The behavior of the BESS as a nonlinear dynamical system, which can be controlled through nonlinear control methods. The control design will be based on separating the control actions of rectifier and DC/DC converter based on simplifying assumptions. In our design, the active power will be controlled by the DC/DC converter through sliding mode control, and the reactive power and the DC voltage will be controlled by the rectifier through linear PI controllers.

Active Power Control:

The charging/discharging power of the battery can be controlled by the duty ratio of the DC/DC converter. For this purpose, sliding mode control method has been used. Based on this method, a positive constant λ, called the convergence factor, is used to force the variable x to approach its desired value x^* by controlling $\dot{x}$ through the below differential equation:

$$\dot{x} = -\lambda(x - x^*)$$

Based on (23), for controlling P_{dc} at its desired value P_{dc}^*, we may control i_{bat} at the desired value i_{bat}^* evaluated as:

$$i_{bat}^* = P_{dc}^*/v_{bat}$$

Based on (23), and using (3), the duty ratio of the DC/DC converter for controlling the injected power can be determined as:

$$d = \frac{\lambda . L_{dc}(i_{bat} - i_{bat}^*) + v_{dc}^* - v_{bat}}{v_{dc}^*}$$

Reactive Power and DC-Link Voltage Control:

For controlling the reactive power Q and the DC-link voltage v_{dc}, Voltage Oriented Control (VOC) method based on [6] is applied to the AC/DC rectifier. Figure 3 depicts the schematics of VOC.

Figure 73: Schematic diagram of Voltage Oriented Control

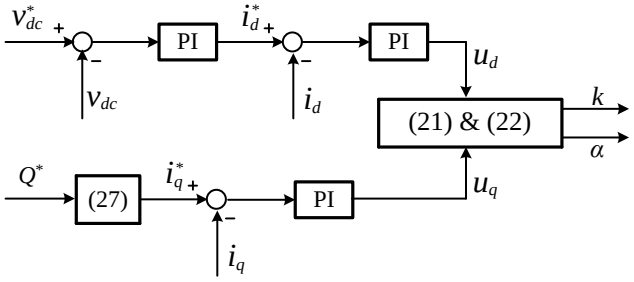

Considering $\theta_0 = 0$ in the rotating dq reference frame, $e_{q=0}$, and the injected reactive power at the entry of the rectifier can be written as:

$$P_{ac} = -1.5 e_d . i_d$$

$$Q = +1.5 e_d . i_q$$

Assuming e_d (maximum value of the grid voltage) to remain fairly constant, change of i_d can directly change $P_{dc}$and hence v_{dc}. Similarly, based on (27), changing i_q can directly change Q. As seen in Figure 3, control of v_{dc} and Q in VOC have been implemented through independent (decoupled) PI controllers.

APPENDIX E:
IKF State Estimation Equations

In this section, IKF SE equations considering PMU data have been derived. It is known that the KF is a method aimed at formulating the SE problem of a general system defined by a set of independent variables $x \epsilon R^n$, where R^n is the n–dimensional field of real numbers whose discrete time–evolution is:

$$\mathbf{x}_k = \mathbf{A}\mathbf{x}_{k-1} + \mathbf{B}\mathbf{u}_{k-1} + \mathbf{w}_{k-1}$$

Where x_k and x_{k-1} are the states of the system in discrete steps of k and k −1 respectively, $u_{k-1} \epsilon R^n$ is a set of h control variables of the system at step k −1, and w_{k-1} represents the assumed white noise with a normal probability distribution. A is a matrix of dimension n x n relating the state of the system at step k −1 with the current step k for the case of null active injections and process noise, B is a matrix of dimension n x h that links the time evolution of the state of the system with h injections at current step k −1 for the case of null process noise.

SE is based on the availability of a set of measurements $z \epsilon R^m$ that in general are non–linearly linked with the system state by the following set of non–linear equations

$$\mathbf{z}_k = h(\mathbf{x}_k) + \mathbf{v}_k$$

Where z_k is the set of the available measurements related to the current time step k; $h(x_k)$ is a measurement function that links the set of measurements with the system state at the step k, for the case of null measurement noise ($h(x_k) \epsilon R^m$). v_k is the measurement noise at the step k which is assumed to be white, with a normal probability distribution and independent from w_k ($v_k \epsilon R^m$).

It is known that the SE problem in a power system is the identification of the phase–to–ground voltage phasors related to the N network buses. Defining the first bus of the network as the slack bus with δ1 = 0, the state vector x is a 2N −1 unknown voltage angle with magnitudes expressed in:

$$\mathbf{x} = \left[\delta^{*,2}, \ldots, \delta^{*,N}, V^1, \ldots, V^N\right]^T$$

where $\delta^{*,i}$ (i = 2,...N) represents the relative angle of the voltage phasor of i^{th} bus with respect to the angle of the slack bus δ^1 ($\delta^{*,i} = \delta^i - \delta^1 = \delta^i$).

We can express the power injections' vector u as:

$$\mathbf{u} = \left[P^1, \ldots, P^N, Q^1, \ldots, Q^N\right]^T$$

Where; P^i and Q^i(i = 1,...N) are the active and reactive power injections (produced by generation systems, absorbed by loads or exchanged by storage systems) of the i^{th} network bus.

Now we present a form of an equation in correspondence to the specific case of power networks. In particular, let make use of the well-known formulation of the power flow problem in the implicit form.

$$f_p^i(\mathbf{x},\mathbf{u}) = P^i - V^i \sum_{h=1}^{N} V^h \left[G^{ih} \cos\left(\delta^i - \delta^h\right) + B^{ih} \sin\left(\delta^i - \delta^h\right) \right] = 0$$

$$f_Q^i(\mathbf{x},\mathbf{u}) = Q^i - V^i \sum_{h=1}^{N} V^h \left[G^{ih} \sin\left(\delta^i - \delta^h\right) - B^{ih} \cos\left(\delta^i - \delta^h\right) \right] = 0$$

If we linearize the above functions as a function of the system state x and power injections u and considering that $f_P^i(x,u)$ and $f_Q^i(x,u)$ are implicit functions, we obtain the following with all variables as defined in:

$$\frac{\partial \mathbf{f}(\mathbf{x},\mathbf{u})}{\partial \mathbf{x}} \Delta\mathbf{x} + \frac{\partial \mathbf{f}(\mathbf{x},\mathbf{u})}{\partial \mathbf{u}} \Delta\mathbf{u} + \mathbf{e} = 0$$

Where;

$$\mathbf{f}(\mathbf{x},\mathbf{u}) = \left[\mathbf{f}_P(\mathbf{x},\mathbf{u}), \mathbf{f}_Q(\mathbf{x},\mathbf{u}) \right]$$

The equation can be also written as:

$$\overbrace{\begin{bmatrix} -\frac{\partial \mathbf{f}_P(\mathbf{x},\mathbf{u})}{\partial \delta} & -\frac{\partial \mathbf{f}_P(\mathbf{x},\mathbf{u})}{\partial V} \\ -\frac{\partial \mathbf{f}_Q(\mathbf{x},\mathbf{u})}{\partial \delta} & -\frac{\partial \mathbf{f}_Q(\mathbf{x},\mathbf{u})}{\partial V} \end{bmatrix}}^{-J} \Delta\mathbf{x} + \overbrace{\begin{bmatrix} I & 0 \\ 0 & I \end{bmatrix}}^{I} \Delta\mathbf{u} + \mathbf{e} = 0$$

therefore:

$$\mathbf{x}_k = \mathbf{x}_{k-1} + \mathbf{J}_k^{-1}\left(\mathbf{u}_k - \mathbf{u}_{k-1}\right) + \mathbf{J}_k^{-1}\mathbf{e}$$

The term $J_k^{-1}e$ of 14 is related to the system process noise w_k of 16 which is due to the error in the linearization process.

It can be considered as the network's pseudo–dynamic model where matrix is the identity matrix. Generally, the closeness of the a–priori values predicted as compared to the real states has a direct effect on the number of iterations to be performed by the KF for convergence. Although this approach needs further investigation, here we are assuming 'flat–start' composed of a zero angle and unity magnitudes for voltages at the a-priori states:

$$\mathbf{x}_{k,0} = \left[\overbrace{0,\ldots,0}^{N-1}, \overbrace{1,\ldots,1}^{N} \right]^T$$

Where; $x_{k,0}$ shows the a-priori state related to the generic k-th time step 4.

The IKF algorithm will then begin an iterative process at the generic time step k to minimize the a-posteriori error by use of a non–linear a–priori estimate combined with a weighted difference separating the measurement z_K and the predicted measurement $h(x_{k,i})$.

$$\mathbf{x}_{k,j+1} = \mathbf{x}_{k,j} + \mathbf{K}_{k,j}\left[\mathbf{z}_k - h\left(\mathbf{x}_{k,j}\right)\right]$$

Where K is defined as the KF blending factor or Kalman gain. Later, we will define in details all the elements of ($\mathbf{x}_{k,j+1} = \mathbf{x}_{k,j} + \mathbf{K}_{k,j}\left[\mathbf{z}_k - h\left(\mathbf{x}_{k,j}\right)\right]$). Now, we should express this equation for our problem. In order to integrate the PMU data in our algorithm, we assume that the set of measurements is composed as follows:

- type–d nodes where we consider to measure phase–to–ground voltage phasors by means of PMU devices;
- type–s nodes where we consider to measure active and reactive power injections so that $d + s \geq N$.

The relevant measurements array z defined by (17) is the following:

$$\mathbf{z} = \left[\overbrace{\delta^2,\ldots,\delta^d,V^1,\ldots,V^d}^{z^d},\overbrace{P^1,\ldots,P^s,Q^1,\ldots,Q^s}^{z^s}\right]^T$$

Since by definition, the Kalman gain K is based on a linearized relation between the system state x and the measurements z, we should derive a linearized version such as:

$$\mathbf{z}_k = \mathbf{H}_k\mathbf{x}_k + \mathbf{v}'_k$$

Where; H_k shows linear dependency and v'_k is a combined measurement and $h(x_k)$ is the linearization errors.

So define a (2d −1) x (2N −1) matrix T to link the first part of the measurement array z^d_k to the system state variables which is composed by the rows of the (2N −1) identity matrix related to the type–d nodes, where phase–to–ground voltage phasors are measured by PMUs.

$$\mathbf{z}^d_k = \mathbf{T}\mathbf{x}_k + \mathbf{v}^d_k$$

Where; the term v^d_k shows the array of the uncertainties of the state variables measured by the

PMUs.

Now, we should link the measured injected power into type–s nodes, namely z^s_k, to the state of the system by means of a linear expression. So we can use:

$$\begin{bmatrix} -\frac{\partial \mathbf{f}_P^s(\mathbf{x},\mathbf{u})}{\partial \delta} & -\frac{\partial \mathbf{f}_P^s(\mathbf{x},\mathbf{u})}{\partial V} \\ -\frac{\partial \mathbf{f}_Q^s(\mathbf{x},\mathbf{u})}{\partial \delta} & -\frac{\partial \mathbf{f}_Q^s(\mathbf{x},\mathbf{u})}{\partial V} \end{bmatrix} (\mathbf{x}_k - \mathbf{x}_{k-1}) + (\mathbf{z}_k^s - \mathbf{z}_{k-1}^s) + \mathbf{e} = 0$$

Where; terms $\frac{\partial .^s}{\partial .}$ refer to the rows of the Jacobian matrix J relevant to type–s nodes along with z^s_k and z^s_{k-1} which are relevant to the measured injected active and reactive powers in correspondence to type–s nodes.

We can then infer z^s_k:

$$\mathbf{z}_k^s = \begin{bmatrix} \frac{\partial \mathbf{f}_P^s(\mathbf{x},\mathbf{u})}{\partial \delta} & \frac{\partial \mathbf{f}_P^s(\mathbf{x},\mathbf{u})}{\partial V} \\ \frac{\partial \mathbf{f}_Q^s(\mathbf{x},\mathbf{u})}{\partial \delta} & \frac{\partial \mathbf{f}_Q^s(\mathbf{x},\mathbf{u})}{\partial V} \end{bmatrix} \mathbf{x}_k + \mathbf{v}_k^s$$

Where; the term v^s_k is given by:

$$\mathbf{v}_k^s = -\begin{bmatrix} \frac{\partial \mathbf{f}_P^s(\mathbf{x},\mathbf{u})}{\partial \delta} & \frac{\partial \mathbf{f}_P^s(\mathbf{x},\mathbf{u})}{\partial V} \\ \frac{\partial \mathbf{f}_Q^s(\mathbf{x},\mathbf{u})}{\partial \delta} & \frac{\partial \mathbf{f}_Q^s(\mathbf{x},\mathbf{u})}{\partial V} \end{bmatrix} \mathbf{x}_{k-1}^s + \mathbf{z}_{k-1}^s - \mathbf{e}$$

The term v^s_k represents an equivalent uncertainty that combines a type–s measurement, with the one related to the approximation of (8) which is clearly not constant with the time step k.

Consequently:

$$\mathbf{z}_k = \overbrace{\begin{bmatrix} \\ \mathbf{T} \\ \frac{\partial \mathbf{f}_P^s(\mathbf{x},\mathbf{u})}{\partial \delta} & \frac{\partial \mathbf{f}_P^s(\mathbf{x},\mathbf{u})}{\partial V} \\ \frac{\partial \mathbf{f}_Q^s(\mathbf{x},\mathbf{u})}{\partial \delta} & \frac{\partial \mathbf{f}_Q^s(\mathbf{x},\mathbf{u})}{\partial V} \end{bmatrix}}^{\mathbf{H}_k} \mathbf{x}_k + \mathbf{v}_k$$

Where

$$\mathbf{v}_k = \begin{bmatrix} \mathbf{v}_k^d \\ \mathbf{v}_k^s \end{bmatrix}$$

With the elements of V_k defined by above.

Now we should just define the blending factor K. The typical form to express the blending matrix to make a converging process as the following:

$$\mathbf{K}_{k,i} = \mathbf{P}_{k,i-1}\mathbf{H}_k^T \left(\mathbf{H}_k \mathbf{P}_{k,i-1}\mathbf{H}_k^T + \mathbf{R}_k\right)^{-1}$$

Where; R_k is the diagonal matrix related to the uncertainties of the measurements:

$$\mathbf{R}_k = \begin{bmatrix} v_{k,11} & \cdots & 0 \\ \vdots & \ddots & \vdots \\ 0 & \cdots & v_{k,mm} \end{bmatrix}$$

Where; $v_{k,jj}$ is the elements of the array v_k, and $P_{k,i-1}$ is the a–priori estimate covariance matrix defined as:

$$\mathbf{P}_{k,i-1} = \mathbf{A}\mathbf{P}_{k-1}\mathbf{A}^T + \mathbf{Q}_{k-1}$$

In our case, matrix A is the identity matrix I and Q_{k-1} is the process covariance matrix, namely the approximations introduced into the linearization of the process. Matrix Q_{k-1} could be computed if the process is known or it can be selected arbitrarily.

As the relative values of Q_{k-1} and R_k directly affect the behavior of the IKF, we will study their sensitivity in the next section. In our case we considered the values of Q_{k-1} as being known and constant for different time steps k (i.e. $Q_{k-1} = Q$).

So the iterative process is the following:

Iteration i = 0:

- forming of the state $x_{k,0}$;
- calculating the error covariance ahead:

$$\mathbf{P}_{k,0} = \mathbf{P}_{k-1} + \mathbf{Q}$$

Iteration i > 0:

- calculation of the blending factor :
- update of the state:

$$\mathbf{x}_{k,i} = \mathbf{x}_{k,i-1} + \mathbf{K}_{k,i}\left[\mathbf{z}_k - \mathbf{h}_k\left(\mathbf{x}_{k,i-1}\right)\right]$$

update of the error covariance matrix:

$$\mathbf{P}_{k,i} = \left(\mathbf{I} - \mathbf{K}_{k,i}\mathbf{H}_k\right)\mathbf{P}_{k,i-1}$$

The stopping criterion is chosen according to the absolute values of differences between two consecutive iterations of phase–to–ground voltage angles and magnitudes. The values of ε_δ and ε_V are suitably chosen as a function of the values of phase–to–ground voltage angles and magnitudes.

$$\max\left(\left|\boldsymbol{\delta}_{k,i} - \boldsymbol{\delta}_{k,i-1}\right|\right) < \varepsilon_\delta$$

$$\max\left(\left|\left|\overline{\mathbf{V}}\right|_{k,i} - \left|\overline{\mathbf{V}}\right|_{k,i-1}\right|\right) < \varepsilon_V$$

APPENDIX F:
Voltage Drop Formula

The approximate formula for Voltage Drop (VD) calculations are given by the following equation, which shows the relationship between the parameters of the system and the load demand. VD is related to the Resistive (R) and Reactive (X_L) parameters of the line, with I_R and I_X flowing through the conductors of the distribution feeder:

$$VD = I_R R + I_X X_L$$

Where I_R and, I_X are the real and the reactive components of the current required by the load, R is the resistive component of the line and X_L is reactive component of the line.

Corrective measures such as adding a shunt Capacitor with reactance X_C in the following equation can reduce the effect of the reactance X_L, lowering the vector magnitude of VD, as demonstrated in Figure 49. This also will lower the magnitude of the current seen by the conductor and lower the line losses caused by I^2R

$$VD = I_R R + I_X X_L - I_C X_C$$

Where I_R, I_X, R, X_L are the parameters as defined above, I_C is the reactive current through the capacitor and Xc is the reactance of the capacitor.

Figure 74: Vector representation of capacitor correction.

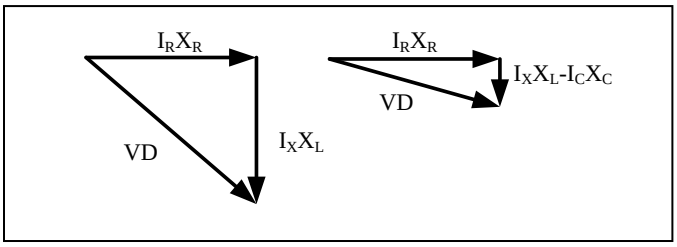

In certain feeders with a small conductor diameter, high impedance, or long lines, R and X_L increase, making VD become more sensitive to the amounts of I_R and I_X that are due to the demand of the load. This high impedance line is often referred to as a weak network and presents additional challenges.

$$VD = |I_L| \times R_{eff} \times \cos\theta + |I_L| \times X_{eff} \times \sin\theta$$

Where $|I_L|$ is the magnitude of the line current, R_{eff} and X_{eff} are the calculated resistance and reactance to the point at distance "d", and θ is the angle difference between current and

Voltage. The Line Drop Compensator (LDC) in voltage regulators actively monitors the line current I_L at the LTC and uses the R/X ratio of the line to predict the VD suggested by the above equation at a point with some distance (d) away from the regulator's location. The accuracy of this predictive measuring point is dependent on the loading before and after the point at the distance (d).